Ghent University
Faculty of Sciences
Department of Chemistry

Copper Nanocrystals-based Conductive Inks for Printed Electronics

Arnau Oliva Puigdomènech

Thesis submitted in fulfillment
of the requirements of the degree of
Doctor in Science: Chemistry
2019

Ghent University
Faculty of Sciences
Department of Chemistry

Promotor	Department
Prof. Dr. Ir. Z. Hens	Chemistry
Co-Promotor	Department
Prof. Dr. C. Detavernier	Solid-State Sciences
Jury members	Affiliation
Prof. Dr. K. De Buysser (chair)	UGent
Prof. Dr. J. Martins	UGent
Prof. Dr. D. Depla	UGent
Prof. Dr. A. Hardy	UHasselt
Dr. Guido Desie	Agfa-Gevaert

This work was realized with the support of:
SIM-Flanders (ICON-Met@link)
University of Ghent (F2018/IOF-StarTT/419)

Acknowledgements

This section was drafted prior to anything else in this thesis. In one of many days that I felt lost I decided to start remembering all the people that had an impact on my life in Ghent. By that time, I was not even sure the thesis will be submitted and I thought I could use this as a farewell letter. This is the result:

I could not start with anyone else than Prof. Zeger Hens. He is the main cause I am here today, in Gent, where I have spent the last 4 years of my life. He believed in me after a crappy interview that luckily I can no longer remember and continuously gave me the confidence to work in the project. Most of the former PhD students praise his intelligence and scientific prowess in this lines which even if fascinating is not what makes him a great promoter. He literally always had the door open to guide, assist or teach me; and did it repeatedly and kindly even if my face was clearly showing that I was completely lost. These meetings with you were not only useful for the scientific input but also to value my work with optimism which I often had difficulties to. The fact that a brilliant person like him is accessible and takes the time to humbly help the more mundane is what really makes him a great promoter and mainly, an excellent man. Thanks for everything Zeger.

The other person that had a considerable scientific impact on the thesis is (already Prof.) Jonathan De Roo. When I joined the group he was an enthusiastic PhD student and by the time I am finishing he is already a professor. This rapid evolution is not just an example of his academic ambition, he really deserves it. Personally, as I was the only student working on the project, having you around was a blessing. I appreciate your guidance, ideas, corrections and most of all, your optimism.

I would also like to thank Prof. José Martins, Prof. Christophe Detavernier and Prof. Klaartje de Buysser. Your collaboration, insights and equipment were of immense value and totally necessary for the completion of this thesis. In terms of research contributions, I would also like to acknowledge some colleagues for teaching or assisting me in specific topics. Thanks Willem for showing me how to use the TEM even if I'm still awful, thanks Pieter S. for teaching me thermodynamics, Hannes for the XRDs, Davy, Filip and Jakob for your help in S1 and of course, thanks Jorick for being there when I had a technical problem.

Before jumping into more personal acknowledgments I would like to show my appreciation to the jury members: Prof. José Martins, Prof. An Hardy, Prof. Diederik Depla and Dr. Guido Desie. I know I am not a great writer and reading all these pages were probably the least enjoyable thing to do with your time. Anyway, thanks for taking your time to read, correct and comment the thesis. Also, I would like to appreciate the funding support that made this thesis possible: SIM-Flanders (ICON-Met@link) and UGent (F2018/IOF-StarTT/419).

I genuinely believe that the key for happiness is to surround yourself with people that you love (i.e. family and friends). Since these 4 years I have been away from home it was necessary for me to meet people with whom I could be myself and build a social relation. Luckily, I did not have to look very far to find them because I can say with full conviction that I have been working with friends. I still remember the first day I walked into the (sick) office and I met Dorian, Mickael and Kishu. The first was seated in an awkward posture, face hidden under his shirt neck and I could not understand a word he said; the second seemed a very serious man and barely said hi; fortunately, the third seemed a friendlier guy. However, one thing I learnt here is that first impressions are usually wrong. They were the first to embrace me, and once I got to know them (and understand their English) we had a great time together. Their friendship helped me to adapt to a new country and research group and their support became crucial to start feeling more like at home. For all these reasons I am very grateful I have met you and I wish to see you in the future in your maisonette.

Continuing in the "sick" office I would like to express my appreciation to Pieter. We spent a lot of time together (sorry Brenda!) and I enjoyed all of it. Concerts, quizzes, brewing beer, board games... we shared almost all

our hobbies! Being friends with you is the easiest thing in the world and I wish you the best for your future projects: saving the human race, getting a PhD, reforming your house, staying vegetarian, cleaning your desk... (in ascending difficulty) we will sure keep in touch. Next, I would like to mention Hannes. The first thing people think when mentioning him would be his happiness and contagious joy but he is much more than that. Now that I know you more I can say that you are a great human being, with a huge heart and I feel fortunate to be your colleague and friend. Ah, and you suck at dards. Still in the sick office I would like to mention Filipe. Anyone that knows him can probably tell that he is a really nice and easy-going person, and I confirm that. I enjoyed having breakfast with you every day. And the latest addition to the office, Kim the Artist. It has been great to have you around during the last months, I appreciate our conversations and I am convinced you will do amazing both with your thesis and your life. To conclude the office, I would like to thank Ivo for never being there so I could comfortably stretch my legs.

Next I will mention the colleagues that inhabit the "cool" office. First, I would like to thank Valeria, it has been a pleasure for me to share the PhD road and many moments with you. I will always be at your feet. Igor, it has been an honor to be your colleague as well, I appreciated our conversations and your help with the IR-lamp. Thanks Jakob for your help in S1 and best regards wherever you are. Good luck Catwoman-Leila with your PhD, your hard-work will have a great pay-off for sure, you deserve it. Federico, Abhi, Vignesh, Ali sadly I did not have the opportunity of working or getting to know you much but I want to wish you the best for the future. Chandu, I am happy I had the opportunity to know you more this last year, you are awesome. Willem, I have really enjoyed having you around either in the lab or outside during the last years. Your open and chill character made it really easy for me and I am glad you took it well when I (continuously) made jokes about your height. Also, I really liked when you took responsibility and improved the functioning of the lab as well as our discussions about TEM, XRD...

The relation with the people I am about to name really evolved during time. To start, Suzanne, we barely talked during the first months I was in the group. With time I got to know more of you and I am really happy about that because I discovered a really interesting person with whom I could talk

about anything and have fun in the leisure time. A similar case goes for Jorick. I knew from the beginning that we would get along but it also took time to build up our friendship. Besides helping me in plenty of work-related problems I had a lot of fun when we had the opportunity to hang out. I admire you and I have great memories of the MRSs conferences with you and Suzanne. Finally, Kim. Our relation has been in a rollercoaster during these years but I can happily say that now we comprehend and trust each other. In general, knowing you all took time still totally worth the effort. Your friendship is an accomplishment that I am really proud of and I will be seeing you all around in the thingy.

The last office of PCN is the "fun" office and I can really say that nowadays is a well-deserved name. That is in great part because of the Italians. Carmelita, Alessio and Gabri, your presence in the group revitalized the atmosphere and is always enjoyable to be around any of you. You are always up for any activity and being in a good mood with you is effortless. Thanks for being there, I take great memories from all the time we spent together. Natalia is another great example of someone you cannot judge from the first impression. I admire your transparency and how natural and unique you are. Emile, if you are reading this during my reception, stop eating, leave some food for the rest. Jokes apart, you are a fine man it was really nice to work with you; I wish you the best in your new group. Jari, you are a better scientist than basketball player. And I do not say that because you suck at ball, it is because you are really becoming a great scientist. I love your sense of humor (still learning from you) and it was always wonderful to spend leisure time with you. Shalini, thanks for the discussions, the support and all the moments of bliss, good luck in your new adventure as professor. Also, I would like to mention Prof. Pieter Geiregat and future Prof. Tangi here, thank you for your insights, help and conversations throughout last years. I wish you the best in your careers. Renu, Pengshang, I enjoyed working next to you in the lab. You are really easy-going and it was a pleasure to have you as colleagues. Good luck for the future.

There are other people in the department of Chemistry that have been essential during these years. Pierre and Kathleen you do an amazing work in secretary day after day and are of huge value in the department. Pat and Bart, you are fascinating people and do your job splendidly; the department

is very lucky to have you both around. Thanks for helping me any time I required it. I would also like to acknowledge Tom, Els and Katrien for your significant help at certain moments. Finally, Hans, Philip, Ilse and Bernard, I enjoyed assisting in the practical exercises and that was mainly because you made things easy for me. I used to look forward to Friday afternoon and the coffee break with Ilse and I take with me a nice experience of this part of the PhD. Finally, I would also like to have a general shout-out to all the rest of personnel from S3 that made my stay here so gratifying.

As can be read in the lines above, it seems I am writing to a bunch of friends instead of colleagues. You might think I have a naive or childish perspective of the working life and you would probably be right. I guess adults know how to separate social relations from work, they know is not always easy feel comfortable with your colleagues. Yet, I simply cannot feel good with myself and be happy if I do not feel comfortable with whom I spend most of my time during the week. I know this will be a future priority, to be part of a working environment like the one I had here in S3 these last years.

Even if my personality does not match with most of the Spanish clichés, coming from the south of Europe and encountering the Flemish culture was a small social impact for me that initially hampered my integration. With time I learnt how to interact better with the people here and at the same time I learnt a lot about the history, traditions, society, etc. All this helped me not feeling like a stranger anymore and I gradually integrated a more Flemish mentality into my identity. Now, even if I do not speak dutch, I think of myself as a "belgianized Catalan", that is the effect that the time here had in me. Because doing a PhD here it was not only about getting results and publications; for me an equally important part of the experience was to LIVE here. And again, I consider myself lucky to have done this experience in Ghent. For example, going home at night after enjoying a beer with some of the people mentioned here, biking by the Leie with the cold wind blowing on my face whilst listening to "Pretty Machines" from Parquet Courts was one of the moments of happiness that I will always remember and associate with Ghent. Also, I take with me plenty of great memories playing basketball in Gentson. Cheers to the guys.

At the end of the day, living in this city was a great experience because I got the opportunity to meet excellent people that accompanied me during these years: An-Sofie, Inge, Benjamin, Sarah, Adriana, Marta, Andrea, Jonas. . . , thanks for sharing so many moments with me.

To finish this acknowledgments I would to like to mention the people that define me and for practical reasons I will do it in Catalan.

Primer de tot, no estaria aquí si no fos pel suport rebut constantment per part meus pares. Vosaltres sempre hi heu sigut i m'heu donat la llibertat d'escollir lliurament el meu camí en tot moment, recolzant-me en tot. Ja sabeu que em costa expressar en persona com em sento i per això ho escric aquí: us estimo. Per altra banda m'agradaria agrair a tots els amics i familiars que en un moment o altre heu vingut a visitar-me. Poder ensenyar-vos la meva vida d'aquests darrers anys i a la vegada compartir estones amb vosaltres m'ha servit per unir els meus dos mons i portar la meva estada aquí de forma molt més suportable. I per acabar, Anna. En poc temps t'has convertit en un suport vital per mi i et valoro moltíssim. Gràcies per ser-hi.

Contents

List of Acronyms

C

COSY ..... Homonuclear Correlation Spectroscopy

D

DLS ..... Dynamic light scattering

DOE ..... Design of experiments

DOSY ..... Diffusion ordered spectroscopy

E

EDX ..... Energy-dispersive X-ray spectroscopy

F

FWHM ..... Full width at half maximum

I

IoT ..... Internet of Things

M

MEEAA ..... 2-[2-(2-methoxyethoxy)ethoxy]acetic acid

N

NC ..... Nanocrystal

NMR ..... Nuclear magnetic resonance spectroscopy

NP ..... Nanoparticle

O

OlNH$_2$ ..... Oleylamine

P

PE ..... Printed electronics

PA ..... Poly(allylamine)

PET ..... Polyethylene terephthalate

PVP ..... Poly(vinylpyrrolidone)

R

RFID ..... Radio-Frequency Identification

S

SEM ..... Scanning electron microscopy

SPR ..... Surface plasmon resonance

T

TEM ..... Transmission electron microscopy

U

UV-Vis ..... UV-Visible spectroscopy

UDA ..... Undecylenic acid

X

XRD ..... X-ray powder diffraction

Nederlandse Samenvatting
–Summary in Dutch–

Koper (Cu) gebaseerde nanodeeltjes (NP's) of nanokristallen (NC's) vormen een kostenefficiënt alternatief voor het gebruik van zilver (Ag) in geprinte elektronica. Koper heeft een gelijkaardige bulkgeleidbaarheid als die van zilver, maar de kostprijs bedraagt slechts 1% van die van Ag. In dit proefschrift behandelen we eerst de state-of-the art, met name de productiemethoden voor Cu nanodeeltjes en strategieën om oxidatie te vermjiden. Vervolgens ontwikkelden we een synthesestrategie voor Cu nanokristallen die gebaseerd is op een thermische ontbinding. Dit liet ons toe om de grootte van de nanokristallen af te stemmen. We hebben onderzocht hoe verschillende liganden interageren met het oppervlak van de Cu nanodeeltjes. Hieruit besloten we dat zowel het ligand als de deeltjesgrootte een effect heeft op het sinteren van de deeltjes in een continue film. Uiteindelijk ontwikkelden we een formulering om de Cu nanokristallen te printen en verkregen we geleidende RFID-antennes.

Allereerst hebben we een uitgebreid onderzoek ondernomen naar de meest aangewende methoden om Cu nanodeeltjes te synthetiseren. Hierbij hebben we de methoden onderverdeeld in 3 categorieën, met name, chemische, fysische en biologische productiemethoden. Chemische productiemethoden worden het meest aangewend in de literatuur vanwege hun toegankelijkheid en het gemak om op een eenvoudige manier de deeltjeseigenschappen aan te passen. Het nadeel van de chemische methoden is het frequente gebruik van gevaarlijke reductiemiddelen en de hoeveelheid afvalproduct die tijdens de synthese vrijkomt. Substitutie van het reductiemiddel door ascorbinezuur lijkt een veelbelovende aanpak om de milieu-impact van de synthese te verminderen en tegelijkertijd de Cu NP's tegen oxidatie te beschermen. Als alternatief zijn methoden op basis van de thermische ontbinding van een

koper precursor veelbelovend omdat er hier geen extra reductiemiddel nodig is. Fysische methoden maken massaproductie mogelijk, maar vereisen veeleer dure apparatuur. Eveneens is er een gebrek aan controle op een aantal cruciale deeltjeseigenschappen, zoals de grootte en de colloïdale stabiliteit. Biologische syntheses van Cu NP's zijn gebaseerd op dezelfde mechanismen als de chemische methoden, maar dit in een milieuvriendelijker perspectief. Hier onderscheidt de synthese op basis van plantenextracten zich van de rest als een groene methode die toelaat om goed gedefinieerde Cu NP's te bereiden. De lage reactietijden en opbrengsten van een dergelijke synthese veroorzaken echter nog steeds geen kosteneffectieve manier om Cu NP's te vervaardigen. Als strategie om oxidatie te voorkomen, zorgde een inbedding in silica en koolstof dat het oxidatieproces op Cu-oppervlakken stopte, dit echter ten koste van een drastische afname van de geleidbaarheid. Omgekeerd bleek het groeien van een zilverlaag op het oppervlak van de NP's, door transmetallatie, de geleidende eigenschappen te behouden terwijl de Cu-kern tegen oxidatie werd beschermd. Een meer economische benadering is gebaseerd op de adsorptie van organische liganden en polymeren op het oppervlak van de NP's. Naast het verlenen van colloïdale stabiliteit, vertraagde hun aanwezigheid op het oppervlak het oxidatieproces voldoende om uiteindelijk de Cu NP's in geleidende films te transformeren.

In hoofdstuk 3 hebben we onze methode geïntroduceerd om Cu NC's te synthetiseren op basis van de thermische ontleding van koperformiaat in oleylamine. Deze methode maakt gebruik van een economische precursor en een snelle één-pot synthese om Cu NC's te verkrijgen. Door het initiële reactievolume te verzadigen met koperformiaat en door implementatie van een specifiek temperatuurprofiel te, laten we een zelfreinigend effect zien. Zuurstof heeft tijdens de reactie geen toegang tot de nanokristallen, wat ons toegang heeft tot niet-geoxideerde nanokristallen te verkrijgen. Dit is echter alleen mogelijk als de reactiesnelheid hoog genoeg is, wat ervoor zorgt dat zuurstof een beperkte toegang heeft tijdens de vorming van Cu^0 monomeren. We hebben aangetoond dat de grootte van de deeltjes kan worden aangepast van 4 tot 200 nm door de beginconcentratie van precursor en de verhoudingen precursor / oleylamine aan te passen.

In hoofdstuk 4 tonen we aan dat we, mits een aanpassing aan de synthese, 4 nm Cu NC's kunnen vormen – deze zijn ideaal voor oppervlaktechemiestudies vanwege hun hoge oppervlakte tot volumeverhouding. We hebben

aangetoond dat de initieel gebonden $OlNH_2$ kan worden vervangen door een carbonzuur door middel van massa-actie. Op basis van een thermodynamische beschrijving van de titratiecurven van amine / carbonzuur argumenteren we aan dat carbonzuren $OlNH_2$ rechtstreeks vervangen en binden aan extra oppervlaktesites die weinig affiniteit vertonen voor $OlNH_2$. We hebben bewezen dat carbonzuren dissociëren bij binding op dergelijke oppervlakken en een X_2 bindend motief vormen. Aangezien een dergelijk bindend motief een amfoteer oppervlak vereist met zure en basische bindingsplaatsen, stellen wij dat ligandbinding aan Cu-nanokristallen wordt bepaald door de aanwezigheid van oppervlakte-oxiden, in plaats van door de eigenschappen van het ongerepte metaaloppervlak.

In hoofdstuk 5 hebben we het effect geanalyseerd dat liganden hebben op de oxidatie en reductie van de NC's en hebben we het sintergedrag van de Cu NC's bestudeerd. We toonden aan dat de Cu NC's in polaire oplosmiddelen kon worden gedispergeerd door het aanvankelijk gebonden $OlNH_2$ te vervangen door MEEAA, een vluchtig carbonzuur. We toonden aan dat carbonzuren, ook al zijn ze licht gebonden, niet in staat zijn om oxidatie van de NC's na blootstelling aan lucht te voorkomen. We hebben echter bewezen dat oxidatie kan worden teruggedraaid door te sinteren onder N_2 en we hebben onderzocht hoe het passiverend ligand en de deeltjesgrootte de reductietemperatuur beïnvloeden. Met MEEAA bedekte deeltjes vertoonden de laagste reductietemperatuur onder de bestudeerde liganden en een verbeterde korrelgrootte van 50 nm, wat MEEAA vooropsteld als een veelbelovende ligand voor Cu NC's in geleidende inktformuleringen. We toonden een duidelijke relatie aan tussen deeltjesgrootte en Cu_2O-Cu overgangstemperatuur. Films bestaande uit grotere deeltjes ($\geq$ 113 nm) vertoonden een verbeterde geleidbaarheid zowel voor als na het thermisch sinteren, ondanks de hoge temperatuur. Over het geheel genomen benadrukken deze conclusies de relevantie van het passiverend ligand en de deeltjesgrootte bij het nastreven van geleidende films en wijzen ze op de relevante deeltjesparameters om een geleidende inkt te formuleren en af te drukken.

Tot slot hebben we een aanpassing van de synthesemethode gepresenteerd, waarbij $\sim$ 6 g per 100 ml niet-geoxideerde Cu NC's in een hoge concentratie werden geproduceerd. De geproduceerde Cu NC's maakten de optimalisatie van een inktformulering met behulp van een definitive screening design (DSD) mogelijk. We hebben de significante factoren bepaald die invloed

hebben op de soortelijke weerstand en de aanhechting van de inkt. Optimale verwerkingscondities leverden hooggeleidende films op, met een weerstand van 2,57 $\mu\Omega \cdot$ cm, een waarde die overeenkomt met 66 % van de bulkgeleidbaarheid van Cu. Vervolgens verhoogden we het volume van de reactie verder tot 1 L, waarbij in een enkele synthese licht geoxideerde $\sim$ 60 g Cu NC's werden geproduceerd. We hebben zeefdrukken en geleidende RFID-antennes geproduceerd door de optimale formulering aan te passen met een thixotroop middel, hierdoor werd weerstand van 0,52 $\Omega/\square$ te verkregen.

1 Introduction

1.1 Problem definition

1.1.1 Internet of Things

Historically, computers, and by extension, the Internet, have been almost fully dependent on people for information. Humans actively coded, typed, recorded or photographed most of the data available on the Internet. We created and established the protocols to process this data and we acted accordingly. This human dependency in gathering the data of our environment and transferring it to the Internet is associated with imperfection due to lack of attention or inaccuracy inherent in our human condition.

What if we had devices that could gather information from the environment, interact with other devices and act on it? We could avoid flaws, spare time and save resources by having interconnected devices that sense the surroundings and inform or react unambiguously. This reflection was made in 1999 by Kevin Ashton, founder of the MIT Auto-ID Center, who dubbed the Radio-frequency identification (RFID) and sensor technology that enable computers to observe, identify and understand the world without the limitations of human-entered data as Internet of Things (IoT). [1]

Today, 20 years after IoT was mentioned for the first time, the term evolved as the technology did and it could be generally defined as the extended network between everyday objects and electronic devices.[2] Some IoT applications are already present in our daily life, for example, temperature sensors interacting with the heating system and precisely adapting the temperature of the house to our liking or sensors informing us of empty spots in parking lots and detecting automatically the car license to relieve the traffic.[3–6] The possibilities are uncountable and the development of technology will have an impact in different fields like healthcare, smart cities, retail, security, etc.[7]

1.1.2 Radio Frequency Identification (RFID)

RFID is an automatic technology that enables distant identification of objects through radio waves. A RFID system consists of a reader (or interrogator) and a tag.[8] The tags have several advantages compared to traditional bar code identification: it can incorporate additional data such as the manufacturer or product type; it can measure environmental factors such as temperature; it does not require physical orientation towards the reader and the readers can discern many different tags located in the same area. These perks link IoT to RFID technology due to its ability to identify objects and interconnect them with the internet without human assistance.[9]

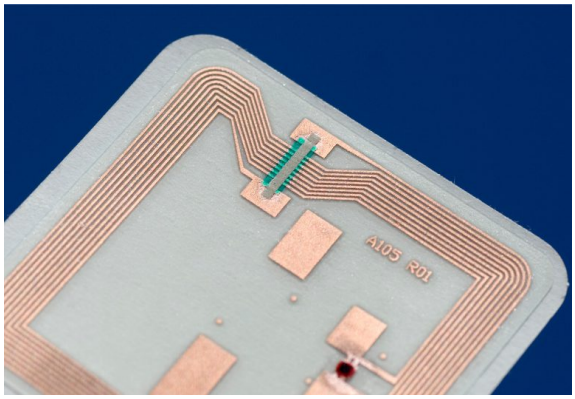

Figure 1.1: Printed RFID tag (Reprinted from reference.[10])

RFIDs are generally classified in two classes depending on their energy source: active and passive. Active tags require an autonomous power source to propagate their signal to the reader and their lifetime, size, applications and cost is usually limited by the battery. On the bright side, they usually

have a stronger signal and longer range making them useful to track high-value assets or vehicles. Active tags represent the smallest market segment within the RFID technology with over 150M tags sold in 2017 - compared with 16B of passive RFID tags.[11]

As the name implies, passive tags do not require an internal power source, drawing their power from the reader radio signal. Then, only two components are imperious in a passive RFID tag: the conductive antenna receives the signal, powers the circuit and transmits a response to the interrogator; and the chip or integrated circuit provides identification and coordinates that response (see Fig 1.1).[9;12] The growth and spreading of RFID technology will depend in large measure on providing the adequate materials to reduce the production costs whilst maintaining performance as well as on the establishment of a suitable method to fabricate the tags, integrating both components in a scalable manner.[13;14]

Table 1.1: Conductivity (σ), redox potential for the redox couple indicated (E°), earth abundance and price of common metals used in conductive applications.[15] Metal prices retrieved from www.metalprices.com (June 2019)

Metal	σ (S/m)	Redox couple	E°(V)	Ab. (ppm)	Price ($/kg)
Ag	$6.3 \cdot 10^7$	Ag^+/Ag	+0.80	0.075	468.76
Cu	$6.0 \cdot 10^7$	Cu^{2+}/Cu	+0.34	60	5.93
Al	$3.8 \cdot 10^7$	Al^{3+}/Al	−1.66	82300	1.74
Zn	$1.7 \cdot 10^7$	Zn^{2+}/Zn	−0.76	70	2.71
Ni	$1.4 \cdot 10^7$	Ni^{2+}/Ni	−0.23	84	11.97
Fe	$1.0 \cdot 10^7$	Fe^{2+}/Fe	−0.41	56300	0.09
Sn	$9.2 \cdot 10^6$	Sn^{2+}/Sn	−0.14	2.3	19.64
Ti	$2.4 \cdot 10^6$	Ti^{4+}/Ti	−0.88	5600	56.99

1.2 Printing of conductive inks

A recurrent method to manufacture RFID's antennas is based on the photolitography of a metal film (typically aluminum) to form the antenna, a tedious process that involves several successive steps and produces a lot of acid-base waste in the etching process. Moreover, Al-based antennas have a limited performance compared to silver or copper-based ones due to their bulk conductivity being $\sim$ 50% lower (see Table 1.1). Other traditional manufacture methods, such as vacuum deposition or electroless plating can

deposit a high-resolution layer though they require a time-consuming stepwise process that require high-cost equipment and hazardous chemicals.[16] An alternative, quick and clean approach consists of depositing the conductive material directly in the desired shape, i.e., the printed electronics (PE) approach (see Fig. 1.2). PE comprises all the devices fabricated with different traditional printing techniques such as screen or ink-jet printing and its advantages in respect to conventional electronics fabrication are their low-cost, high-throughput and the possibility to print on flexible surfaces.[17]

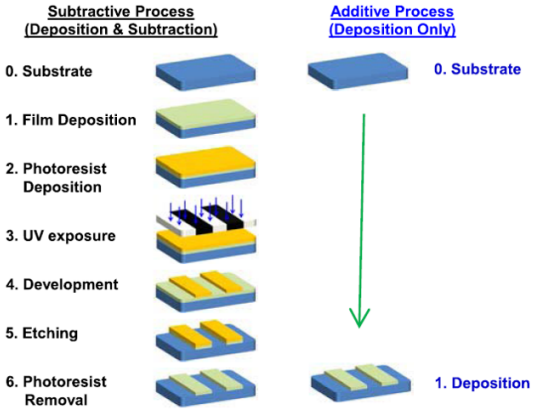

Figure 1.2: The traditional photolitography procedure compared to the PE approach for producing RFID antennas. (Reprinted from reference.[18])

To enable electric conductors to be printed, so-called conductive inks are needed that contain, for example, a conductive precursor or metallic particles, just like a regular ink contains pigment particles. At present, the most widely used material in conductive inks is silver, which has the highest conductivity of all metals while suffering little from oxidation (see Table 1.1).[19] However, one of the key trends for IoT is a progressive reduction of the device footprint and cost which can hardly be achieved with the use of high-priced raw material. At almost the same bulk conductivity value though far more abundant and economical, copper appears as an intuitive cost-effective solution to replace silver as the material required to mass-print conductive features.[13]

1.3 Copper in conductive inks

An ink is a multi-component system composed of a liquid carrier, i.e. a solvent; a filler, i.e. a pigment or nanoparticles; and additives (such as rheology and surface tension modifiers, wetting agents or binders). The function of the additives is to enable optimal printing, adhesion and performance of the whole system. Inks can be separated in graphic and conductive inks depending on the type of filler used. Graphic inks are made from pigments capable of providing color whereas conductive inks are made of conductive materials such as copper to provide the desired electrical characteristic of conductivity.[20] Copper, like most metals, is encountered in a solid state at room temperature. Therefore, in order to incorporate it into a printable ink formulation as the conductive filler, it must be dispersed as nanoparticles or dissolved as an organometallic compound.[16]

Copper-based organometallic or metal-organic inks are composed of compounds consisting in copper in the cuprous (+1) or cupric (+2) oxidation state coordinated to different organic ligands. The stability of such copper complexes prevents the formation of undesired copper oxide or precipitation of the metal source during ink formulation or storage, a recurrent problem encountered in nanoparticle-based inks.[21] Despite the aforementioned advantages, there have been limited studies on copper-based organometallic inks, and these inks have two shortcomings that make them hard to apply commercially. First, most of them require a reducing atmosphere to reduce the copper complex from the monovalent or divalent state into the metallic state (e.g., hydrogen gas or formic acid gas), which should be avoided for the industrial production of printed electronics because of safety and cost concerns. Second, these inks have an inherent limited copper-loading and performance. Each copper atom is required to coordinate with at least a ligand, which establishes an upper limit in the weight of copper that can be incorporated per volume of ink. Also, the presence of the ligands restricts the density of the printed layer due to the volume of organic molecules, negatively affecting the continuity of the film and hence the conductivity.[16;22]

A nanoparticle could be defined as a conglomerate of atoms in the diameter range of 1-100 nm.[23;24] Nanoparticles can be also referred as nanocrystals if they are composed of atoms in a crystalline arrangement.[25] Dispersion of nanoparticles in the ink vehicle is enabled by ligands attached to the surface of the colloids granting stability in the media - typically by steric hindrance - avoiding agglomeration and preventing precipitation. Nanoparticle-based copper inks are gaining a greater deal of attention due to their properties and they are particularly more suited as fillers for conductive inks than

organometallic complexes due to two main features:

1. A precursor already in the metallic state. The convenience of depositing copper atoms in the metallic state results in saving energy because treatment in reducing atmosphere is not required.

2. A larger copper atoms/organic ligands ratio compared to organometallic inks. Nanoparticles are composed of thousands of atoms whereas only the surface is covered by organic molecules, thus less non-conductive species are present in the ink and higher solid-loadings can be achieved.

On the negative side, copper is intrinsically prone to oxidation, which if not dealt with, results in considerable loss of conductivity. A simple extrapolation of typical oxidation rates of bulk copper, even if they amount to a mere one micrometer *per annum*,[26] indicates that nanometer-sized Cu crystallites can be expected to oxidize completely within a few hours or days.[27] This issue demands a strategy to prevent or reverse the oxide formation in order to obtain conductive and functional devices. A strategy to protect or reverse particles oxidation (i), a suitable sintering method to form interconnected particles (ii) and a cost-efficient approach to synthesize copper nanocrystals (iii) constitute the essence of this thesis and will be addressed in the upcoming pages. In the next chapter, we will present a comprehensive literature study in the field of synthesis of copper nanoparticles as well as strategies to prevent or counter the oxidation tendency.

1.4 Thesis outline

This thesis discusses the development of a copper nanocrystals-based conductive ink. The manuscript covers the synthesis of copper nanocrystals, a detailed characterization of the surface chemistry of the colloids, the analysis of the sintering properties of the particles depending on different properties and an optimization of an ink in order to obtain an economical and efficient conductive ink suitable for printed electronics.

In the second chapter, a literature overview of the synthesis of Cu nanoparticles is given. Different synthesis methods to materialize in a pristine unoxidized material that can yield to a conductive pattern are reviewed. Strategies to protect the colloids by a shell against corrosion are investigated and compared.

In the third chapter, we propose a synthesis of metallic copper nanocrystals based on copper formate, which does not need an additional reducing agent

nor a protective atmosphere to yield metallic copper. By saturating the initial solution with copper formate and implementing a specific temperature profile, we demonstrate a self-cleaning effect. Oxygen cannot access the nanocrystals during the reaction with non-oxidized nanocrystals as result. A clear influence of the reaction rate was established and the mechanism of oxygen exclusion is discussed. Furthermore, the size of the NCs can be tuned by adjusting precursor and ligand concentrations.

In the fourth chapter, we perform an in-depth study of the surface chemistry of the Cu NCs, focusing on the synthesis of 4 nm Cu colloids as a study model due to their high surface/volume ratio. We demonstrate that oleylamine is initially capping the surface as a tightly bound ligand. We illustrate that addition of undecylenic acid triggers an exchange reaction on the surface of the colloids. We propose and discuss different models to describe this exchange reaction.

In the fifth chapter, we analyze the sintering behavior of the Cu NCs depending on different particle properties. In the first part we study the transformation into films of 4 nm particles capped with different ligands upon thermal sintering with different gases. We analyze the grain size and reduction temperature of the resulting layer depending on the capping ligand. In the second part we evaluate different particle sizes and the effect that the sintering temperature has on the conductivity of the patterns.

In the sixth chapter, we introduce an upscaled synthesis with potential to be taken in industrial facilities. We use a design of experiments to optimize an ink formulation in terms of adhesion and resistivity. We formulate an ink paste for screen printing, producing conductive RFID antennas.

1.5 Scientific output

1.5.1 Publications in international journals

This work is based on the following publications:

1. **Arnau Oliva Puigdomènech**, Jonathan De Roo, Jakob Kuhs, Christophe Detavernier, Jose C. Martins, Zeger Hens. *Ligand Binding to Copper Nanocrystals: Amines and Carboxylic Acids and the Role of Surface Oxides.* Chemistry of Materials, 31 (6), 2058–2067, **2019**.

2. **Arnau Oliva Puigdomènech**, Jonathan De Roo, Hannes Van Avermaet, Klaartje De Buysser, Zeger Hens. *Oxidation Prevention of Copper Nanocrystals Synthesized in Ambient Atmosphere.* Submitted December 2019.

1.5.2 Patents

1. **Arnau Oliva Puigdomènech**, Zeger Hens. *A method to form copper nanoparticles.* Priority filled November 2019 (EP19210653.2.)

1.5.3 Conference contributions

1. **Arnau Oliva Puigdomènech**, Jonathan De Roo, Jose C. Martins, Zeger Hens. *Self-reducing Copper Nanocrystals -How Surface Chemistry affects Sintering*, 2017 E-MRS Spring Meeting, Strasbourg (France), May 22-26 (Presentation).

2. **Arnau Oliva Puigdomènech**, Jonathan De Roo, Jose C. Martins, Zeger Hens. *Self-reducing Copper Nanocrystals -How Surface Chemistry affects Sintering*, 2017 E-MRS Spring Meeting, Strasbourg (France), May 22-26 (Poster).

3. **Arnau Oliva Puigdomènech**, Filip Geenen, Christophe Detavernier, Zeger Hens. *From the synthesis of Cu Nanocrystals to the formation of conductive layers*, 2018 SIM User Meeting, Gent (Belgium), May 16 (Poster Award).

4. **Arnau Oliva Puigdomènech**, Jonathan De Roo, Filip Geenen, Christophe Detavernier, Jose C. Martins, Zeger Hens. *In-situ analysis of conductive films formation by adaptable Cu nanocrystals*, 2018 MRS Fall Meeting, Boston (MA,USA), November 25-30 (Poster).

References

[1] Kevin Ashton. *That 'Internet of Things' Thing.* RFiD J., 2009.

[2] Jayavardhana Gubbi, Rajkumar Buyya, Slaven Marusic, and Marimuthu Palaniswami. *Internet of Things (IoT): A vision, architectural elements, and future directions.* Futur. Gener. Comput. Syst., 29(7):1645–1660, 2013.

[3] Sean Dieter Tebje Kelly, Nagender Kumar Suryadevara, and Subhas Chandra Mukhopadhyay. *Towards the implementation of IoT for environmental condition monitoring in homes.* IEEE Sens. J., 13(10):3846–3853, 2013.

[4] Muftah Fraifer and Mikael Fernstrom. *Smart car parking system prototype utilizing CCTV nodes: A proof of concept prototype of a novel approach towards IoT-concept based smart parking.* 2016 IEEE 3rd World Forum Internet Things, WF-IoT 2016, pages 649–654, 2017.

[5] Zeydin Pala and Nihat Inanç. *Smart parking applications using RFID technology.* 2007 1st Annu. RFID Eurasia, 2007.

[6] Sergey Andreev, Olga Galinina, Alexander Pyattaev, Mikhail Gerasimenko, Tuomas Tirronen, Johan Torsner, Joachim Sachs, Mischa Dohler, and Yevgeni Koucheryavy. *Understanding the IoT connectivity landscape: A contemporary M2M radio technology roadmap.* IEEE Commun. Mag., 53(9):32–40, 2015.

[7] Ovidiu Vermesan, Mark Harrison, Harald Vogt, Kostas Kalaboukas, Maurizio Tomasella, Karel Wouters, Sergio Gusmeroli, and Stephan Haller. *Cluster of European Research Projects on the Internet of Things: Vision and Challenges for Realising the Internet of Things.* CERP-IoT, 2010.

[8] Vipul Chawla and Dong Sam Ha. *An Overview of Passive RFID.* IEEE Commun. Mag., 45(9):11–17, 2007.

[9] Xiaolin Jia, Quanyuan Feng, Taihua Fan, and Quanshui Lei. *RFID technology and its applications in Internet of Things (IoT).* 2012 2nd Int. Conf. Consum. Electron. Commun. Networks, CECNet 2012 - Proc., pages 1282–1285, 2012.

[10] Nadine Cranenburgh. *Engineers teach RFID tags new tricks to lower the cost of smart technologies*, 2019.

[11] Raghu Das. *RFID 2018-2028: RAIN and NFC Market Status, Outlook and Innovations.* Technical report, IDTechEx, 2018.

[12] Roy Want. *An introduction to RFID Technology.* Ind. Commer. Train., 10(1):11–18, 2008.

[13] Shlomo Magdassi, Michael Grouchko, and Alexander Kamyshny. *Copper Nanoparticles for Printed Electronics: Routes Towards Achieving Oxidation Stability.* Mater. (Basel)., 3(9):4626–4638, 2010.

[14] Vivek Subramanian, Paul C. Chang, Josephine B. Lee, Steven E. Molesa, and Steven K. Volkman. *Printed organic transistors for ultra-low-cost RFID applications.* IEEE Trans. Components Packag. Technol., 28(4):742–747, 2005.

[15] Raymond A. Serway and John W. Jewett Jr. *Physics for Scientists - with Modern Physics.* Mary Finch, 8th edition, 2010.

[16] Alexander Kamyshny and Shlomo Magdassi. *Conductive nanomaterials for printed electronics.* Small, 10(17):3515–3535, 2014.

[17] Wei Wu. *Inorganic nanomaterials for printed electronics: A review.* Nanoscale, 9(22):7342–7372, 2017.

[18] Tong Ge, Jia Zhou, Yang Kang, and Joseph S. Chang. *Review: A fully-additive printed electronics process with very-low process variations (Bent and unbent substrates) and PDK.* Proc. - IEEE Int. Symp. Circuits Syst., 2017.

[19] Alessandro Chiolerio, Krishna Rajan, Ignazio Roppolo, Annalisa Chiappone, Sergio Bocchini, and Denis Perrone. *Silver nanoparticle ink technology: state of the art.* Nanotechnol. Sci. Appl., page 1, 2016.

[20] Gerard Cummins and Marc P.Y. Desmulliez. *Inkjet printing of conductive materials: A review.* Circuit World, 38(4):193–213, 2012.

[21] Pascal Lignier, Ronan Bellabarba, and Robert P Tooze. *Scalable strategies for the synthesis of well-defined copper metal and oxide nanocrystals.* Chem. Soc. Rev., 41(5):1708, 2012.

[22] James E. Huheey, Ellen A. Keiter, and Richard L. Keiter. *Química inorgánica. Principios de estructura y reactividad.* Oxford, 4th edition, 2007.

[23] Mihail C Roco. *Nanotechnology: convergence with modern biology and medicine.* Curr. Opin. Biotechnol., 14(3):337–46, 2003.

[24] Marzie Hejazy, Mohammad Kazem Koohi, Adele Bassiri Mohamad Pour, and Davood Najafi. *Toxicity of manufactured copper nanoparticles - A review.* Nanomedicine Res. J., 3(1):1–9, 2018.

[25] C. Amiens, D. Ciuculescu-Pradines, and K. Philippot. *Controlled metal nanostructures: Fertile ground for coordination chemists.* Coord. Chem. Rev., 308(July 2015):409–432, 2016.

[26] D W Rice. *Atmospheric Corrosion of Copper and Silver.* J. Electrochem. Soc., 128(2):275, 1981.

[27] Jérémy Cure, Arnaud Glaria, Vincent Collière, Pier Francesco Fazzini, Adnen Mlayah, Bruno Chaudret, and Pierre Fau. *Remarkable Decrease in the Oxidation Rate of Cu Nanocrystals Controlled by Alkylamine Ligands.* J. Phys. Chem. C, 121(9):5253–5260, 2017.

2

Copper Nanoparticles Synthesis: State-of-the-art

Copper nanoparticles (Cu NPs) have generated a great deal of interest due to their versatility and properties. The advantage of Cu-based systems is their lower cost compared to alternative noble metals. Here, we give a literature overview of the synthesis of Cu nanoparticles. Different synthesis methods are reviewed, with a focus on unoxidized particles that are suitable for conductive patterns. We also investigate and compare strategies to protect or shell the colloids against oxidation.

2.1 Introduction

In the last 20 years, reports dealing with the synthesis and characterization of copper-based nanoparticles were prevalent in the scientific literature. This growing attention is ascribed to their size-dependent unique magnetic, electrical, chemical, physical and optical properties.[1–5] For instance, Cu NPs-based catalysts can be used in the reduction of nitrates from drinking water.[6] Here, high surface-to-volume ratios are of utmost importance for the selection of a metal catalyst. By using Cu NPs, the cost of the cata-

lysts, which commonly consist of rare noble metals such as Pd or Pt, can be greatly reduced.[7] Other potential applications of the Cu NPs are based on its unique localized surface plasmon resonance (SPR).[8] For example, the SPR oscillations can enhance the local electromagnetic field, enabling the use of surface-enhanced spectroscopy for single-molecule detection.[9] In the field of electronics Cu NPs are also gaining a great deal of attention.[10] As seen in table 1.1 of this thesis introduction, the electrical conductivity of Cu is almost on a par with the most conductive metal, Ag, whilst being $\sim 1\%$ of its cost, advocating its case as the material of choice for cost-efficient conductive applications. Even in terms of thermal conductivity, the presence of Cu NPs in fluids was proven to enhance thermal conductivity.[11]

For all that, Cu NPs have been proven valuable in a wide variety of applications such as antimicrobial agent,[12] sensing,[13;14] heat transfer,[11] light emission,[15;16] surface-enhanced Raman scattering,[17;18] catalysis,[19] and electronics.[20;21] In this chapter, different routes to achieve copper nanoparticles will be listed and compared. The assessment of the known methods will serve as preamble to the synthesis method developed in the context of this PhD which will be described in chapter 3. With a focus on preserving the electrical properties of the NPs, we will also provide an overview of different strategies to prevent or protect the metallic Cu from oxidation.

In this chapter we divided the synthesis methods for Cu NPs in three categories depending on the nature of the process: chemical, physical and biological.

2.2 Chemical methods

Chemical synthesis methods of colloids is a bottom-up process, meaning that the particles are grown from its elemental metallic atoms. This process is divided in three stages by the LaMer model (see figure 2.1). First, the precursor is either reduced or decomposed to its metallic state, increasing the concentration of the monomers that will constitute the particles. Once the concentration reaches the supersaturation point, seeds are formed by clustering of the monomers into nuclei. Finally, the seeds grow rapidly, thereby causing the concentration of metal ions in solution to drop. The size and morphology of the colloids are affected by the binding of the stabilizer during the growth stage.[22;23]

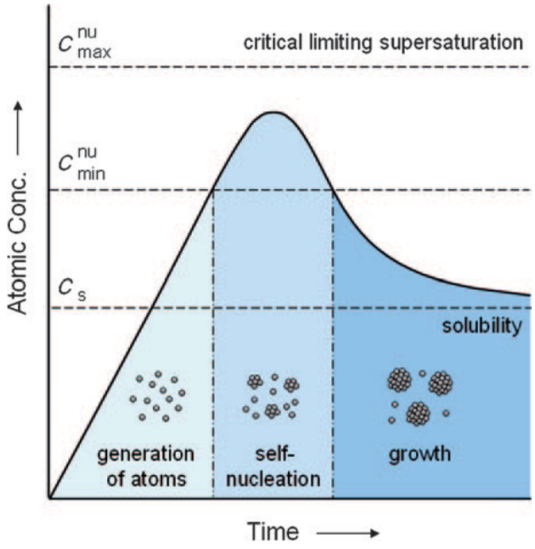

Figure 2.1: Schematic representation of the LaMer model in a plot of atomic concentration against time, illustrating the generation of monomer, nucleation, and subsequent growth of colloidal nanoparticles. C_{min}^{nu} indicates the saturation point for atoms in solution, when nucleation events start to occur. C_s indicates the equilibrium state reached between the atoms in the nanoparticles and the atoms in solution. Reprinted from reference[22]

2.2.1 Chemical reduction

Back in 1857, Michael Faraday published the first synthesis of metal colloids when he reported the formation of gold colloids and observed different optical properties from the bulk material. In his work, he formed Au colloids by the wet chemical reduction of chloroauric acid in the presence of phosphor.[24] Currently, the chemical reduction of metal salts has become the most used technique to synthesize a large variety of metal nanoparticles, including copper. Here, the driving force for the copper salt reduction is the difference in the redox potentials of the reagents which correlate with the Gibbs' free energy of the reaction.[3] Compared to Au and Ag, Cu has a relatively low redox potential (see table 1.1) offering a challenge to the production of Cu NPs by this method.

Typically, strong reducing agents such as hydrazine[8;17;25;26] or sodium borohydrate[27;28] are used to reduce the copper to its metallic state. Despite the

hazards, these methods benefit of good control of the particle growth and morphology upon reducing agent injection and can be carried out at low or even room temperature. Similarly, Lee *et al.* patented a method to manufacture Cu NPs from different copper salts in the presence of a fatty acid and a reducing agent.[29] Some researchers proved that unoxidized Cu NPs could also be formed by employing a milder reducing agent, sodium hypophosphite.[30;31] All these aforementioned methods are usually coupled with the addition of poly(vinylpyrrolidone)(PVP) or poly(allylamine)(PA) to control the growth and stabilize the NPs by steric hindrance. Alternatively, more environmentally-friendly synthesis procedures used ascorbic acid as reducing agent.[2;32;33] Besides having the role of reducing agent, ascorbic acid also binds to the Cu surfaces, removing the need of adding an extra stabilizer. Polyol methods are also included in the chemical reduction subcategory; here, the glycol-based solvent serves as solvent, capping agent and sometimes, reducing agent.[34] Overall, methods based on chemical reduction are simple and straight-forward to carry out in a laboratory-scale and at the same time they allow adaptation of particle size and morphology.[35] Note that some of the techniques mentioned in this section are based on a chemical reduction even if included in another category.

2.2.2 Electrochemical

In an electrochemical synthesis, a current is passed between the electrodes in an electrolyte solution of a copper salt. The voltage difference triggers reduction of copper onto the surface of the cathode.[36] This method has a lower cost and environmental impact than most, owing to the fact that is a flow process that occurs at room temperature. However, size control and re-dispersion of the NPs becomes more difficult due to lack of surfactant.[37] For example, Zhang and co-workers studied how the electrode potential and temperature affect nucleation and growth of the Cu NPs, demonstrating that size of the colloids can be tuned from 36 to 130 nm by adapting those parameters .[38]

2.2.3 Microemulsion

A microemulsion is a synthesis route for nanoparticles that consists of forming a thermodynamically stable solution of two immiscible fluids such as water-in-oil or viceversa. To achieve miscibility, a surfactant is added to bridge the interfacial surface tension between the two fluids. For instance, in Ahmed *et al.*[39] copper nitrate is dissolved in aqueous media and mixed

with the octane oil phase containing the surfactants, cetyltrimethyl ammonium bromide and 1-butanol. Upon addition of the reducing agent, micelles of Cu are formed between 7-30 nm. In another work, Solanki and co-workers studied in detail the ratio water-to-surfactant required to form different sizes of Cu NPs by a similar method.[40] Salzemann *et al*[41] presented an in-depth study on the anisotropic growth and morphology of the particles obtained via a reverse micelles method, observing cubes, flat triangles, pentagons and elongated forms.

2.2.4 Microwave

In a microwave synthesis, microwave radiation is used to trigger the reaction to form Cu NPs (i.e. reduction, thermal decomposition). By using microwaves as heating method, large volumes can be heated rapidly and uniformly resulting in shorter reaction times and improved size-control. In Yamauchi *et al.* Cu, Ni and Cu-Ni NPs are formed by irradiating a solution of metal formate/oleylamine complexes at 1.25 kW, yielding monodisperse metallic particles and alloys between 13 and 22 nm.[1] Polyol methods are widely used in microwave synthesis. Zhao and co-workers presented that different morphologies of Cu NPs could be obtained by this method.[42] Similarly, Blosi *et al.* used polyol chemistry to synthesize Cu NPs under microwave radiation.[43] In this work, different range of Cu colloid diameters (90-260 nm) were obtained by studying in detail the different parameters that have an effect on the size. Different range of particles sizes were achieved by Kawasaki *et al.*.[44] In their work, an ethylene glycol solution of copper chloride was reduced with sodium hydroxide to produce 2 nm Cu NPs *via* a microwave-assisted polyol method.

2.2.5 Photochemical

Formation of Cu NPs can be triggered by light absorption of a photoreactive copper precursor. For example, bis(2,4-pentanedionate)copper(II) undergoes photoreduction upon light irradiation at 254 nm. This phenomenon, coupled with the addition of a stabilizer such as PVP can be used to obtain colloidally stable Cu NPs without the use of a reducing agent or high temperatures.[45] Similarly, a solution of copper sulphate with PVP can be photoreduced in the presence of benzophenone by irradiation at 253.7 nm, producing polydisperse Cu NPs.[46]

2.2.6 Solvothermal

In a solvothermal (hydrothermal for aqueous systems) synthesis of Cu NPs the process takes place in a sealed reactor or autoclave. Here, the reaction mixture is brought to a temperature above the boiling point of the solvent, increasing the pressure of the system and facilitating solvent-precursor interaction. For example, Chen *et al.*[47] prepared a solution of copper chloride, hydrazine and dodecyl benzenesulfonate in water and transferred the reaction mixture to an autoclave, where the temperature was raised to 100°C. By adapting the synthesis parameters, particles with a variety of shapes and diameters from 40 to 300 nm were obtained. Another report by Shi and co-workers described the hydrothermal synthesis of Cu nanowires with an aspect ratio of 10^5 by using octadecylamine as surfactant.[48]

2.2.7 Sonochemical

Sonochemical synthesis of colloids is based on the radiation of ultrasonic waves into the reaction solution (see figure 2.2). These waves generate bubbles in solution, a phenomenon known as cavitation. The collapse of these cavities results in an increase of the local energy of the sonicated liquid, enhancing the chemical reactivity of the solution.[49] By this principle, Dhas *et al*,[50] formed a copper hydrazine carboxylate and exposed it to ultrasound radiation, forming 50-70 nm Cu metallic particles with catalytic activity. In another report, amorphous Cu NPs were formed and embedded in a polyaniline matrix.[51]

Combining both sonochemistry and electrochemistry, increased mass transport and reaction rates can be achieved. Several sonoelectrochemistry synthesis methods for Cu NPs are reported. For example, Haas and co-workers synthesized copper nanoparticles from an aqueous solution of copper sulfate using PVP as ligand.[52] Monodisperse Cu NPs with a diameter range between 25 and 60 nm were obtained by applying a current density between 55 and 100 mA cm^{-2}.

2.2.8 Thermal Decomposition

Thermal decomposition synthesis of Cu NPs are based on the decomposition upon heating of a copper precursor in the presence of ligands. Thus, this method differs from chemical reduction in the choice of a precursor that can decompose in reducing entities. This results in a cleaner and simpler process since no extra reducing agents are required to be added separately.[53]

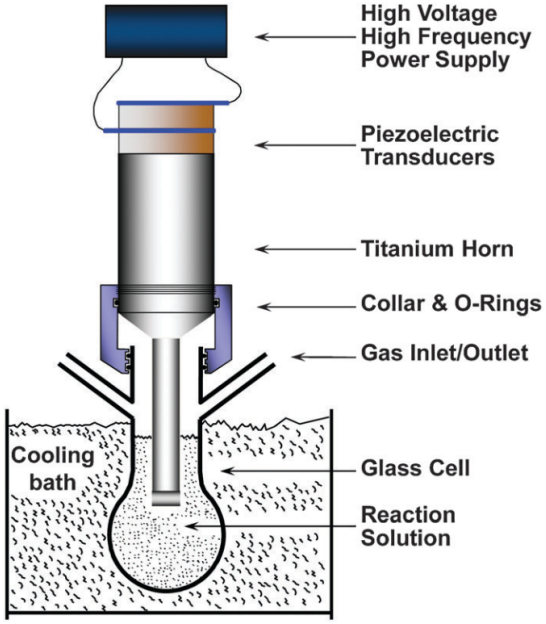

Figure 2.2: Schematic representation of a typical laboratory rig for sonochemical reactions using a high intensity ultrasonic horn. Reprinted from reference[49]

It has also been reported that some surfactants such as oleylamine, PVP or ascorbic acid play a double role and aid in the reduction process.[2;54;55].

For example, Sun *et al.* first reported the thermolysis of metal formates in the presence of oleylamine and oleic acid to form metal and metal oxides NPs.[56] Other precursors such [bis(2-hydroxy-1-naphthaldehydato)copper(II)], [bis(salicylaldiminato)copper(II)] or copper oxalate were succesfully employed by Salavati-Niasari and co-workers to synthesize Cu NPs of different diameters.[53;57;58]. Similarly, copper(II) 2-ethylhexanoate was employed by Kim *et al.* to form 70-80 nm Cu NPs further shelled with copper formate to stall oxidation.[59] Alternatively, other researchers first synthesized copper oleate, which can be thermally decomposed into Cu NPs without adding extra stabilizers.[60;61] Overall, long alkylamines or carboxylic acids play a large role in the aforementioned syntheses, where its complexation with the copper precursors both lowers the decomposition temperatures of the precursors and stabilizes the resulting Cu NPs in apolar solutions.

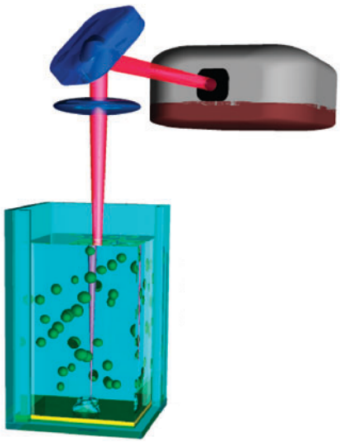

Figure 2.3: Schematic representation of a laboratory experimental set-up for a laser ablation system in solvent. Reprinted from reference[64]

2.3 Physical methods

Physical methods of nanoparticle synthesis are typically based on a top-down approach. Here, the material (i.e. metallic bulk copper) is reduced to smaller entities to produce nanoparticles by structured decomposition with different techniques. However, NPs formed by some physical methods such as wire discharge or laser ablation follow a growth profile similar to the chemical methods yet in different media. Even if energetically efficient, physical methods are considered in general less suitable for mass production than the chemical ones due to the high cost of the equipment and expensiveness of the process.[62]

2.3.1 Laser ablation

To produce nanoparticles by laser ablation, a high-power beam is focused in a vacuum chamber, towards a metal plate of the desired material. At high laser flux, plasma is formed at the surface of the material. By performing this process in solution, the plasma condenses in the liquid, forming nanoparticles (see Figure 2.3).[63;64]

This method has been used by some researchers to synthesize Cu NPs. For example, colloidal Cu NPs were synthesized by pulsed Nd:YAG laser ablation.[65] In this report, colloids of 30 nm were synthesized in water and 3 nm in acetone, only the later being stable for months. Colloidal stability in

water was achieved by Muniz-Miranda *et al.* by incorporating ligands such 1,10-phenanthroline or 4,4'-bipyridine to stabilize the NPs.[66] However, Cu NPs dispersed in water media oxidize quickly. To avoid it, Saito and co-workers successfully synthesized colloidally stable Cu NPs in polysiloxane oil, obtaining a wide size dispersion between 2 and 20 nm.[67]

2.3.2 Mechanical milling

Milling has been historically used to form uniform dispersions of powders.[68] Currently, micron and nano-powders can be obtained by milling and are commercialized and used in a wide variety of applications. The process consists of grinding the powdered material in a rotary milling bowl in the presence of ceramic or steel balls lined with an abrasion-resistant material such as manganese steel or rubber. This method is suitable for industrialization, allowing mass-production, however, size control is problematic and generation of sub-100nm particles is laborious and costly. Besides straight synthesis of the material, high-energy ball milling is a way of modifying the conditions in which chemical reactions usually take place either by inducing reactions during milling or changing the reactivity of as-milled solids.[69] This has been used by some researchers to form nanocrystalline Cu metal alloys, achieving adaptability in mechanical properties of the solids such hardness.[70;71]

2.3.3 Pulsed wire discharge

In a pulsed wire discharge synthesis method (or electric explosion of a wire), a wire of the metal of choice is placed in a chamber filled with ambient gas. Then, a discharge current is passed through the wire, initially flowing through it. At a given time, hot points are created and develop quickly along the wire. Within 100 ns after the first hot points appeared, the entire wire is evaporated and becomes a plasma. The expansion of the plasma results in a large volume of hot metal vapor that further condenses into nanoparticles.[72] This method for the synthesis of NPs was first reported by Jiang and Yatsui, who successfully synthesized metallic Cu NPs of 62 nm among other materials.[72] Later, Suematstu and co-workers developed a pulsed wire discharge apparatus for the mass production of Cu NPs, producing up to 2 g in 90 s.[73] Lee and fellow researchers investigated the effect of the ambient air pressure on the size of the produced Cu NPs, demonstrating that size tuning from 23 to 31 nm was possible when pressure was changed from 50 mbar to 1 bar.[74] To protect the particles from oxidation, Murai and co-workers carried out the process in the presence of oleic acid

vapor. By doing that, 25 nm Cu NPs coated with an organic shell of a few nanometers were obtained and the oxidation successfully stalled after for at least 2 months.[75] In another report by Kawamura *et al.*, the chamber was filled with deionized water and ascorbic acid before placing the copper wire between the electrodes. When the discharge was triggered, Cu NPs were formed in solution facilitating collection and processing into a conductive ink. Moreover, they demonstrated that increasing presence of ascorbic acid as a mild reducing agent decrease the oxidation of the Cu NPs.[76] Overall, pulsed wire discharge has been proved to be an energy efficient method that allows for a high production rate of pure Cu NPs. On the negative side, particles monodisperse in size are difficult to produce by this method.[62;76]

2.3.4 Alternative methods

The amount of reports in literature dealing with the synthesis of Cu nanomaterial is uncountable. In this subsection we will introduce the work of some researchers that successfully synthesized Cu NPs by an innovative physical method not exemplary enough to include it in a new category yet worth mentioning.

Li *et al.* reported the production of Cu NPs by a flow-levitation method (see Figure 2.4).[77] First, the solid metal is heated by a high-frequency electromagnetic induction coil forming a metal liquid droplet. The droplet is levitated and heated continuously under its interaction with the magnetic field generated by another reverse electromagnetic induction coil. The continuous heating start to evaporate atoms at the surface of the droplet. These evaporated atoms are quickly cooled through their collision with the inert gas and form nanoparticles. The inert gas gradient pressure guides the formed nanoparticles towards the collector in a definite direction preventing adherence to the reactor wall. This results in the formation of high yield and purity nanoparticles.

Nasibulin and co-workers designed and built a vertical laminar flow reactor for the investigation of Cu acetylacetonate$_2$ thermal decomposition under controlled conditions to form Cu NPs.[78] In their work, they claim that precursor decomposition is followed by dimerization of the copper atoms at high temperatures prior to nucleation. They developed a semi-empirical model to account for the elemental copper dimer reaction with carbon dioxide caused the formation of Cu_2O NPs. Alternatively, low partial pressure of carbon dioxide resulted in the formation of metallic Cu NPs from 4 to 27 nm depending on the experimental conditions.

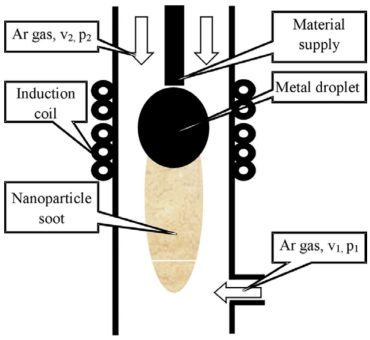

Figure 2.4: Schematic representation of the flow-levitation synthesis method for Cu nanoparticles. Reprinted from reference [77]

Similar to the laser ablation synthesis method, an electron beam can be utilized to evaporate a copper plate into NPs. This has been reported by Zavjalov *et al.* who used the beam of an industrial linear accelerator of electrons with a power up to 5 MW/cm^2 to irradiate a copper ingot.[79] The evaporated copper particles are collected by an argon flux (20 L/min) at a rate of >500 g of nanopowder per hour. Characterization of the NPs however shows that a polydisperse range of sizes from 15 to 700 nm were formed and that precise control of argon flux rate is necessary to avoid oxidation.

2.4 Biological methods

Biological synthesis of Cu NPs comprehends all the synthesis methods based on the use of plants, plants extracts, enzymes or bacteria with the help of biotechnological tools. Other biological methods based on yeast or algae are known for Ag NPs synthesis and could possibly be adapted for Cu NPs.[80]Biological methods, often labeled as green, blossomed in literature due to the need of finding a more economical and environmentally-friendly alternative to the chemical methods. Biological-based synthesis resembles chemical methods by both being bottom-up methods that rely on a reduction agent and stabilizer to produce Cu^0 colloids.[81]

2.4.1 Bacteria

Bacteria-mediated synthesis of NPs are of interest due to their abundance in the environment, fast-growing times and low cost. Compared to well-known Ag NPs, bacterial synthesis of Cu NPs is still an unexplored field

with just a few reports present in literature. A pioneer article by Saif Hasan and co-workers reported that the incubation of $CuSO_4$ with *Serratia sp.*, a gram-negative bacterium, resulted in an intracellular synthesis of Cu and Cu_2O NPs.[82] More recently, an innovative approach to synthesize Cu NPs from bacteria was reported by Varshney *et al.*.[83] A non-patogenic bacteria strain, *Pseudomonas stutzeri*, was isolated from soil and incubated with the effluent waste-water around the sewage outfall of an electroplating industry. The researchers characterized the product with XRD, SEM, UV-Vis and EDX, confirming that it produced 50-150 nm sized cubical Cu NPs.

2.4.2 Fungi

Compared to bacteria, the use of fungi for the synthesis of NPs offers *a priori* some advantages: ease of scaling up and a downstream processing, an economical process and an increased surface area due to the presence of mycelia. Also, fungi secrete significantly higher amounts of proteins than bacteria, amplifying in that manner the NP productivity.[84;85] For example, Pavani *et al.* synthesized $\sim$ 600 nm Cu NPs by growing the fungus strain *Aspergillus* in an aqueous $CuSO_4$ solution for 96 hrs at pH-5 in an incubator.[86] Likewise, Honary and co-workers synthesized Cu_2O NPs incubating different strains of the fungus *Penicillium* with $CuSO_4$ for 24 h, obtaining a range of particle sizes from 80 to 300 nm depending on the experiment conditions.[84]

2.4.3 Plants

Here copper nanoparticles are synthesized using plant leaf extract which acts as both reducing and capping agent. For example, Cu NPs were successfully synthesized by using novel *Capparis zeylanica* plant leaves extract as a reducing agent in aqueous $CuSO_4$ solution. The NPs were fabricated for 12 h and resulted in nanocubes in the size range 50–100 nm. Then, the Cu NPs were used in an antimicrobial study to determine their zone of inhibition against both gram positive (*Staphylococcus aureus*) and gram negative (*Escherichia coli* and *Pseudomonas aeruginosa*), showing an improved inhibition in the gram negative bacteria.[87] Similarly, Subbaiya and Selvam published that *Hibiscus rosa-sinensis* leaf extract can reduce a $CuNO_3$ solution and form Cu NPs with antimicrobial activity against *Bacillus subtilis* and *Escherichia coli.*[88] Shorter reaction times (8-10 min) were reported by Kulkarni and Kulkarni with the use of *Ocimum sanctum* leaf extracts to reduce $CuSO_4$. However, the metallic state of the NPs is doubtful and the reaction times variable along the article.[89] Overall, a large number of

plant extracts are reported to successfully reduce Cu precursors and produce metallic NPs in generally long reaction times. An extensive review on this trending topic has been published in 2017 by Rafique and co-workers, presenting a large number of plant-based synthesis methods for Cu NPs.[90]

2.5 Oxidation prevention strategies

The inherent oxidation tendency of Cu in ambient conditions is a well-known phenomenon.[91] In the case of nanoscale Cu, this process is accelerated to a great extent.[92] Yanase and Komiyama studied the oxidation kinetics of Cu NPs in different atmospheres and found that the oxidation involves a fast reaction of Cu to CuO_x, (x=0.67) with Cu_2O structure and afterwards, a slow reaction from CuO_x, (x=0.67) to CuO_x, (x=1).[93] Cure *et al.* tracked the oxidation of 7 nm Cu NPs capped with hexadecylamine by the surface plasmon resonance and determined that the oxidation process is divided in three regimes: a first - in the seconds range - corresponding to O_2 adsorption, a second - in the minutes range - where a complete Cu_2O monolayer is formed and a third - in the hours/day range - corresponding to the full oxidation of the colloid.[94] The presence of copper oxides on the surface of the NPs has two negative effects towards conductive applications: the sintering temperature is increased and the electrical conductivity is reduced.[3]

Since the scope of this thesis is to produce conductive inks, avoiding the oxidation during storage becomes crucial to ensure proper performance of the printed patterns. Here, we explore the literature in the search of approaches that are meant to achieve air stable metallic Cu NPs. The strategies to protects the colloids by a shell can be classified according to the coating material in: carbon, ligand, metal, polymer and silica.

2.5.1 Carbon-based shell

Protecting the Cu NPs with a carbon shell has been proven to prevent oxidation. For example, Li *et al.* presented a solid-state synthesis of Cu NPs from copper carbonate and glucose, which carbonizes at high temperatures.[95] They found out that carbon could simultaneously reduce and shell Cu NPs, protecting them from oxidation. In another example, Athanassiou *et al.* produced air-stable Cu NPs with a coating of carbon by a reducing flame spray synthesis.[96]

As presented in the works of Chen *et al.* or Luechinger *et al.*, graphene can also successfully passivate Cu surfaces, preventing the diffusion of O_2.[97;98]

More precisely, Luechinger and co-workers synthesized graphene-coated Cu NPs in a one-step process and utilized such particles to formulate a conductive ink. Despite, the achieved conductivity was very low (1.56 $S \cdot cm^{-1}$), graphene seems an economically attractive route to the use of Cu nanoparticles in ambient conditions.

2.5.2 Ligand adsorption on the surface

Molecules are usually present on the surface of colloids enabling dispersion in solvents and preventing aggregation. These molecules, generally known as ligands, are typically long organic molecules present at the surface at a density of about 1-5 ligands$\cdot nm^{-2}$.[99] Several reports have been published studying the effect of the ligands on the oxidation of the Cu NPs.

For example, Ziegler and co-workers showed that hexanethiol, a well known ligand for metal nanocrystals, made copper nitrate react to form Cu instead of CuO nanocrystals, an observation these authors attributed to the formation of a hexanethiol capping at the NP surface.[100] A similar conclusion followed from the work of Kanninen *et al.*[101] who studied the oxidation of Cu NPs capped by aliphatic carboxylic acids and thiols and found that the oxidation rate differed depending on the type of ligand and the length of the aliphatic chain, as the oxidation resistance improved with increasing chain length. Glaria *et al.*[102] analyzed Cu NPs synthesized in the presence of either alkyl amines or phosphonic acids, and showed that stabilization by alkylamines lead to a marked reduction of the oxidation rate. The authors followed the study with a detailed analysis of the oxidation regimes of Cu NPs capped with hexadecylamine, also demonstrating a stalled oxidation rate with increasing concentration of ligand.[94] Shi and co-workers[103], on the other hand, synthesized Cu NPs capped with mercaptocarboxylic acids and studied the reactive oxygen species generated during the oxidation process to assess the cytotoxicity related to this process. In line with the aforementioned studies, these authors found that a longer ligand length prevented the formation of oxygen radicals that lead to cell damage; an indirect indication of the suppression of Cu oxidation. In general, long ligand chains and increased surface coverage have been proven to improve the oxidation resistance of the Cu NPs. However, to the best of our knowledge, long-term protection in ambient conditions has not been demonstrated so far.

2.5.3 Metal-based shell

The formation of a metallic shell on metallic NPs has been established by different methods such as pulsed wire evaporation,[104] seeded growth,[105] electroless plating,[106;107], thermal evaporation under ultrahigh vacuum,[108] self-assembly[109] or galvanic displacement/transmetallation.[110;111] Here, the interest is to shell the Cu NPs with a metal that is both resistant to oxidation and conductive (i.e. Au or Ag). For example, Stewart *et al.* synthesized Cu/Ag, Cu/Au and Cu/Pt nanowires by a room-temperature, non-etching process with the aid of ascorbic acid, which removed the superficial oxide and protected the Cu core while reducing the other metal precursors on the surface of the Cu nanowires.[112] The importance of nanowires is normally associated with the formation of transparent conductors as an alternative to Indium Tin Oxide.

Formation of Cu/Ag core-shell NPs has been widely studied by the research group of Professor Magdassi.[113–115] They developed two-step transmetallation process based on the work of Lee *et al.* to shell the Cu NPs with Ag.[116] First, Cu NPs are formed in aqueous solution by the reduction of copper nitrate with hydrazine or sodium formaldehyde sulfoxylate dihydrate in the presence of polyacrylic acid sodium salt as stabilizer. Then, the particles were washed and redispersed in a solution of ascorbic acid and silver ammonia to form the Cu/Ag NPs. The resulting NPs were formulated, printed and sintered, resulting in layers that reached a conductivity 16% of bulk Cu.[113] In a simpler and cleaner process, Lee *et al.* produced Cu NPs by thermal decomposition of copper acetylacetonate in oleylamine at 235°C, then the solution was cooled down to 80°C and silver nitrate added and left stirring for 2 hours, resulting in monodisperse Cu/Ag of 13.5 nm.[110] Even if some oxidation species were present after some months of storage, the particles were coated and sintered at 350°C, resulting in a conductive layer with a resistivity of 12 $\mu\Omega \cdot$ cm. An improved conductivity was achieved by Kim and co-workers with Cu/Ag NPs synthesized by coupling a pulsed-wire discharge synthesis of Cu NPs with a surface transmetallation to Ag on solution. In their synthesis no organic stabilizer was utilized, reducing in that manner both the required sintering temperature to 200°C and the resulting resistivity to only 8.2 $\mu\Omega \cdot$cm. Overall, the use of an Ag shell seems a promising solution to protect the Cu core from oxidation while keeping conductive properties intact. Despite the longer processing time and higher costs of shelling Cu cores with Ag, companies like Samsung already are the assignee of patents regarding this strategy.[117]

Kim *et al.* introduced an alternative method to protect the colloids based

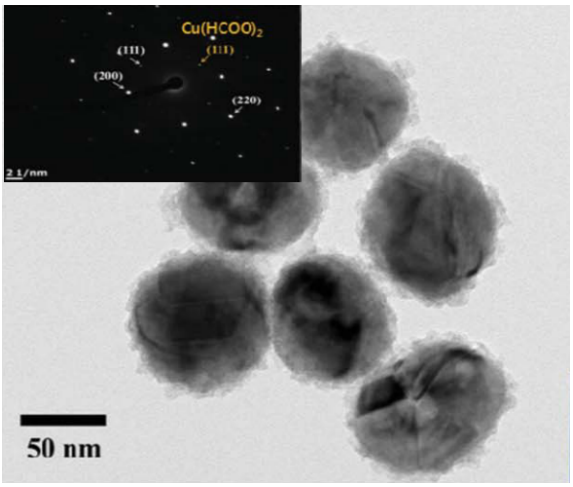

Figure 2.5: Transmission electron microscopy image showing the $Cu/Cu(HCO_2)_2$ core–shell particles. Inset: selected area electron diffraction pattern of a high resolution image showing the presence of crystalline $Cu(HCO_2)_2$. Reprinted from reference[59]

on the formation of a $Cu(HCO_2)_2$ shell around the as-synthesized NPs.[59] First, Cu NPs were synthesized by thermal decomposition of copper(II) 2-ethylhexanoate in oleylamine. Then, the capping oleylamine was exchanged by pyridine to alter the compatible solvents for the NPs, enabling dispersion in polar solvents such as acetonitrile. By injecting formic acid to the NPs, this reacted with superficial oxides and hydroxides, forming copper formate in the surface of the NPs (see figure 2.5). The $Cu(HCO_2)_2$ shell could, besides avoiding oxidation, cleanly decompose to metallic Cu upon sintering at low temperatures (150°C). The resulting sintered layers presented a low resistivity of 13.5 $\mu\Omega \cdot$ cm.

2.5.4 Polymer embedding/surface adsorption

As seen previously, a commonly used practice in the synthesis of Cu NPs is the addition of a polymeric stabilizer. Polymer ligands have also been observed to retard the oxidation of NPs.[118] Among the polymeric stabilizers, PVP is the most widely used to control the size growth of Cu NPs during synthesis and stabilize and protect them during storage.[55] Jeong *et al.* studied the effect of the molecular weight of PVP on the oxidation of Cu NPs.[119] In their work, they demonstrated that the molecular weight of PVP determines their conformation when chemisorbed on the Cu surface.

This has a significant effect on the formation of the surface oxide layer, with higher molecular weight PVP yielding thinner oxide shells. They correlated this results with the conductivity of the layers manifesting that the thinner the initial oxide shell of the NPs is, the lower is the resistivity of the printed layer, attaining a minimum resistivity of 11 $\mu\Omega \cdot$cm after sintering at 275°C by using the highest molecular weight PVP (40,000 g/mol). In another report by Lee *et al.*, Cu NPs were synthesized through a relatively large-scale (5 L) in the presence of PVP.[30] The resulting Cu NPs presented slight oxidation after 20 days under ambient storage conditions and the printed layers reached a surprisingly low resistivity at 3.6 $\mu\Omega \cdot$cm after 60 min of sintering at 200°C in reducing atmosphere. Similarly, Kobayashi and co-workers used another polymer, polypyrrole, to stabilize and coat the Cu NPs, showing just slight presence of Cu_2O after 50 days of storage under ambient conditions.[120] Alternatively, Pham *et al.* embedded Cu NPs in a conductive composite of poly(3,4-ethylenedioxythiophene)/poly(styrenesulfonate).[121] Despite obtaining an air stable paste and successfully print it, the measured conductivity of the layers was orders of magnitude far from the bulk value.

2.5.5 Silica encapsulation

Just a few reports dealing with Cu/SiO_2 NPs are present in literature. In a prior work, Kobayashi and Sakuraba reported the growth of a silica shell around Cu NPs in aqueous media by reaction of (3-aminopropyl)trimethoxysilane with sodium silicate.[122] The shelled Cu NPs maintained their SPR and were stable after air exposure in aqueous media. Later, Shiomi *et al.* reported the synthesis of Cu NPs in ammonia with gelatin as dispersant and hydrazine as reducing agent.[123] Then rapidly, a solution of tetraethylorthosilicate in ethanol was added to the particles, forming stable Cu/SiO_2 NPs by a sol-gel method. These particles featured a ∼30 nm Cu core and a ∼40 nm SiO_2 shell. Similar to carbon coating, addition of silica can efficiently stall the oxidation. However, as an insulating material, a silica shell would hamper the conductivity of the printed films and render sintering more difficult.

2.6 Assessment

In this chapter we divided the synthesis methods for Cu NPs in three categories: chemical, physical an biological. Even if most synthesis methods allow adaptation within, a general trend depending on the nature of the process can be distinguished.

Chemical methods are the most frequently used since they offer the most control on the synthesis. In general, energy is supplied to the system to trigger the reduction of copper to its metallic state and facilitate their growth into NPs following the LaMer model. Size, morphology, oxidation state, yield and processing can easily be overseen and manipulated depending on the desired properties of the Cu NPs. Moreover, chemical methods usually require shorter reaction times, increasing the productivity. The downsides of the chemical methods are the frequent use of hazardous reducing agents and the amount of waste-product from the synthesis. There are also few articles reporting a large-scale production of Cu NPs. Substitution of the reducing agent by ascorbic acid seems to be a promising approach to reduce the environmental impact of the synthesis and at the same time protect the Cu NPs from oxidation. Alternatively, shifting to methods based on thermal decomposition of copper precursors are promising since no extra reducing agent is required.

Physical methods stand out as rapid and clean processes to obtain pure Cu NPs. Especially, mechanical milling and pulsed wire discharge methods offer a productivity unachievable by other means. The negative aspect of the physical methods is the lack of control on the size and morphology of the NPs and the high cost of the equipment. Therefore, Cu NPs produced by such methods typically find their spot in mass-production of nanopowders yet not for applications were precise particle properties are desired.

Biological methods are considered an alternative to chemical methods. Such methods are based on the use of more environmentally-friendly and non-toxic reagents as compared to conventional methods. In spite of that, biological synthesis of Cu NPs is still a novel field of research. Especially in microorganism-mediated synthesis, the reaction mechanisms are completely unknown and the produced NPs are of dubious condition. Plant-based synthesis are gaining emphasis and are widely reported in the last years. More controlled sizes and reproducible synthesis are accomplished *via* plant extract reduction. The main downside of the method is still the low productivity due to the long reaction times.

Different strategies to deal with the oxidation tendency of Cu NPs are described in the literature. Shelling the Cu NPs with a carbon or silica layer has been proven to fully halt the oxidation. However, due to to the low conductivity or insulating properties of such shells, the resistivity of the printed patterns is concomitantly increased. An alternative to maintain the oxidation resistance while keeping the electrical properties intact is in the usage of noble metal shell. Here, several shelling methods are already widely reported and conductivity of layers close to bulk values of Cu are

already reported. The issue with this strategy is economical. The low-cost advantage of Cu against other metals is forfeited by adding extra processing steps and using costly reagents or methods. A trade-off solution dwells in the use of ligands or polymers. Since both are frequently used during synthesis to control particle growth and stabilize the NPs in solution no extra means are required to implement them. Organic ligands are typically thiols, phosphates, amines or carboxylic acids with an aliphatic chain in the range of C_{10}-C_{20}. Careful choice of these ligands has been proven to somewhat decrease the oxidation rate yet not protect the NPs for a long time in ambient conditions. Polymer-based stabilizers, especially PVP, are established as an excellent method to stabilize and decently stall oxidation for some weeks. The downside of polymer stabilizers is their low volatility, which demands harsher sintering conditions to obtain conductive layers. Nonetheless, since the oxidation is mainly superficial, different sintering strategies such as thermal sintering under inert atmosphere have demonstrated to reverse the oxidation. Hence, highly conductive films have been printed with both ligand or polymer-capped Cu NPs, supporting a cost-effective approach to obtain conductive patterns not specifically based on oxidation protection.

References

[1] Tomohisa Yamauchi, Yasunori Tsukahara, Takao Sakata, Hirotaro Mori, Takeshi Yanagida, Tomoji Kawai, and Yuji Wada. *Magnetic Cu-Ni (core-shell) nanoparticles in a one-pot reaction under microwave irradiation.* Nanoscale, 2(4):515–523, 2010.

[2] Chia-Yang Tsai, Wei-Chen Chang, Guan-Lin Chen, Cheng-Huan Chung, Jun-Xiang Liang, Wei-Yang Ma, and Tsun-Neng Yang. *A Study of the Preparation and Properties of Antioxidative Copper Inks with High Electrical Conductivity.* Nanoscale Res. Lett., 10(1):357, 2015.

[3] Shlomo Magdassi, Michael Grouchko, and Alexander Kamyshny. *Copper Nanoparticles for Printed Electronics: Routes Towards Achieving Oxidation Stability.* Mater. (Basel)., 3(9):4626–4638, 2010.

[4] Sawsan Dagher, Yousef Haik, Ahmad I Ayesh, and Nacir Tit. *Synthesis and optical properties of colloidal CuO nanoparticles.* J. Lumin., 151:149–154, 2014.

[5] Katherine P. Rice, Edwin J. Walker, Mark P. Stoykovich, and Aaron E. Saunders. *Solvent-dependent surface plasmon response and oxidation of copper nanocrystals.* J. Phys. Chem. C, 115(5):1793–1799, 2011.

[6] N. Barrabés, J. Just, A. Dafinov, F. Medina, J. L.G. Fierro, J. E. Sueiras, P. Salagre, and Y. Cesteros. *Catalytic reduction of nitrate on Pt-Cu and Pd-Cu on active carbon using continuous reactor: The effect of copper nanoparticles.* Appl. Catal. B Environ., 62(1-2):77–85, 2006.

[7] Manoj B. Gawande, Anandarup Goswami, François Xavier Felpin, Tewodros Asefa, Xiaoxi Huang, Rafael Silva, Xiaoxin Zou, Radek Zboril, and Rajender S. Varma. *Cu and Cu-Based Nanoparticles: Synthesis and Applications in Catalysis.* Chem. Rev., 116(6):3722–3811, 2016.

[8] Isabel Pastoriza-Santos, Ana Sánchez-Iglesias, Benito Rodríguez-González, and Luis M. Liz-Marzán. *Aerobic synthesis of Cu nanoplates with intense plasmon resonances.* Small, 5(4):440–443, 2009.

[9] Encai Hao and George C. Schatz. *Electromagnetic fields around silver nanoparticles and dimers.* J. Chem. Phys., 120(1):357–366, 2004.

[10] Alexander Kamyshny and Shlomo Magdassi. *Conductive Nanomaterials for Printed Electronics.* Small, 10(17):3515–3535, 2014.

[11] S. Lee, S. U.-S. Choi, S. Li, and J. A. Eastman. *Measuring Thermal Conductivity of Fluids Containing Oxide Nanoparticles.* J. Heat Transfer, 121(2):280, 1999.

[12] Avinash P. Ingle, Nelson Duran, and Mahendra Rai. *Bioactivity, mechanism of action, and cytotoxicity of copper-based nanoparticles: A review.* Appl. Microbiol. Biotechnol., 98(3):1001–1009, 2014.

[13] Jiatao Zhang, Junfeng Liu, Qing Peng, Xun Wang, and Yadong Li. *Nearly Monodisperse Cu O and CuO Nanospheres: Preparation and Applications for Sensitive Gas Sensors.* Chem. Mater., 18(4):867–871, 2006.

[14] Qin Xu, Yu Zhao, Jin Zhong Xu, and Jun Jie Zhu. *Preparation of functionalized copper nanoparticles and fabrication of a glucose sensor.* Sensors Actuators, B Chem., 114(1):379–386, 2006.

[15] Qusai Darugar, Wei Qian, Mostafa A. El-Sayed, and Marie Paule Pileni. *Size-dependent ultrafast electronic energy relaxation and enhanced fluorescence of copper nanoparticles.* J. Phys. Chem. B, 110(1):143–149, 2006.

[16] Zhenguang Wang, Bingkun Chen, and Andrey L. Rogach. *Synthesis, Optical Properties and Applications of Light-Emitting Copper Nanoclusters.* Nanoscale Horiz., 2(3):135–146, 2017.

[17] Yanfei Wang and Tewodros Asefa. *Poly(allylamine)-stabilized colloidal copper nanoparticles: Synthesis, morphology, and their surface-enhanced raman scattering properties.* Langmuir, 26(10):7469–7474, 2010.

[18] Thekkathu Ramani, K. Leon Prasanth, and Bojja Sreedhar. *Air Stable Colloidal Copper Nanoparticles: Synthesis, Characterization and their Surface-Enhanced Raman Scattering Properties.* Phys. E Low-dimensional Syst. Nanostructures, 77:65–71, 2016.

[19] Pinhua Zhang, Yongming Sui, Chao Wang, Yingnan Wang, Guangliang Cui, Chunzhong Wang, Bingbing Liu, and Bo Zou. *A One-Step Green Route to Synthesize Copper Nanocrystals and their Applications in Catalysis and Surface Enhanced Raman Scattering.* Nanoscale, pages 5343–5350, 2014.

[20] Rui Dang, Lingling Song, Wenjun Dong, Chaorong Li, Xiaobo Zhang, Ge Wang, and Xiaobo Chen. *Synthesis and self-assembly of large-area cu nanosheets and their application as an aqueous conductive ink on flexible electronics.* ACS Appl. Mater. Interfaces, 6(1):622–629, 2014.

[21] Jin Sung Kang, Hak Sung Kim, Jongeun Ryu, H Thomas Hahn, Seonhee Jang, and Jae Woo Joung. *Inkjet Printed Electronics Using Copper Nanoparticle Ink.* J. Mater. Sci. Mater. Electron., 21(11):1213–1220, 2010.

[22] Younan Xia, Yujie Xiong, Byungkwon Lim, and Sara E. Skrabalak. *Shape-controlled synthesis of metal nanocrystals: Simple chemistry meets complex physics?* Angew. Chemie - Int. Ed., 48(1):60–103, 2009.

[23] Alessandro Chiolerio, Krishna Rajan, Ignazio Roppolo, Annalisa Chiappone, Sergio Bocchini, and Denis Perrone. *Silver nanoparticle ink technology: state of the art.* Nanotechnol. Sci. Appl., page 1, 2016.

[24] Michael Faraday. *The Bakerian Lecture: Experimental Relations of Gold (and Other Metals) to Light.* Philos. Trans. R. Soc. London, 147:145–181, 1857.

[25] Dunying Deng, Yunxia Jin, Yuanrong Cheng, Tianke Qi, and Fei Xiao. *Copper nanoparticles: Aqueous phase synthesis and conductive films fabrication at low sintering temperature.* ACS Appl. Mater. Interfaces, 5(9):3839–3846, 2013.

[26] Arijit Kumar Chatterjee, Raj Kumar Sarkar, Asoke Prasun Chattopadhyay, Pulakesh Aich, Ruchira Chakraborty, and Tarakdas Basu. *A simple robust method for synthesis of metallic copper nanoparticles of high antibacterial potency against E. coli.* Nanotechnology, 23(8), 2012.

[27] Robert Prucek, Libor Kvítek, Ale Panáek, Lenka Vanurová, Jana Soukupová, Dalibor Janík, and Radek Zboil. *Polyacrylate-assisted synthesis of stable copper nanoparticles and copper(I) oxide nanocubes with high catalytic efficiency.* J. Mater. Chem., 19(44):8463–8469, 2009.

[28] I. Lisiecki, F. Billoudet, and M. P. Pileni. *Control of the shape and the size of copper metallic particles.* J. Phys. Chem., 100(10):4160–4166, 1996.

[29] Kwi-jong Lee, Jae-woo Joung, Young-il Lee, and Byung-ho Jun. *US 2008/0138643 A1*, 2008.

[30] Youngil Lee, Jun-rak Choi, Kwi Jong Lee, Nathan E Stott, and Donghoon Kim. *Large-scale synthesis of copper nanoparticles by chemically controlled reduction for applications of inkjet-printed electronics.* Nanotechnology, 19(41):415604, 2008.

[31] Dongzhi Lai, Tao Liu, Guohua Jiang, and Wenxing Chen. *Synthesis of highly stable dispersions of copper nanoparticles using sodium hypophosphite.* J. Appl. Polym. Sci., 3(128):1443–1449, 2012.

[32] Shaeel Ahmed Al-Thabaiti, Abdullah Yousif Obaid, Zaheer Khan, Ommer Bashir, and Shokit Hussain. *Cu nanoparticles: synthesis, crystallographic characterization, and stability.* Colloid Polym. Sci., 293(9):2543–2554, 2015.

[33] Jing Xiong, Ye Wang, Qunji Xue, and Xuedong Wu. *Synthesis of highly stable dispersions of nanosized copper particles using l-ascorbic acid.* Green Chem., 13(4):900, 2011.

[34] Kyler J. Carroll, J. Ulises Reveles, Michael D. Shultz, Shiv N. Khanna, and Everett E. Carpenter. *Preparation of elemental Cu and Ni nanoparticles by the polyol method: An experimental and theoretical approach.* J. Phys. Chem. C, 115(6):2656–2664, 2011.

[35] Bahareh Khodashenas and Hamid Reza Ghorbani. *Synthesis of copper nanoparticles: An overview of the various methods.* Korean J. Chem. Eng., 31(7):1105–1109, 2014.

[36] Mohan Raja, J. Shuba, Fathilah Binti Ali, and Sung Hun Ryu. *Synthesis of copper nanoparticles by electroreduction process.* Mater. Manuf. Process., 23(8):782–785, 2008.

[37] T. Theivasanthi and M. Alagar. *Nano sized copper particles by electrolytic synthesis and characterizations.* Int. J. Phys. Sci., 6(15):3662–3671, 2011.

[38] Q. B. Zhang and Y. X. Hua. *Electrochemical synthesis of copper nanoparticles using cuprous oxide as a precursor in choline chloride-urea deep eutectic solvent: Nucleation and growth mechanism.* Phys. Chem. Chem. Phys., 16(48):27088–27095, 2014.

[39] Jahangeer Ahmed, Kandalam V. Ramanujachary, Samuel E. Lofland, Anthony Furiato, Govind Gupta, S. M. Shivaprasad, and Ashok K. Ganguli. *Bimetallic Cu-Ni nanoparticles of varying composition (CuNi3, CuNi, Cu3Ni).* Colloids Surfaces A Physicochem. Eng. Asp., 331(3):206–212, 2008.

[40] Jignasa N. Solanki, R. Sengupta, and Z. V P Murthy. *Synthesis of copper sulphide and copper nanoparticles with microemulsion method.* Solid State Sci., 12(9):1560–1566, 2010.

[41] C. Salzemann, I. Lisiecki, J. Urban, and M. P. Pileni. *Anisotropic copper nanocrystals synthesized in a supersaturated medium: Nanocrystal growth.* Langmuir, 20(26):11772–11777, 2004.

[42] Yu Zhao, Jun Jie Zhu, Jian Min Hong, Ningsheng Bian, and Hong Yuan Chen. *Microwave-induced polyol-process synthesis of copper and copper oxide nanocrystals with controllable morphology.* Eur. J. Inorg. Chem., 2004(20):4072–4080, 2004.

[43] M. Blosi, S. Albonetti, M. Dondi, C. Martelli, and G. Baldi. *Microwave-assisted polyol synthesis of Cu nanoparticles.* J. Nanoparticle Res., 13(1):127–138, 2011.

[44] Hideya Kawasaki, Yuka Kosaka, Yuki Myoujin, Takashi Narushima, Tetsu Yonezawa, and Ryuichi Arakawa. *Microwave-assisted polyol synthesis of copper nanocrystals without using additional protective agents.* Chem. Commun., 47(27):7740–7742, 2011.

[45] Salvatore Giuffrida, Lucia L. Costanzo, Giorgio Ventimiglia, and Corrado Bongiorno. *Photochemical synthesis of copper nanoparticles incorporated in poly(vinyl pyrrolidone).* J. Nanoparticle Res., 10(7):1183–1192, 2008.

[46] Sudhir Kapoor and Tulsi Mukherjee. *Photochemical formation of copper nanoparticles in poly(N-vinylpyrrolidone).* Chem. Phys. Lett., 370(1-2):83–87, 2003.

[47] Huiyu Chen, Jong-Hak Lee, Yu-Hee Kim, Dong-Wook Shin, Sang-Cheol Park, Xianhui Meng, and Ji-Beom Yoo. *Metallic Copper Nanostructures Synthesized by a Facile Hydrothermal Method.* J. Nanosci. Nanotechnol., 10(1):629–636, 2010.

[48] Yu Shi, Hong Li, Liquan Chen, and Xuejie Huang. *Obtaining ultralong copper nanowires via a hydrothermal process.* Sci. Technol. Adv. Mater., 6(7):761–765, 2005.

[49] Hangxun Xu, Brad W Zeiger, and Kenneth S Suslick. *Sonochemical synthesis of nanomaterials.* Chem. Soc. Rev., 42(7):2555–2567, 2012.

[50] N. Arul Dhas, C. Paul Raj, and A. Gedanken. *Synthesis, Characterization, and Applications of Copper Nanoparticles.* Chem. Mater., 10(1):1446–1452, 1998.

[51] R. Vijaya Kumar, Y. Mastai, Y. Diamant, and A. Gedanken. *Sonochemical synthesis of amorphous Cu and nanocrystalline Cu2O embedded in a polyaniline matrix.* J. Mater. Chem., 11(4):1209–1213, 2001.

[52] Iris Haas, Sangaraju Shanmugam, and Aharon Gedanken. *Pulsed Sonoelectrochemical Synthesis of Size-Controlled Copper Nanoparticles Stabilized by Poly (N -vinylpyrrolidone).* J.Phys Chem.B, 110(34):16947–16952, 2006.

[53] Masoud Salavati-Niasari and Fatemeh Davar. *Synthesis of copper and copper(I) oxide nanoparticles by thermal decomposition of a new precursor.* Mater. Lett., 63(3-4):441–443, 2009.

[54] Stefanos Mourdikoudis and Luis M Liz-Marzán. *Oleylamine in nanoparticle synthesis.* Chem. Mater., 25(9):1465–1476, 2013.

[55] Kallum M. Koczkur, Stefanos Mourdikoudis, Lakshminarayana Polavarapu, and Sara E. Skrabalak. *Polyvinylpyrrolidone (PVP) in nanoparticle synthesis.* Dalt. Trans., 44(41):17883–17905, 2015.

[56] Xlao Sun, Ya Wen Zhang, Rui Si, and Chun Hua Yan. *Metal (Mn, Co, and Cu) oxide nanocrystals from simple formate precursors.* Small, 1(11):1081–1086, 2005.

[57] Masoud Salavati-Niasari, Fatemeh Davar, and Noshin Mir. *Synthesis and characterization of metallic copper nanoparticles via thermal decomposition.* Polyhedron, 27(17):3514–3518, 2008.

[58] Masoud Salavati-Niasari, Noshin Mir, and Fatemeh Davar. *A novel precursor for synthesis of metallic copper nanocrystals by thermal decomposition approach.* Appl. Surf. Sci., 256(12):4003–4008, 2010.

[59] Inhyuk Kim, Youngwoo Kim, Kyoohee Woo, Eui-Hyun Ryu, Kyung-Yol Yon, Guozhong Cao, and Jooho Moon. *Synthesis of oxidation-resistant core–shell copper nanoparticles.* RSC Adv., 3(35):15169, 2013.

[60] Young Hwan Kim, Don Keun Lee, Beong Gi Jo, Ji Hean Jeong, and Young Soo Kang. *Synthesis of oleate capped Cu nanoparticles by thermal decomposition.* Colloids Surfaces A Physicochem. Eng. Asp., 284-285:364–368, 2006.

[61] R. Betancourt-Galindo, P. Y. Reyes-Rodriguez, B. A. Puente-Urbina, C. A. Avila-Orta, O. S. Rodríguez-Fernández, G. Cadenas-Pliego,

R. H. Lira-Saldivar, and L. A. García-Cerda. *Synthesis of Copper Nanoparticles by Thermal Decomposition and Their Antimicrobial Properties.* J. Nanomater., 2014:1–5, 2014.

[62] Asim Umer, Shahid Naveed, Naveed Ramzan, and Muhammad Shahid Rafique. *Selection of a Suitable Method for the Synthesis of Copper Nanoparticles.* Nano, 7(5):1230005, oct 2012.

[63] Myungjoon Kim, Saho Osone, Taesung Kim, Hidenori Higashi, and Takafumi Seto. *Synthesis of nanoparticles by laser ablation: A review.* KONA Powder Part. J., 2017(34):80–90, 2017.

[64] Vincenzo Amendola and Moreno Meneghetti. *Laser ablation synthesis in solution and size manipulation of noble metal nanoparticles.* Phys. Chem. Chem. Phys., 11(20):3805–3821, 2009.

[65] R. M. Tilaki, A. Iraji Zad, and S. M. Mahdavi. *Size, composition and optical properties of copper nanoparticles prepared by laser ablation in liquids.* Appl. Phys. A Mater. Sci. Process., 88(2):415–419, 2007.

[66] Maurizio Muniz-Miranda, Cristina Gellini, and Emilia Giorgetti. *Surface-enhanced Raman scattering from copper nanoparticles obtained by laser ablation.* J. Phys. Chem. C, 115(12):5021–5027, 2011.

[67] M. Saito, K. Yasukawa, T. Umeda, and Y. Aoi. *Copper nanoparticles fabricated by laser ablation in polysiloxane.* Opt. Mater. (Amst)., 30(7):1201–1204, 2008.

[68] C. C. Koch. *Top-down synthesis of nanostructured materials: Mechanical and thermal processing methods.* Rev. Adv. Mater. Sci., 5(2):91–99, 2003.

[69] W. Cao. *Synthesis of Nanomaterials by High Energy Ball Milling.*

[70] T. D. Shen and C. C. Koch. *Formation, solid solution hardening and softening of nanocrystalline solid solutions prepared by mechanical attrition.* Acta Mater., 44(2):753–761, 1996.

[71] E. Gaffet, M. Harmelin, and F. Faudot. *Far-from-equilibrium phase transition induced by mechanical alloying in the CuFe system.* J. Alloys Compd., 194(1):23–30, 1993.

[72] Weihua Jiang and Kiyoshi Yatsui. *Pulsed wire discharge for nanosize powder synthesis.* IEEE Trans. Plasma Sci., 26(5):1498–1501, 1998.

[73] H. Suematsu, S. Nishimura, K. Murai, Y. Hayashi, T. Suzuki, T. Nakayama, W. Jiang, A. Yamazaki, K. Seki, and K. Niihara. *Pulsed wire discharge apparatus for mass production of copper nanopowders.* Rev. Sci. Instrum., 78(5):2005–2008, 2007.

[74] Y. S. Lee, B. Bora, S. L. Yap, and C. S. Wong. *Effect of ambient air pressure on synthesis of copper and copper oxide nanoparticles by wire explosion process.* Curr. Appl. Phys., 12(1):199–203, 2012.

[75] K. Murai, Y. Watanabe, Y. Saito, T. Nakayama, H. Suematsu, W. Jiang, K. Yatsui, K.B. Shim, and K. Niihara. *Preparation of copper nanoparticles with an organic coating by a pulsed wire discharge method.* J. Ceram. Process. Res., 8(2):114–118, 2007.

[76] Go Kawamura, Samuel Alvarez, Ian E. Stewart, Matthew Catenacci, Zuofeng Chen, and Yoon Cheol Ha. *Production of Oxidation-Resistant Cu-Based Nanoparticles by Wire Explosion.* Sci. Rep., 5:1–8, 2015.

[77] C. M. Li, H. Lei, Y. J. Tang, J. S. Luo, W. Liu, and Z. M. Chen. *Production of copper nanoparticles by the flow-levitation method.* Nanotechnology, 15(12):1866–1869, 2004.

[78] Albert G. Nasibulin, P. Petri Ahonen, Olivier Richard, and Esko I. Kauppinen. *Copper and copper oxide nanoparticle formation by chemical vapor nucleation from copper (II) acetylacetonate.* J. Aerosol Sci., 31(Ii):552–553, 2003.

[79] A. P. Zavjalov, K. V. Zobov, I. K. Chakin, V. V. Syzrantsev, and S. P. Bardakhanov. *Synthesis of copper nanopowders using electron-beam evaporation at atmospheric pressure of inert gas.* Nanotechnologies Russ., 9(11-12):660–666, 2014.

[80] Ratnika Varshney, Seema Bhadauria, and Mulayam S. Gaur. *A Review: Biological Synthesis Of Silver and Copper Nanoparticles.* Nano Biomed. Eng., 4(2):99–106, 2013.

[81] Priyanka Singh, Yu Jin Kim, Dabing Zhang, and Deok Chun Yang. *Biological Synthesis of Nanoparticles from Plants and Microorganisms.* Trends Biotechnol., 34(7):588–599, 2016.

[82] Syed Saif Hasan, Sanjay Singh, Rasesh Y. Parikh, Mahesh S. Dharne, Milind S. Patole, B. L. V. Prasad, and Yogesh S. Shouche. *Bacterial Synthesis of Copper/Copper Oxide Nanoparticles.* J. Nanosci. Nanotechnol., 8(6):3191–3196, 2008.

[83] Ratnika Varshney, Seema Bhadauria, M.S. Gaur, and Renu Pasricha. *Copper Nanoparticles Synthesis from Electroplating Industry Effluent.* Nano Biomed. Eng. Nano Biomed. Eng, 3(32):115–119, 2011.

[84] Soheyla Honary, Hamed Barabadi, Eshrat Gharaei-Fathabad, and Farzaneh Naghibi. *Green synthesis of copper oxide nanoparticles using Penicillium aurantiogriseum, Penicillium citrinum and Penicillium waksmanii.* Dig. J. Nanomater. Biostructures, 7(3):999–1005, 2012.

[85] Nikolaos Pantidos. *Biological Synthesis of Metallic Nanoparticles by Bacteria, Fungi and Plants.* J. Nanomed. Nanotechnol., 05(05), 2014.

[86] Kantabathini Venkata Pavani, Nandigam Srujana, Guntur Preethi, and Tandale Swati. *Synthesis of Copper Nanoparticles by Aspergillus Species.* Lett. Appl. NanoBioScience, 2(2):110–113, 2013.

[87] K. Saranyaadevi, V. Subha, R. S. Ernest Ravindran, and S. Renganathan. *Synthesis and characterization of copper nanoparticle using capparis zeylanicaleaf extract.* Int. J. ChemTech Res., 6(10):4533–4541, 2014.

[88] R. Subbaiya and M. N. Selvam. *Green Synthesis of Copper Nanoparticles from Hibicus Rosasinensis and their antimicrobial, antioxidant activities.* Res. J. Pharm. Biol. Chem. Sci., 6(2):1183–1190, 2015.

[89] Vasudev D Kulkarni and Pramod S Kulkarni. *Green Synthesis of Copper Nanoparticles Using Ocimum Sanctum Leaf Extract.* Int. J. Chem. Stud., 1(3):1–4, 2013.

[90] Muhammad Rafique, Ahson J. Shaikh, Reena Rasheed, Muhammad Bilal Tahir, Hafiz Faiq Bakhat, Muhammad Shahid Rafique, and Faiz Rabbani. *A Review on Synthesis, Characterization and Applications of Copper Nanoparticles Using Green Method.* Nano, 12(04):1750043, 2017.

[91] D. W. Rice, P. Peterson, E.B. Rigby, P.B.P. Phipps, R.J. Cappell, and R. Tremoureux. *Atmospheric Corrosion of Copper and Silver.* J. Electrochem. Soc., 128(2):275, 1981.

[92] Xianping Xia, Changsheng Xie, Shuizhou Cai, Zhihong Yang, and Xiangliang Yang. *Corrosion characteristics of copper microparticles and copper nanoparticles in distilled water.* Corros. Sci., 48(12):3924–3932, 2006.

[93] Akihisa Yanase and Hiroshi Komiyama. *In situ observation of oxidation and reduction of small supported copper particles using optical absorption and X-ray diffraction.* Surf. Sci., 248(1-2):11–19, 1991.

[94] Jérémy Cure, Arnaud Glaria, Vincent Collière, Pier Francesco Fazzini, Adnen Mlayah, Bruno Chaudret, and Pierre Fau. *Remarkable Decrease in the Oxidation Rate of Cu Nanocrystals Controlled by Alkylamine Ligands.* J. Phys. Chem. C, 121(9):5253–5260, 2017.

[95] Jing Li and Chun Yan Liu. *Carbon-coated copper nanoparticles: Synthesis, characterization and optical properties.* New J. Chem., 33(7):1474–1477, 2009.

[96] E. K. Athanassiou, R. N. Grass, and W. J. Stark. *Large-scale production of carbon-coated copper nanoparticles for sensor applications.* Nanotechnology, 17(6):1668–1673, 2006.

[97] Norman A. Luechinger, Evagelos K. Athanassiou, and Wendelin J. Stark. *Graphene-stabilized copper nanoparticles as an air-stable substitute for silver and gold in low-cost ink-jet printable electronics.* Nanotechnology, 19(44), 2008.

[98] Shanshan Chen, Lola Brown, Mark Levendorf, Weiwei Cai, Sang-Yong Ju, Jonathan Edgeworth, Xuesong Li, Carl W. Magnuson, Aruna Velamakanni, Richard D. Piner, Junyong Kang, Jiwoong Park, and Rodney S. Ruoff. *Oxidation Resistance of Graphene-Coated Cu and Cu/Ni Alloy.* ACS Nano, 5(2):1321–1327, feb 2011.

[99] Z Hens and J C Martins. *A Solution NMR Toolbox for Characterizing the Surface Chemistry of Colloidal Nanocrystals.* Chem. Mater., 25(8):1211–1221, 2013.

[100] K. J. Ziegler, R. C. Doty, K. P. Johnston, and B. A. Korgel. *Synthesis of organic monolayer-stabilized copper nanocrystals in supercritical water.* J. Am. Chem. Soc., 123(32):7797–7803, 2001.

[101] Petri Kanninen, Christoffer Johans, Juha Merta, and Kyösti Kontturi. *Influence of ligand structure on the stability and oxidation of copper nanoparticles.* J. Colloid Interface Sci., 318(1):88–95, 2008.

[102] Arnaud Glaria, Jérémy Cure, Kilian Piettre, Yannick Coppel, Cédric Olivier Turrin, Bruno Chaudret, and Pierre Fau. *Deciphering ligands' interaction with Cu and Cu2O nanocrystal surfaces by NMR solution tools.* Chem. - A Eur. J., 21(3):1169–1178, 2015.

[103] Miao Shi, Hyun Soo Kwon, Zhenmeng Peng, Alison Elder, and Hong Yang. *Effects of Surface Chemistry on the Generation of Reactive Oxygen Species by Copper Nanoparticles.* ACS Nano, 6(3):2157–2164, 2012.

[104] Chang Kyu Kim, Gyoung Ja Lee, Min Ku Lee, and Chang Kyu Rhee. *A novel method to prepare Cu@Ag core-shell nanoparticles for printed flexible electronics.* Powder Technol., 263:1–6, 2014.

[105] Robert W. Lord, Cameron F. Holder, Julie L. Fenton, and Raymond E. Schaak. *Seeded Growth of Metal Nitrides on Noble-Metal Nanoparticles to Form Complex Nanoscale Heterostructures.* Chem. Mater., 31(12):4605–4613, 2019.

[106] Chang Hyun Song, Youngmin Kim, Byeong Kwon Ju, and Jong Woong Kim. *Preparation of core-shell microstructures using an electroless plating method.* Mater. Des., 89:1278–1282, 2016.

[107] Yoshio Kobayashi, Verónica Salgueiriño-Maceira, and Luis M. Liz-Marzán. *Deposition of Silver Nanoparticles on Silica Spheres by Pretreatment Steps in Electroless Plating.* Chem. Mater., 13(5):1630–1633, 2001.

[108] M. Cazayous, C. Langlois, T. Oikawa, C. Ricolleau, and A. Sacuto. *Cu-Ag core-shell nanoparticles: A direct correlation between micro-Raman and electron microscopy.* Phys. Rev. B - Condens. Matter Mater. Phys., 73(11):1–4, 2006.

[109] Liuye Mo, Eng Toon Saw, Yonghua Du, Armando Borgna, Ming Li Ang, Yasotha Kathiraser, Ziwei Li, Warintorn Thitsartarn, Ming Lin, and Sibudjing Kawi. *Highly dispersed supported metal catalysts prepared via in-situ self-assembled core-shell precursor route.* Int. J. Hydrogen Energy, 40(39):13388–13398, 2015.

[110] Changsoo Lee, Na Rae Kim, Jahyun Koo, Yung Jong Lee, and Hyuck Mo Lee. *Cu-Ag core-shell nanoparticles with enhanced oxidation stability for printed electronics.* Nanotechnology, 26(45):455601, 2015.

[111] Changyong Yim, Allen Sandwell, and Simon S. Park. *Hybrid Copper-Silver Conductive Tracks for Enhanced Oxidation Resistance under Flash Light Sintering.* ACS Appl. Mater. Interfaces, 8(34):22369–22373, 2016.

[112] Ian E Stewart, Shengrong Ye, Zuofeng Chen, Patrick F Flowers, and Benjamin J Wiley. *Synthesis of Cu–Ag, Cu–Au, and Cu–Pt Core–Shell Nanowires and Their Use in Transparent Conducting Films.* Chem. Mater., 27(22):7788–7794, nov 2015.

[113] Anna Pajor-Świerzy, Yousef Farraj, Alexander Kamyshny, and Shlomo Magdassi. *Air stable copper-silver core-shell submicron particles: Synthesis and conductive ink formulation.* Colloids Surfaces A Physicochem. Eng. Asp., 521:272–280, 2017.

[114] Michael Grouchko, Alexander Kamyshny, and Shlomo Magdassi. *Formation of air-stable copper–silver core–shell nanoparticles for inkjet printing.* J. Mater. Chem., 19(19):3057, 2009.

[115] Anna Pajor-Świerzy, Yousef Farraj, Alexander Kamyshny, and Shlomo Magdassi. *Effect of carboxylic acids on conductivity of metallic films formed by inks based on copper@silver core-shell particles.* Colloids Surfaces A Physicochem. Eng. Asp., 522:320–327, 2017.

[116] Woo-Ram Lee, Joon-Rak Choi, Seung Jin Ko, Jinwoo Cheon, Min Gyu Kim, Jong-Il Park, and Sang Jun Oh. *Redox-transmetalation process as a generalized synthetic strategy for core-shell magnetic nanoparticles.* J. Am. Chem. Soc., 127(46):16090–16097, 2005.

[117] In-Keun Shim, Oh Young-Soo, and Jae-Woo Joung. *US7611644B2*, 2009.

[118] Robert B. Grubbs. *Roles of polymer ligands in nanoparticle stabilization.* Polym. Rev., 47(2):197–215, 2007.

[119] Sunho Jeong, Kyoohee Woo, Dongjo Kim, Soonkwon Lim, Jang Sub Kim, Hyunjung Shin, Younan Xia, and Jooho Moon. *Controlling the thickness of the surface oxide layer on Cu nanoparticles for the fabrication of conductive structures by ink-jet printing.* Adv. Funct. Mater., 18(5):679–686, 2008.

[120] Yoshio Kobayashi, Satoshi Ishida, Kazuaki Ihara, Yusuke Yasuda, Toshiaki Morita, and Shinji Yamada. *Synthesis of metallic copper nanoparticles coated with polypyrrole.* Colloid Polym. Sci., 287(7):877–880, 2009.

[121] Long Quoc Pham, Jong Hwa Sohn, Chang Woo Kim, Ji Hyun Park, Hyun Suk Kang, Byung Cheol Lee, and Young Soo Kang. *Copper nanoparticles incorporated with conducting polymer: Effects of copper concentration and surfactants on the stability and conductivity.* J. Colloid Interface Sci., 365(1):103–109, 2012.

[122] Y Kobayashi and T Sakuraba. *Silica-coating of metallic copper nanoparticles in aqueous solution.* Colloids Surfaces A Physicochem. Eng. Asp., 317:756–759, 2008.

[123] Shohei Shiomi, Makoto Kawamori, Shunsuke Yagi, and Eiichiro Matsubara. *One-pot synthesis of silica-coated copper nanoparticles with high chemical and thermal stability.* J. Colloid Interface Sci., 460:47–54, 2015.

3

Synthesis of Copper Nanocrystals: A cost-effective approach

We propose a synthesis of metallic copper nanocrystals based on copper formate, which does not need an additional reducing agent nor a protective atmosphere to yield metallic copper. By saturating the initial solution with copper formate and implementing a specific temperature profile, we demonstrate a self-cleaning effect. Oxygen cannot access the nanocrystals during the reaction with non-oxidized nanocrystals as result. A clear influence of the reaction rate was established and the mechanism of oxygen exclusion is discussed. Furthermore, the size of the NCs can be tuned by adjusting precursor and ligand concentrations.

3.1 Introduction

In chapter 2, we presented an overview of different methods to synthesize Cu NCs. A common issue encountered in most of the published research on Cu NCs synthesis is the limited amount of conductive material produced per unit reaction volume and the questionable scalability of the described methods. Both factors cast doubts on the economical feasibility of imple-

menting Cu NCs in industrial processes. Some researchers tackled these issues; for instance Lee *et al.*[1] introduced a large scale (5 L), relatively high concentration (0.2 M) method of producing 30-65 nm Cu NCs by the chemical reduction of copper sulfate with sodium hypophosphite in the presence of polyvinylpyrrolidone. In another publication,[2] Li *et al.* produced 2.1 g of copper nanowires in a 4 L reaction by reducing copper chloride with glucose in the presence of oleic acid and oleylamine using an electrical-pressure cooker. Although these proposed methods produced valuable material for conductive applications, the scale is still insufficient to consider them relevant to raise industrial interest.

In this chapter, we propose an economic synthesis with a high solid content per reaction volume. The process is based on the low-temperature decomposition of copper(II) formate, an inexpensive precursor bearing the reducing agent within (formate). Oleylamine is present as the sole surfactant. By saturating the reaction with precursor, we achieved two significant benefits. First, we greatly increased the amount of Cu NCs produced per volume of reaction (>50 g/L). Second, we suppressed the need of a protective atmosphere to perform the reaction. Metallic Cu NCs were obtained under air. The size of the Cu NCs could be conveniently tuned from 10 nm to 200 nm by adjusting the reagent ratios.

3.2 Experimental Section

Chemicals. Copper(II) formate tetrahydrate (Alfa Aesar, 98%), oleylamine (Acros Tech, 80-90%), n-dodecane (Merck Millipore, ≤99%), diacetone alcohol (Sigma-Aldrich, ≤99%), disperbyk 180 (BYK)

Synthesis of Cu NCs. Copper nanocrystals were synthesized by revising a method originally introduced by Sun *et al.*[3] and adapted in recent publications[4;5]. A solution of copper(II) formate in an oleylamine:dodecane mixture was formed by heating the mixture at 60°C until the copper(II) formate was fully dissolved. Unless mentioned otherwise, the temperature was raised to 140°C in a constant heating rate of 10°C/min and kept at this temperature for 10 minutes before cooling down. Cu NCs where extracted from the reaction mixture and further purified by repetitive precipitation/resuspension cycles using toluene as solvent and ethanol or methanol as non-solvent.

Quantification of Cu^+ and Cu^0. The amount of Cu^+ and Cu^0 was quantified by taking aliquots from the reaction mixture at different stages

of the reaction. For the quantitative analysis of Cu^+, these aliquots were weighted, diluted in hexane and loaded in a small glass vial. Right after, a known concentration of bicinchoninic acid dissolved in DMSO was added to the vial, which resulted in a 2-phase system. Upon shaking, the Cu^+ could be extracted from the reaction mixture, and an intensely colored Cu^+ complex with bicinchoninic acid was formed in the DMSO phase. Subsequently, the amount of Cu^+ was determined colorimetrically, from the absorbance of the DMSO phase at 562 nm using a molar extinction coefficient of $7.7\,10^3 l/(mol \cdot cm)$.[6] For the quantification of Cu^0, the aliquots were diluted in hexane and the absorbance spectra of the resulting dispersion was directly recorded. The intrinsic absorption coefficient of Cu^0 at 400 nm in hexane was calculated using its optical constants: $n = 1.32, k = 2.12$.[7] From the combination of the intrinsic absorption coefficient and the absorbance of the Cu NC dispersions at 400 nm, the volume fraction of Cu in the dispersion was obtained, a number that directly yields the amount of Cu^0 formed in the reaction.[8]

Structural Characterization. Transmission electron microscopy (TEM) images were recorded on a Cs-corrected JEOL 2200-FS TEM operated at 200 kV. X-ray diffraction (XRD) analysis was conducted on a Thermo Scientific ARL XTra diffractometer, operated at 40 kV/30 mA using Cu-Kα radiation (λ = 1.5406 Å) and a Peltier cooled Si(Li) solid-state detector. Scanning electron microscopy (SEM) images were recorded on a JEOL JSM-7600F Schottky Field Emission.

Rietveld refinement. The XRD data were collected on a Thermo Scientific ARL X'tra Diffractometer equipped with a Peltier cooled detector. Samples were measured in θ-2θ geometry over an angular range of 20-80 D2θ (CuKα radiation) using a 0.02 D2θ step size and 1 s/step counting time. The Rietveld method for whole-powder pattern fitting was used and the Topas Academic V4.1 software was used for Rietveld refinement. The refined parameters were the measurement specific or sample displacement error, a cosine Chebyshev function of 10 polynomial terms for background correction, phase specific scale factors, unit cell parameters and Lorentzian peak shape broadening parameters.

3.3 The Standard Synthesis

3.3.1 Protective and Ambient Atmosphere

As described in the Experimental Section, any synthesis described in this work starts with the formation of a solution of copper formate ($Cu(HCO_2)_2$) in oleylamine ($OlNH_2$) and dodecane. Here, $OlNH_2$ is used to as a complexing agent to bring the copper precursor in solution. Moreover, $OlNH_2$ is known to reduce the overall decomposition temperature of the $Cu(HCO_2)_2$:$OlNH_2$ complex, originally around 200°C for pure $Cu(HCO_2)_2$, to only 120°C.[9;10] Different hypotheses have been presented to explain this decrease in reduction temperature. Here, the work from Marchal *et al.* shown that the in-situ reduction mechanisms of copper formate proceed via a transient Cu(I) intermediate.[11] Compared to other Cu(II) complexes, it was inferred that the decrease on the $Cu(HCO_2)_2$ reduction temperature arose from the low stability of the Cu(I) intermediate and the structural differences between Cu(II) and Cu(I) species along the thermal decomposition route.

Figure 3.1 presents the characterization of the products obtained from the decomposition of a $Cu(HCO_2)_2$ solution containing 2 g/L of Cu and featuring a 2:1 molar ratio of $OlNH_2$: $Cu(HCO_2)_2$. The difference between Figure 3.1a and 3.1b is the synthesis atmosphere, where the former was run under ambient and the second under inert atmosphere. The bright field transmission electron microscopy (TEM) images show that the morphology and size of the NCs are similar, regardless of the synthesis environment. As can be seen, these specific synthesis conditions lead to a polydisperse distribution of NCs, with an average size of 240 ± 40 nm and 280 ± 150 nm for syntheses under ambient and nitrogen, respectively. One sees that in both cases, the NCs exhibit a projected hexagonal shape, suggesting that the crystallites are cuboctahedrons.[12;13] The fact that such large NCs maintain a cuboctahedral shape points towards a similar growth rate of both (100) and (111) facets, suggesting a non-preferential binding of $OlNH_2$ to either facet.[14;15]

Despite the similar morphology, a very different crystallographic structure is obtained depending on the synthesis atmosphere. Figure 3.1c shows that the X-ray diffraction pattern of NCs synthesized under ambient conditions corresponds to that of Cu_2O (JCPDS 05-0667) and features a diffraction peak characteristic to the (111) lattice plane of CuO at 38.75° (JCPDS 80-1268). The oxidized nature of the NCs is not unexpected since an inert atmosphere is typically used to prevent oxidation during the formation of Cu NCs.[16] On the other hand, the NCs obtained through a synthesis performed

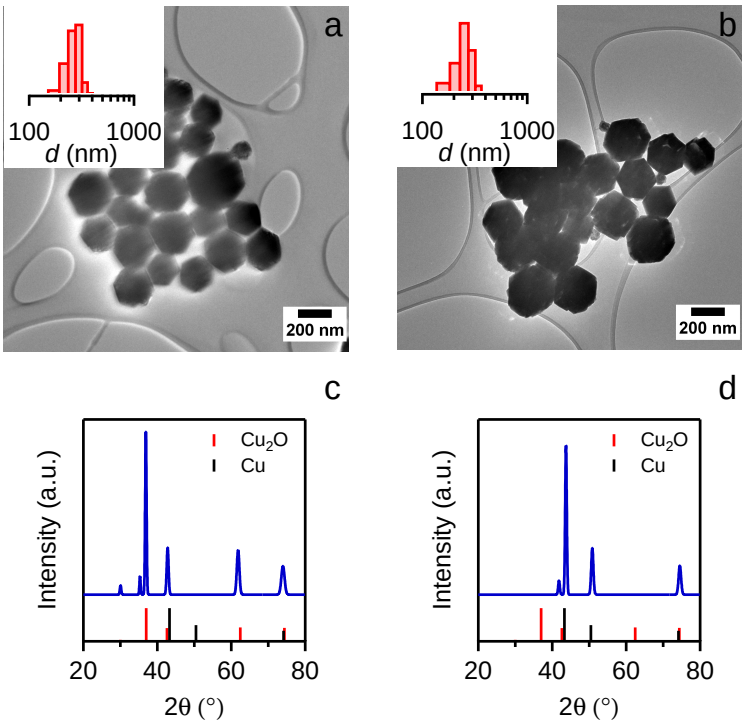

Figure 3.1: Low-resolution, brightfield TEM image of Cu NCs formed by a 2 g/L, 2:1 oleylamine:$Cu(HCO_2)_2$ synthesis under (a) ambient and (b) nitrogen atmosphere; (insets) Size histograms determined based on the analysis of 200 NCs in TEM images. XRD pattern of pristine NCs synthesized under (c) ambient and (d) nitrogen atmosphere. The mixture for the synthesis under nitrogen was degassed prior to the reaction.

under inert conditions exhibit the X-ray diffraction pattern of metallic Cu^0 in its cubic structure (JCPDS 04-0836), confirming that formate and $OlNH_2$ can fully reduce Cu^{2+} to Cu^0 under inert conditions without the addition of an extra reducing agent.[17]

3.3.2 Two-Step Reduction of Copper Formate

To study the decomposition of copper formate in more detail, we performed a synthesis while taking aliquots after regular time intervals. Under nitrogen atmosphere, a 0.2 M (12.7 g/L) solution of $Cu(HCO_2)_2$ in a 1:1 mixture of $OlNH_2$ and dodecane was heated to 140°C and kept at that temperature

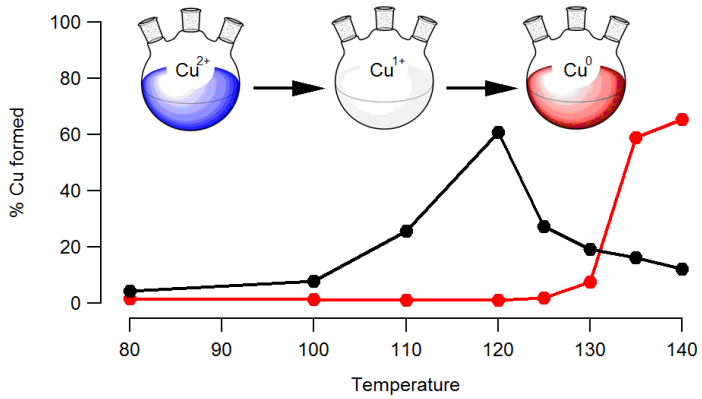

Figure 3.2: Development of the yield of (black) Cu^{1+} and (red) Cu^0 during a Cu NC synthesis based on heating of a 0.2M copper formate solution in an 1:1 oleylamine:dodecane mixture up to 140°C. All datapoints at intermediate temperatures were obtained by analyzing aliquots taken from the reaction mixture during the temperature sweep. In the case of the datapoint at 140°C, the reaction was kept at that final temperature for 5 minutes before the aliquot was taken.

for 5 minutes. Upon heating at a rate of approximately 10°C/min, the deep blue color of the initial solution first became transparent at around 120°C, after which the reaction mixture quickly turned dark red; a color typical of dispersions of Cu NCs. We hypothesized that these color changes reflect the successive reduction of Cu^{2+} into Cu^{1+} and, finally, metallic Cu^0. To confirm this, we quantified the amount of Cu^{1+} and Cu^0 in the reaction mixture at different stages of the reaction using colorimetry, where we quantified Cu^{1+} through selective complexation with bicinchoninic acid, and Cu^0 by means of the absorption coefficient of metallic Cu NCs (see Experimental Section).

Figure 3.2 represents the composition of the reaction mixture obtained in this way. In line with our hypothesis and the study from Marchal *et al.*, metallic Cu is indeed formed in a two-step process.[11] The initially present Cu^{2+} is first reduced at temperatures between 100 and 120°C to form Cu^{1+}, which only gives way to metallic copper at temperatures above 130°C. When keeping the reaction mixture at 140°C for 5 minutes, we estimate that ~65% of the Cu^{2+} originally present is converted into metallic Cu. Such a yield is similar to what was reported by Sun *et al.*,[3] yet the reaction is carried out at only 140°C during 5 minutes instead of 250°C for 20

minutes. We project that longer reaction times would lead to almost full yield.

3.4 Oxidation Suppression During Cu Nanocrystal Synthesis

3.4.1 The Impact of Initially Dissolved Oxygen

In an effort to reduce the synthesis complexity, we aimed at defining synthesis conditions for which Cu^0 NCs are formed under ambient. In principle, this would require us to strictly avoid exposure to oxygen at all stages of the synthesis. As a first oxygen source, we considered all oxygen initially dissolved in the $OlNH_2$-dodecane solvent mixture at the start of the reaction. In chemical laboratories, it is common practice to protect oxygen-sensitive compounds during a reaction by degassing the initial reaction mixture under vacuum. However, degassing is a time-consuming process that is impractical for large volumes. Moreover, if a reaction under ambient atmosphere is envisaged, initial degassing seems futile since oxygen can dissolve back into the solvent prior to the reaction.

To evaluate the impact of dissolved oxygen on the formation of Cu NCs, we estimated the concentration of dissolved oxygen in the initial $OlNH_2$-dodecane solvent mixture. According to published data,[18] the solubility of oxygen in n-dodecane amounts to 54.9 mg/L at 35°C and atmospheric pressure. Using that value, we calculated that for the 2 g/L synthesis described in the previous section, the molar ratio between Cu formate and dissolved O_2 amounts to ∼18. To interpret the consequence of such an equivalence, we considered the formation of Cu_2O from Cu and O_2:

$$4Cu_{(s)} + O_{2(sol)} \rightleftharpoons 2Cu_2O_{(s)} \tag{3.1}$$

According to Equation 3.1, 4 moles of Cu are oxidized by 1 mole of O_2. Therefore, a sizable fraction of about 20% of the reduced copper could be re-oxidized by the oxygen initially dissolved in the reaction mixture of that 2 g/L synthesis. This suggests that further increasing the $Cu(HCO_2)_2$ concentration in the reaction mixture could be an efficient strategy to suppress oxidation. Indeed, such reaction mixtures would have an increased initial Cu/O_2 ratio and, consequently, a smaller fraction of re-oxidized Cu as a final product. For example, an increase of the Cu content to 40 g/L could decrease the expected fraction of re-oxidized copper to less than 1% of the total amount of Cu formed. Using such an approach, the initial oxidation

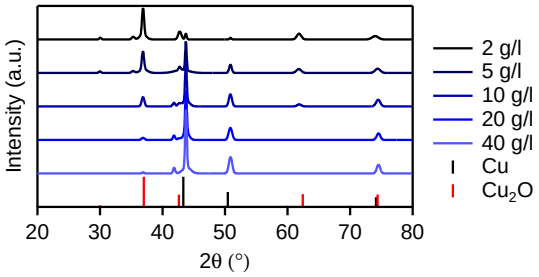

Figure 3.3: XRD patterns of Cu NCs synthesized with different concentrations of Cu without protective atmosphere. The molar ratio of $OlNH_2$:$Cu(HCO_2)_2$ has been kept at 2:1 and the heating rate at $20^{\circ}C/min$ for all syntheses. The NCs were purified and dried in ambient conditions prior to measurement.

Table 3.1: Copper ratios extracted from Rietveld refinement analysis of the XRD data from Figure 3.3.

[Cu]	Cu (%)	Cu_2O(%)
2 g/L	8.8 ± 0.5	91.2 ± 0.5
5 g/L	43.9 ± 0.5	56.1 ± 0.5
10 g/L	73.5 ± 0.6	26.5 ± 0.6
20 g/L	92.7 ± 0.7	7.3 ± 0.7
40 g/L	97.3 ± 0.6	2.7 ± 0.6

of this small amount of Cu may lead to an oxygen-free reaction mixture; a *self-cleaning* effect that creates the inert environment necessary for the formation of metallic Cu NCs.

We tested this possible self-cleaning of the reaction mixture by running the $Cu(HCO_2)_2$ decomposition under ambient conditions in reaction mixtures with a different solid loading. Figure 3.3 presents the XRD patterns of the thus obtained NCs, for Cu loadings increasing from 2 to 50 g/L. As can be seen, the initial concentration of the copper precursor has a large impact on the oxidation state of the resulting NCs. At low precursor concentration, the NCs mainly consist of Cu_2O. In synthesis conditions expected to produce 2 g/L of Cu, the XRD pattern obtained is similar the data presented in 3.1c since the synthesis conditions are equivalent. As the concentration of the initial precursor is increased, the crystallographic phases gradually shift from Cu_2O to Cu^0. Table 3.1 summarizes the results of a Rietveld

refinement of these diffractograms, showing that the metallic Cu content increases from 8.8% to 97.3% by increasing the concentration from 2 g/L to 40 g/L. Note that the oxidized fraction is about 2 % for the 40 g/L synthesis, close to the estimated value based on the room temperature solubility of oxygen in dodecane. As an additional benefit, a larger concentration of precursor results in a higher amount of material produced per volume of reaction; synthesis conditions that reduce the overall cost of producing Cu NCs and limit the generated waste.

3.4.2 Oxygen intake during synthesis

Apart from the initially dissolved oxygen, the influx of oxygen from the ambient surroundings can be a second oxygen source in an open reaction vessel, which we succinctly describe as a transition from gaseous to dissolved oxygen:

$$O_{2(g)} \rightleftharpoons O_{2(sol)} \tag{3.2}$$

This process will promote redissolution of oxygen as already dissolved oxygen is consumed by the oxidation of Cu^0 as described by Eq 3.1. Hence, to prevent further formation of copper oxide, the influx of oxygen in the reaction mixture should be restricted during the decomposition of the precursor and the nucleation and growth of Cu NCs. However, the flask cannot simply be sealed to block any gas inflow since the decomposition of $Cu(HCO_2)_2$ releases water, carbon dioxide and hydrogen:[9]

$$Cu(HCO_2)_2 \cdot 4H_2O_{(sol)} \rightarrow Cu_{(s)} + H_{2(g)} + 2CO_{2(g)} + 4H_2O_{(g)} \tag{3.3}$$

Clearly, such gas evolution would result in a problematic pressure increase in a closed flask.

To evaluate the impact of redissolved oxygen on the reaction, we started from the idea that gasses released from the reaction mixture as $Cu(HCO_2)_2$ decomposes can suppress oxygen redissolution in the reaction mixture. Indeed, considering that the reaction occurs in an open flask exposed to ambient atmosphere, the total pressure in the headspace must remain constant. When the decomposition of $Cu(HCO_2)_2$ starts, evaporation of water and the generation of hydrogen and carbon dioxide from the solution increase the partial pressure of such gases above the liquid and decrease the oxygen partial pressure to keep the total pressure constant. According to Henry's law, a lower partial pressure of oxygen implies that less oxygen will dissolve in the reaction mixture, thus protecting the Cu NCs formed from oxidation.

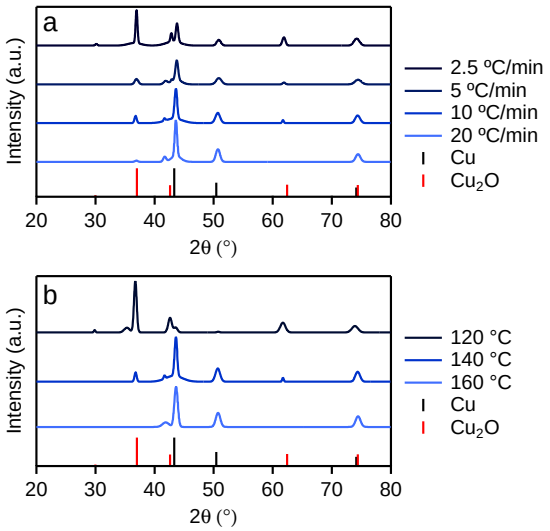

Figure 3.4: (a) XRD patterns of Cu NCs synthesized at different heating rates without protective atmosphere, to a final temperature of 140°C. (b) XRD patterns of Cu NCs synthesized without protective atmosphere, at 10°C/min to different final temperatures and held at these temperature for 10 min. The concentration of copper was set at 20 g/L and the molar ratio of $OlNH_2$:$Cu(HCO_2)_2$ 2:1 for all syntheses. The NCs were purified and dried in ambient conditions prior to characterization.

Importantly, the formation of such an oxygen-poor atmosphere in the reaction vessel will strongly depend on the reaction rate, where slow reactions will have hardly any impact, whereas fast reactions may strongly influence oxygen redissolution.

We evaluated the impact of the reaction rate on the formation of copper and copper oxide during $Cu(HCO_2)_2$ decomposition by either changing the rate at which the a final reaction temperature of 140°C is reached, or by changing that reaction temperature. Figure 3.4 illustrates the x-ray diffractogram recorded on the reaction product obtained for these different syntheses, which give evidence of an increased copper oxide content for slower heating rates or lower reaction temperatures, *i.e.*, conditions in which the overall reaction rates is lowest. This qualitative picture is confirmed by a Rietveld analysis, the results of which are summarized in Tables 3.2 and 3.3. One sees that at the lowest heating rate used, a mixed copper/copper oxide product is obtained whereas a heating rate at 20 °C/min leads to a

Table 3.2: Copper ratios extracted from Rietveld refinement analysis of the XRD data from Figure 3.4a.

Heating rate (°C/min)	Cu (%)	Cu_2O(%)
2.5	43.5 ± 0.7	56.5 ± 0.7
5	77.6 ± 1.2	22.4 ± 1.2
10	82.5 ± 0.8	17.5 ± 0.8
20	92.4 ± 1.6	7.6 ± 1.6

Table 3.3: Copper ratios extracted from Rietveld refinement analysis of the XRD data from Figure 3.4b.

Final temperature (°C)	Cu (%)	Cu_2O(%)
120	8.5 ± 0.7	91.5 ± 0.7
140	82.5 ± 0.8	17.5 ± 0.8
160	90.1 ± 4.4	9.9 ± 4.4

NC product composed for ∼92% of Cu^0. Note that the latter result is in close agreement with the data listed in Table 3.1 for the same precursor concentration. Similarly, Table 3.3) indicates that changing the reaction temperature from 120°C to 160°C induces a shift of the end product composition from 90% copper oxide to 90% copper. Hence, we conclude that a lower reaction rate strongly promotes the formation of copper oxide, probably by enabling redissolution of ambient atmosphere in the reaction mixture. On the other hand, high reaction rates can effectively suppress the redissolution of oxygen, which lead to an oxygen-poor reaction mixture in which Cu NCs can be formed, even under ambient conditions.

3.5 Size-Tuning During Cu Nanocrystal Synthesis

The size of Cu NCs is an important characteristic of a conductive ink based on a copper nanocolloid. For example, NCs with sizes larger than 50 nm can clog the nozzles of an ink-jet printer. On the other hand, smaller NCs have large surface-to-volume ratios. This makes that larger amounts of organic ligands are needed to stabilize a conductive ink, which limits the maximum solid loading of such inks.[19] For these reasons, a synthesis method that

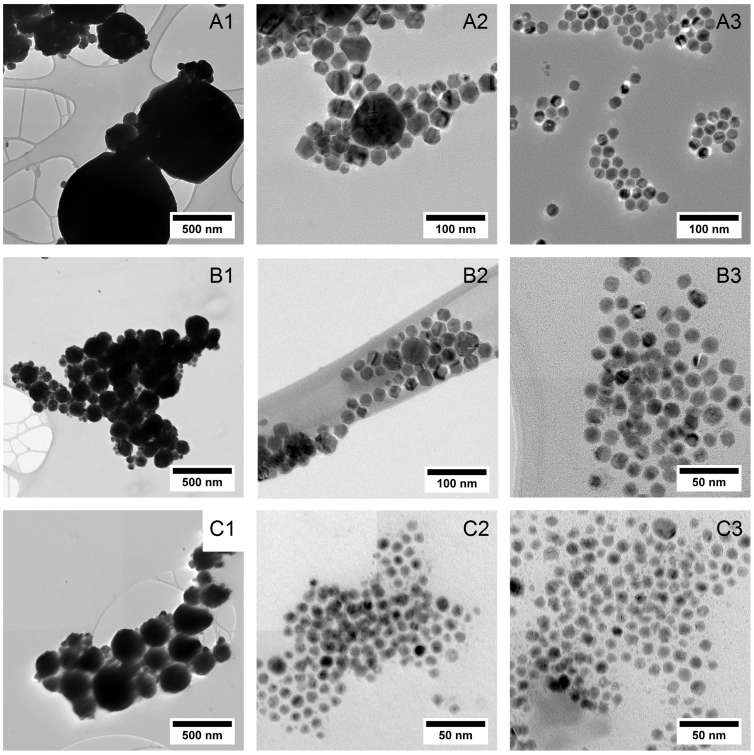

Figure 3.5: Low-resolution, brightfield TEM images of Cu NCs synthesized with different concentrations of copper: (A) [Cu]=10 g/L, (B) [Cu]=20 g/L, (C) [Cu]=40 g/L and different molar ratio between $OlNH_2$ and copper formate: (1) $OlNH_2$:$Cu(HCO_2)_2$=1:1, (2) $OlNH_2$:$Cu(HCO_2)_2$=2:1, (3) $OlNH_2$:$Cu(HCO_2)_2$=3:1.

enables the nanocrystal size to be varied by minimal changes to the composition of the reaction mixtures is of high interest. To obtain such a level of control, we explored the influence of the reagent ratios, most notably the $OlNH_2$:$Cu(HCO_2)_2$ equivalence and the $Cu(HCO_2)_2$ concentration, on the reaction outcome while keeping other relevant parameters such as heating rate, synthesis time and reaction temperature constant. This approach is inspired by literature results on the synthesis of CdSe NCs, where both the reaction rate and the surfactant concentration proved useful knobs to tune the resulting nanocrystal size.[20] Figure 3.5 and Table 3.4 present the different nanocrystal sizes we obtained in this study, where we either modified the $OlNH_2$ equivalence (left to right) or changed the $Cu(HCO_2)_2$ concentration (top to bottom).

Table 3.4: Particle size and standard deviation of the Cu NCs from Figure 3.5. Sizes are determined based on the analysis of 200 NCs in the images.

[Cu]	$OlNH_2$:$Cu(HCO_2)_2$		
	1:1	2:1	3:1
10 g/L	197.6 ± 182.8 nm	34.1 ± 16.9 nm	19.3 ± 2.9 nm
20 g/L	100.9 ± 54.4 nm	27.2 ± 9.2 nm	13.7 ± 1.3 nm
40 g/L	107.6 ± 85.3 nm	10.0 ± 1.4 nm	9.4 ± 1.4 nm

As can be seen, a low concentration of $OlNH_2$ concurs with the formation of large NCs, whereas a high ligand concentration leads to small NCs. A similar observation was made in parallel by Dai *et al.*[4], confirming our results. In the case that the $OlNH_2$ equivalence is further increased to 8/1, the particle size is reduced to 4 nm; a figure in line with results we published previously.[5] Note that these trends are different from what is often found in semiconductor NC synthesis, where larger ligand concentrations typically lead to larger NCs.[21] Possibly, the impact of ligand concentration on the size of Cu NCs reflects the lower growth rate of facets covered with a high surface density of ligands. It is also noteworthy that lower ligand concentration yield broader size distributions, a relation that complicates the determination of the average NC size. For instance, using 1 equivalent of $OlNH_2$ yields an end product in which the NC diameter varies between 20 and 400 nm. Note that these trends are different from what is often found in semiconductor NC synthesis, where larger ligand concentrations typically lead to larger NCs.[21] However, this argumentation is only valid if the ligand has no interaction with the solvent and no effect on the overall reaction rate. In this case, the difference in particle growth can be linked to the solubility of $Cu(HCO_2)_2$, which is only soluble in non-polar solvents when complexed with $OlNH_2$. Since Cu^{2+} can coordinate with six donor atoms, the 1 equivalent reaction mixture will comprise $Cu(HCO_2)_2$ complexed by 0,1 or 2 $OlNH_2$ ligands. Possibly, this diversity leads to a heterogeneous mixture in which $Cu(HCO_2)_2$ reacts at different rates and NC with a broad range of sizes are formed.

Similarly, the initial concentration of $Cu(HCO_2)_2$ in the reaction mixture has an effect on the nanocrystal size. In that case, we find that a lower concentration of copper precursor in the reaction mixture leads to larger NCs, as can be seen in Figure 3.5 and Table 3.4 from top to bottom. This relation between NC size and precursor concentration is in line with previ-

ous results on the formation of CdSe NCs.[20] In that study, the link between higher precursor concentration and larger NCs was assigned to the underlying relation between the reaction rate and the NC size, where more rapid reactions promote nucleation over growth and lead to the formation of more, albeit smaller NCs.

3.6 Conclusion

We demonstrated an economic route to produce copper nanocrystals based on the thermal decomposition of copper formate in oleylamine. Based on a self-cleaning effect, saturation of the initial reaction mixture with the precursor leads the exclusion of oxygen and thus the production of metallic copper nanocrystals. We showed that a high reaction rate is crucial to ensure that oxygen has little access during the formation of the monomers of Cu^0. By adapting the synthesis conditions, a wide range of sizes was obtained granting flexibility to the printing method of choice. Ultimately, we proved that metallic Cu NCs can be obtained by using low-cost reagents and conditions, a fundamental step towards the development and capitalization of Cu NCs as a cost-effective filler for conductive inks.

References

[1] Youngil Lee, Jun-rak Rak Choi, Kwi Jong Lee, Nathan E. Stott, and Donghoon Kim. *Large-scale synthesis of copper nanoparticles by chemically controlled reduction for applications of inkjet-printed electronics.* Nanotechnology, 19(41):415604, 2008.

[2] Shenjie Li, Yanyan Chen, Lijian Huang, and Daocheng Pan. *Large-scale synthesis of well-dispersed copper nanowires in an electric pressure cooker and their application in transparent and conductive networks.* Inorg. Chem., 53(9):4440–4444, 2014.

[3] Xiao Sun, Ya-Wen Zhang, Rui Si, and Chun-Hua Yan. *Metal (Mn, Co, and Cu) Oxide Nanocrystals from Simple Formate Precursors.* Small, 1(11):1081–1086, 2005.

[4] Xiaofeng Dai, Wen Xu, Teng Zhang, and Tao Wang. *Self-Reducible Cu Nanoparticles for Conductive Inks.* Ind. Eng. Chem. Res., 57(7):2508–2516, 2018.

[5] Arnau Oliva-Puigdomènech, Jonathan De Roo, Jakob Kuhs, Christophe Detavernier, Jose C Martins, and Zeger Hens. *Ligand Binding to Copper Nanocrystals : Amines and Carboxylic Acids and the Role of Surface Oxides.* Chem. Mater., 2019.

[6] Andrew J. Brenner and Edward D. Harris. *A quantitative test for copper using bicinchoninic acid.* Anal. Biochem., 226(1):80–84, 1995.

[7] P B Johnson and R W Christy. *Optical Constants of the Noble Metals*, 1972.

[8] Zeger Hens and Iwan Moreels. *Light absorption by colloidal semiconductor quantum dots.* J. Mater. Chem., 22(21):10406, 2012.

[9] Andrew Knox Galwey, David M. Jamieson, Michael Ewart Brown, Andrew Knox Galwey, David M. Jamieson, and Michael Ewart Brown. *Thermal Decomposition of THree Crystalline Modifications of Anhydrous Copper (II) Formate.* J. Phys. Chem., 78(11):2664–2670, 1974.

[10] Dong Hun Shin, Seunghee Woo, Hyesuk Yem, Minjeong Cha, Sanghun Cho, Mingyu Kang, Sooncheol Jeong, Yoonhyun Kim, Kyungtae Kang, and Yuanzhe Piao. *A self-reducible and alcohol-soluble copper-based metal-organic decomposition ink for printed electronics.* ACS Appl. Mater. Interfaces, 6(5):3312–3319, 2014.

[11] Wouter Marchal, Alessandro Longo, Valérie Briois, Kristof Van Hecke, Ken Elen, Marlies K Van Bael, and An Hardy. *Understanding the Importance of Cu(I) Intermediates in Self- Reducing Molecular Inks for Flexible Electronics* . Inorg. Chem., 57:15205–15215, 2018.

[12] Yu Zhao, Jun Jie Zhu, Jian Min Hong, Ningsheng Bian, and Hong Yuan Chen. *Microwave-induced polyol-process synthesis of copper and copper oxide nanocrystals with controllable morphology.* Eur. J. Inorg. Chem., 2004(20):4072–4080, 2004.

[13] C. Salzemann, I. Lisiecki, J. Urban, and M. P. Pileni. *Anisotropic copper nanocrystals synthesized in a supersaturated medium: Nanocrystal growth.* Langmuir, 20(26):11772–11777, 2004.

[14] Pascal Lignier, Ronan Bellabarba, and Robert P. Tooze. *Scalable strategies for the synthesis of well-defined copper metal and oxide nanocrystals.* Chem. Soc. Rev., 41(5):1708–1720, 2012.

[15] Younan Xia, Yujie Xiong, Byungkwon Lim, and Sara E. Skrabalak. *Shape-controlled synthesis of metal nanocrystals: Simple chemistry meets complex physics?* Angew. Chemie - Int. Ed., 48(1):60–103, 2009.

[16] Derrick Mott, Jeffrey Galkowski, Lingyan Wang, Jin Luo, and Chuan Jian Zhong. *Synthesis of size-controlled and shaped copper nanoparticles.* Langmuir, 23(10):5740–5745, 2007.

[17] Stefanos Mourdikoudis and Luis M. Liz-Marzán. *Oleylamine in nanoparticle synthesis.* Chem. Mater., 25(9):1465–1476, 2013.

[18] Wang Jianlong. *Enhancement of citric acid production by Aspergillus niger using n -dodecane as an oxygen-vector.* Process Biochem., 35:1079–1083, 2000.

[19] Sze Kee Tam, Ka Yip Fung, Grace Sum, Hang Poon, and Ka Ming Ng. *Product Design : Metal Nanoparticle-Based Conductive Inkjet Inks.* Am. Inst. Chem. Eng., 62(8):2740–2753, 2016.

[20] Sofie Abe, Richard Karel Čapek, Bram De Geyter, and Zeger Hens. *Tuning the postfocused size of colloidal nanocrystals by the reaction rate: From theory to application.* ACS Nano, 6(1):42–53, 2012.

[21] Sofie Abe, Richard K. Capek, Bram De Geyter, and Zeger Hens. *Reaction chemistry/nanocrystal property relations in the hot injection synthesis, the role of the solute solubility.* ACS Nano, 7(2):943–949, 2013.

4

Surface Chemistry of Copper Nanocrystals: Amines and Carboxylic Acids and the Role of Surface Oxides[1]

We perform an in-depth study of the surface chemistry of the Cu NCs. We focus on the synthesis of 4 nm Cu colloids as a study model due to their high surface/volume ratio. We demonstrate that oleylamine is initially capping the surface as a tightly bound ligand. We illustrate that addition of undecylenic acid triggers an exchange reaction on the surface of the colloids. We propose and discuss different models to describe this exchange reaction.

4.1 Introduction

In chapter 3, we presented how to prevent oxidation and modify the size of the Cu nanocrystals from a synthesis perspective. However, in order to

[1] *Adapted from:* **Arnau Oliva Puigdomènech**, Jonathan De Roo, Jakob Kuhs, Christophe Detavernier, Jose C. Martins, Zeger Hens. *Ligand Binding to Copper Nanocrystals: Amines and Carboxylic Acids and the Role of Surface Oxides.* Chemistry of Materials, 31 (6), 2058–2067, **2019**.

preserve the conductive properties oxidation must be prevented during all stages. An interesting approach to suppress or control oxidation involves capping Cu NCs by surface-bound ligands.[1] An important step towards designing a surface termination that protects Cu NCs from oxidizing is understanding how ligands bind and pack on the surface of Cu NCs. This is by no means straightforward. Several methods have been developed to analyze the binding of ligands to NCs, such as thermogravimetry, infrared spectroscopy, mass spectrometry or nuclear magnetic resonance (NMR) spectroscopy.[2] Among these different methods to study the surface chemistry of NCs, solution NMR spectroscopy stands out due to its unique capability to identify and quantify NC ligands, and study ligand exchange reactions *in-situ*.[3]

In this chapter, we address the binding of amines and carboxylic acids to Cu NCs, two commonly used ligands in NC research, by combining solution NMR spectroscopy with judicious ligand exchange experiments. As a study object, we use ~ 4 nm Cu NCs synthesized by the decomposition of Cu formate in the presence of oleylamine. We show that the crude reaction product can be purified by means of standard purification protocols to obtain dispersions that contain, next to the solvent and the Cu NCs, almost exclusively surface-bound ligands. Using a set of 1D and 2D ^{1}H NMR techniques,[3] we demonstrate that oleylamine is a tightly bound ligand and we estimate a sample-dependent surface concentration in the range $1.4 - 2.5\ \mathrm{nm}^{-2}$. A most remarkable finding is that addition of undecenoic acid to oleylamine-stabilized Cu NCs results in the nearly 1 equivalent exchange at the Cu surface, which again results in a tightly-bound ligand shell. Importantly, this surface reaction results in the binding of a dissociated acid on the Cu surface, a reaction similar to what was described by De Roo *et al.* in the case of metal oxide nanocrystals.[4] We therefore propose that ligands such as amines and carboxylic acids mostly interact with Cu NCs through surface bound copper oxide.

4.2 Experimental Section

Chemicals. In this work, the following chemicals were used: copper(II) formate tetrahydrate (Alfa Aesar, 98%), bicinchoninic acid disodium salt hydrate (Sigma-Aldrich ≤98%), oleylamine (Acros Tech, 80-90%), n-dodecane (Merck Millipore, ≤99%), acetonitrile (VWR, ≤99.5%), n-hexane (VWR, 98%), methanol (VWR, ≤99.8%), undecenoic acid (Sigma-Aldrich, 98%), deuterated toluene (Sigma-Aldrich, ≤99.6%). All the solvents utilized during synthesis and purification were degassed prior to use by freeze-thawing

method to remove dissolved oxygen.

Synthesis of copper nanocrystals. Copper nanocrystals were synthesized by an adaptation of the method originally introduced by Sun *et al.*[5]. In brief, a solution of copper(II) formate tetrahydrate (0.2 mol/L) in an 20 mL oleylamine:dodecane mixture (1:1 by volume) was formed by heating the mixture at 60°C until the copper(II) formate was fully dissolved. Next, the solution was held at 60°C under vacuum for 1 hour to remove excess water. Upon raising the temperature to 140°C, the color of the reaction mixture changed from blue to dark red, indicating the reduction of copper(II) to metallic copper. This reaction mixture was kept at 140°C for 5 minutes, cooled down and diluted with hexane to prevent nanocrystal aggregation. Finally, the resulting solution was washed multiple times using acetonitrile and methanol as non-solvents and hexane as a solvent.

NMR analysis. Samples for NMR analysis were prepared by drying the purified reaction product under a nitrogen flow and redispersing the resulting powder in toluene-d_8. To prevent oxidation, all purification and sample preparation was performed under an inert atmosphere in a nitrogen-filled glovebox and the samples were loaded in air-tight screw-capped NMR tubes. NMR spectra were recorded either on a Bruker Avance III Ascend Spectrometer operating at a ^{1}H frequency of 500.13 MHz and equipped with a BBI-Z probe or on a Bruker Avance II Spectrometer operating at a ^{1}H frequency of 500.13 MHz and equipped with a TXI-Z probe. The sample temperature was set at 298.15 K. Quantitative ^{1}H spectra were recorded with 20 s delay between scans to ensure full relaxation of all NMR signals and concentrations were determined using the Digital ERETIC method. Diffusion-Ordered Spectroscopy (DOSY) experiments were performed using a double stimulated echo sequence for convection compensation and with monopolar gradient pulses. The diffusion decay was recorded in 64 steps of squared gradient strength from 95% to 2% of the probe's maximum value. The gradient pulse duration and diffusion delay were optimized so as to guarantee at least a 10-fold attenuation of the signal throughout the gradient strength scan.

Structural Characterization. Transmission electron microscopy (TEM) images were recorded on a Cs-corrected JEOL 2200-FS TEM operated at 200 kV. FTIR samples were prepared under inert atmosphere by dispersing a solution of Cu NCs in tetrachloroethylene and measuring them inside a KBr coated cuvette using a Nicolet 6700 FTIR. UV/Vis measurements were performed using an Avantes Ava-Spec-2048 spectrometer using

Avantes Avalight-DH-S-BAL as a light source.

Ligand Surface Concentration. The surface concentration of bound ligands was estimated by combining (1) the overall concentration of bound ligands as determined using NMR spectroscopy (see paragraph on NMR analysis), (2) the average surface area of the Cu NCs as determined using TEM imaging, and (3) the concentration of Cu NCs in the dispersion. For the latter, we used spectrophotometry to determine the total amount of Cu in the dispersion (see paragraph on quantification of Cu^+ and Cu^0) and TEM to determine the average NC volume. The ligand surface concentration is then obtained as the ratio between the number of ligands in the dispersion and the total area of the Cu NCs in the dispersion.

Ligand Exchange to UDA. In an oxygen-free environment, excess UDA (5-fold to $OlNH_2$) was added to a dispersion of $OlNH_2$ capped Cu NCs in hexane. After keeping the dispersion at room temperature for 30 minutes, the Cu NCs were precipitated by addition of acetonitrile and methanol as non-solvents and the thus obtained Cu NC powder was redispersed in hexane. This process was repeated a second time, followed by multiple purification cycles.

Titration of $OlNH_2$-capped Cu NCs with UDA. A solution of UDA and dibromomethane was prepared in toluene-d8. A quantitative ^1H spectra was recorded with 60 s delay between scans to ensure full relaxation of all NMR signals and concentrations and ratios were determined using the Digital ERETIC method. Then, a known volume of the previous solution was added to a purified solution of $OlNH_2$-capped Cu NCs with known $OlNH_2$ concentration. The sharp signal of dibromomethane at 4ppm was integrated to know the total amount of added UDA. Then, the concentration of bound $OlNH_2$ and UDA was deduced from the integration of the free ligand signal.

4.3 Results

4.3.1 Copper Nanocrystals, Synthesis and Characterization

Copper NCs were synthesized by the thermal decomposition of copper formate ($Cu(HCO_2)_2$) in a mixture of dodecane and oleylamine ($OlNH_2$), an approach inspired by the method proposed by Sun *et al.*[5] and developed

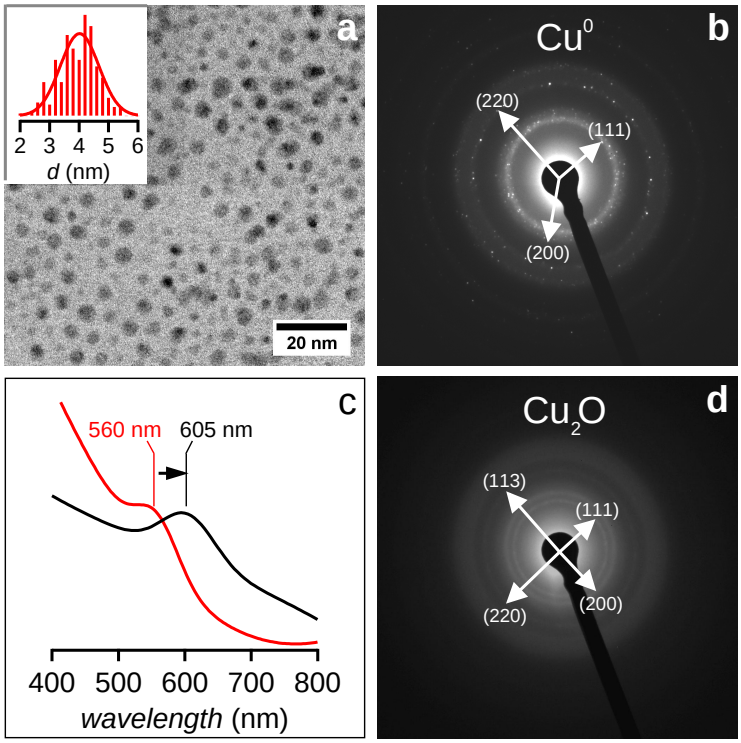

Figure 4.1: (a) Low-resolution, brightfield TEM image of a typical synthesis of Cu NCs; (inset) Size histogram determined based on the analysis of 300 NCs in TEM images. (b) Selected Area Electron Diffraction (SAED) pattern of a sample of pristine (i.e., no air exposure) Cu NCs. (c) UV-Vis spectra of a sample of Cu NCs, (red) pristine, (black) after 120 seconds of air exposure. Spectra have been normalized at the maximum intensity of the plasmon resonance. (d) Selected Area Electron Diffraction (SAED) pattern of a Cu NCs sample exposed to air for 5 days.

in the previous chapter. In practice, a 0.2 M solution of $Cu(HCO_2)_2$ in a 1:1 mixture of $OlNH_2$ and dodecane was heated to 140°C and kept at that temperature for 5 minutes. Figure 4.1a represents a typical bright field transmission electron microscopy (TEM) image of the reaction product obtained from the decomposition of $Cu(HCO_2)_2$. As can be seen, the synthesis method resulted in quasi-spherical particles with an average diameter of 3.95 ± 0.64 nm and a size dispersion of $\sim 20\%$. According to the selected area electron diffraction (SAED) pattern shown in Figure 4.1b, the particles are crystalline and feature lattice spacings characteristic of metallic

Cu. The formation of Cu NCs is further confirmed by the UV-Vis spectra of the purified reaction product (in red), which feature the absorbance maximum at 560 nm that is characteristic of the surface plasmon resonance (SPR) of spherical Cu NCs (see Figure 4.1c).[6] In line with previous studies,[7;8] exposing the Cu NCs to air resulted in a gradual redshift of the SPR, which reached 605 nm after 120 seconds of permanent air exposure for the example shown in Figure 4.1c. Further air exposure resulted in the complete disappearance of the SPR. Such a variation of the absorbance spectrum is typically attributed to the progressive oxidation of the Cu NCs, an interpretation we confirmed by means of an SAED analysis of the NCs after air exposure. As can be seen in Figure 4.1d, the SAED patterns of a sample exposed to air for 5 days indeed features four diffraction rings that can be assigned to diffraction from the (111), (200), (220) and (113) lattice planes of Cu_2O, corroborating the conclusion that the 4 nm copper NCs studied here rapidly oxidize when exposed to air.

4.3.2 Surface Chemistry of As-Synthesized Cu Nanocrystals

Figure 4.2a shows a 1D ^{1}H NMR spectrum recorded on a purified dispersion of Cu NCs in toluene-d_8, synthesized as described above. As the Cu NCs studied here are prone to oxidation, air exposure was avoided during all stages of the synthesis, sample preparation and analysis. In practice, this means that all work was carried out in a nitrogen-filled glovebox, until samples were loaded in air-tight NMR tubes. Next to the narrow resonances of residual toluene at around 7.0 and 2.1 ppm, the spectrum is dominated by broad resonances that are assigned to the different protons in the oleyl chain, as indicated. The resonance of the alkene protons **4** is retrieved at around 5.5 ppm, whereas most of the methyl protons **2** contribute to the broad resonance that peaks at around 1.5 ppm and the methyl protons **1** yield a minor shoulder at 1.0 ppm. Line broadening reduces the resonance of the protons **3** to a slight shoulder at around 2.2 ppm and makes that the resonance of the α-proton **5** cannot be discerned at all. In addition, the spectrum features resonances of methanol and hexane, which were used as non-solvent and solvent in the purification process. For a more detailed account of the resonance assignment, see Appendix (A.1.1).

Figure 4.2b represents the DOSY spectrum of the same sample, which shows that the broad oleyl resonances are linked to species with a diffusion coefficient that is markedly smaller than the self-diffusion coefficient of toluene. A detailed analysis of the signal intensity as a function of the field gradient

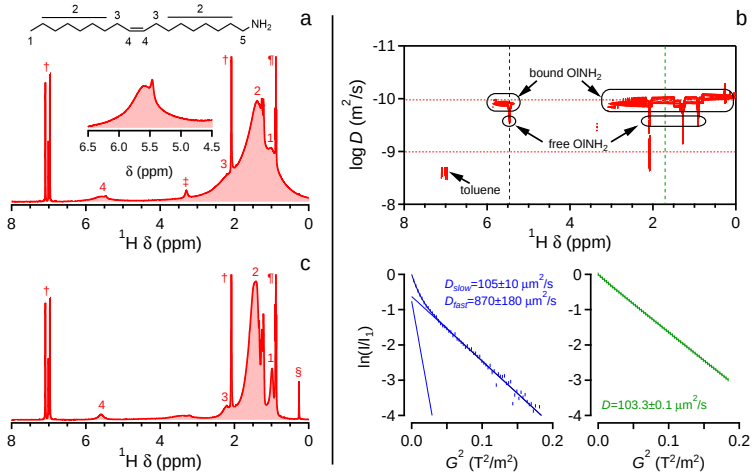

Figure 4.2: (a) 1D ^{1}H NMR spectrum of Cu NCs capped with $\mathrm{OlNH_2}$ in toluene-d_8. (b) (top) DOSY NMR spectrum of the same Cu NC dispersion and (bottom) decay of the signal intensity as a function of the square of the field gradient strength as obtained at chemical shifts as indicated with dashed lines in the DOSY spectrum. (c) 1D ^{1}H NMR spectrum of Cu NCs capped with $\mathrm{OlNH_2}$ after air exposure. Labeled resonances are identified as (1-5) $\mathrm{OlNH_2}$ resonances, (‡) residual methanol, (¶) hexane, (†) toluene-d_8 and (§) silicon grease.

strength at around 1.7 ppm – a chemical shift where only the broad $\mathrm{OlNH_2}$ resonance is observed – yields a diffusion coefficient of $103.3 \pm 0.1\ \mu\mathrm{m}^2/\mathrm{s}$ (see Figure 4.2b). In toluene, such a diffusion coefficient corresponds to a solvodynamic diameter of $7.16 \pm 0.01\mathrm{nm}$. Since this number corresponds to the sum of the NC diameter (4.0 nm) and twice the estimated length of an oleyl chain ($1.5 - 2.0$ nm), we conclude that in the case of Cu NCs, $\mathrm{OlNH_2}$ acts as a tightly bound ligand.

As shown in the inset of Figure 4.2a, the signal of the alkene protons feature next to the broad resonance of bound $\mathrm{OlNH_2}$ a more narrow resonance. According to the DOSY spectrum, this latter resonance comes with a larger diffusion coefficient than bound $\mathrm{OlNH_2}$. This point can be clearly seen in the decay of the resonance intensity with increasing field gradient strength as shown in Figure 4.2b. As shown in the bottom section of Figure 4.2b, fitting the intensity decay to a bi-exponential, yields a diffusion coefficient of the slow and the fast component of $105 \pm 10\,\mu\mathrm{m}^2/\mathrm{s}$ and $870 \pm 180\,\mu\mathrm{m}^2/\mathrm{s}$. Since the latter value is only slightly smaller than the diffusion coefficient of

Table 4.1: Full width at half maximum of 3 selected resonances of the oleyl chain as measured on dispersions of as-synthesized and oxidized Cu NCs, and a dispersion of CdSe NCs in toluene-d_8.

Resonance	Cu as-synthesized	Cu oxidized	CdSe as-synthesized
2	400 Hz	145 Hz	140 Hz
4	235 Hz	85 Hz	75 Hz
1	NA	50 Hz	42.5 Hz

$OlNH_2$ in toluene ($1022 \pm 4 \mu m^2/s$), we conclude that this resonance pertains to free $OlNH_2$ in the Cu NC dispersion.

The most striking feature of the spectrum shown in Figure 4.2a is the excessive broadening of the oleyl resonances, in line with the previous study of Glaria *et al.*[8]. As shown in Table 4.1, the alkene proton resonance **2** at 5.58 ppm has a full width at half maximum of 235 Hz, whereas the bulk methylene resonance **1** and the methyl resonance **3** yield one broad resonance that is 400 Hz wide. These numbers are about 3 times larger than the corresponding resonances in the case of semiconductor NCs, such as CdSe (see Appendix A.1.2). Possibly, this line broadening results from both the different magnetic environments experienced by $OlNH_2$ when bound to Cu NCs and the paramagnetic contribution of the Cu NCs.[9] Even if Cu^0 is considered diamagnetic, the presence of an unpaired electron can result in frequency shifts due to chemical shielding.[10] A study with electron paramagnetic resonance spectroscopy might have been appropriate to assess the paramagnetic nature of the nanocrystals.

Despite the pronounced line broadening, the alkene proton resonance **4** remains well resolved, and based on its integrated intensity, we estimated that the sample analyzed here has a surface concentration of bound $OlNH_2$ of $1.4\,nm^{-2}$. As compared to semiconductor NCs, which often have ligand surface concentrations in the range $3.0 - 5.0\,nm^{-2}$, this number is rather low. Possibly, this is due to the significant line broadening, which can make that the resonance intensity is partially lost in the background noise. On the other hand, such surface concentrations are not unrealistic, since they suffice to preserve colloidal stability.[2]

Figure 4.2c displays the ^1H NMR spectrum of a dispersion of Cu NCs in toluene-d_8 that was opened to air after sample preparation. As compared to the spectrum shown in Figure 4.2a, one sees that oxidation results in a significant narrowing of the resonances of bound $OlNH_2$, which now feature line

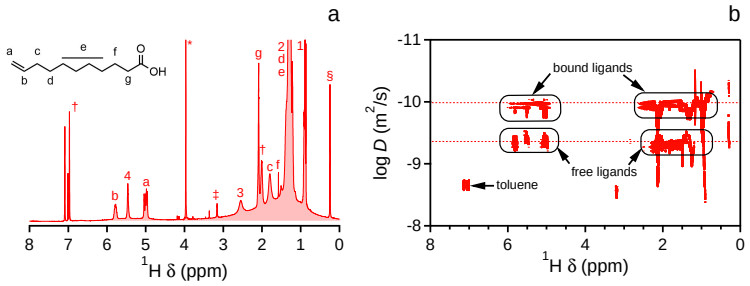

Figure 4.3: (a) 1D ^{1}H NMR spectrum of Cu NCs after addition of UDA in toluene-d_8. (b) DOSY NMR spectrum of the same Cu NCs dispersion. Labeled resonances are identified as (a-g) UDA signals, (1-5) $OlNH_2$ signals, (*) dibromomethane, (§) residual grease, (‡) methanol and (†) toluene-d_8.

widths comparable to what is typically recorded for semiconductor NCs (see Table 4.1). Importantly, we proved that oxidation does not affect the diffusion coefficient of the $OlNH_2$ resonances as shown in the Appendix A.1.3, *i.e.*, $OlNH_2$ remains a tightly bound ligand even in Cu_2O NCs. This suggests that the narrowing of the $OlNH_2$ resonances upon oxidation is not caused by bound $OlNH_2$ assuming a different physical state. However, it may reflect the loss of the specific magnetic environment of Cu NCs upon oxidation, with the resulting Cu_2O NCs being a diamagnetic material similar to the CdSe NCs we used as a reference in Table 4.1.

Among the signals assigned to methanol and hexane, the behavior of the methanol (MeOH) resonance stands out. The resonance is broadened and shifted from its expected position, which suggests that it interacts with the NC surface. Support for this hypothesis comes from the DOSY spectrum, where the MeOH resonance comes with a diffusion coefficient of $166 \pm 18\ \mu m^2/s$. That changes after oxidation of the particles, which results in a marked increase of the diffusion coefficient, up to a value of $D = 1046 \pm 145\,\mu m^2/s$. As this number remains well below the diffusion coefficient of MeOH in toluene, which was determined at $2834 \pm 41\,\mu m^2/s$, this indicates that the MeOH still interacts, albeit more weakly, with oxidized Cu NCs.

4.3.3 Carboxylic Acids as Ligands for Cu Nanocrystals

To have more versatility to design the ligand shell of Cu NCs, we analyzed the exchange of the originally present $OlNH_2$ ligands for carboxylic acids, a class of ligands widely used with semiconductor and metal oxide NCs.

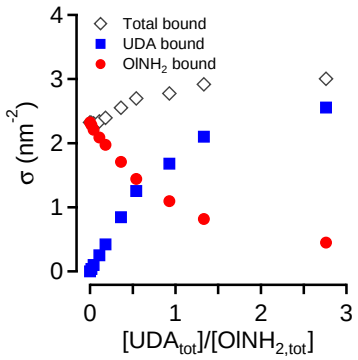

Figure 4.4: Evolution of the bound ligands in the surface of Cu NCs during the progressive addition of UDA on $OlNH_2$-capped NCs.

To monitor the possible exchange of $OlNH_2$ for carboxylic acids, we used undecenoic acid (UDA) as the carboxylic acid of choice since it features two distinct alkene resonances that show little overlap with the resonances of $OlNH_2$ (detailed resonance assignment available in the Appendix A.1.4). As shown in Figure 4.3a, addition of UDA gave rise to several new signals in the ^{1}H NMR spectrum of as-synthesized Cu NCs. The multiple narrow resonances in the aliphatic region can be attributed to protons of both UDA and $OlNH_2$, as indicated. Interestingly, upon adding the carboxylic acid, the appearance of the alkene resonance of $OlNH_2$ at 5.58 ppm changed dramatically. The initially broad resonance has been mostly replaced by a narrow resonance at 5.47 ppm. Such a change points towards the release of the bound $OlNH_2$ from the Cu surface. Finally, the characteristic alkene resonances of UDA show up as narrow signals 4.98 and 5.78 ppm on top of a broad background feature. The DOSY spectrum shown in Figure 4.3b confirms that the signals of the alkene resonances of both UDA and $OlNH_2$ come with two distinct diffusion coefficients; a small diffusion coefficient characteristic of surface-bound ligands, and a larger diffusion coefficent that is consistent with a pool of free ligands. Interestingly, also the diffusion coefficient of MeOH markedly increases after UDA addition, up to a value characteristic of free MeOH. We thus conclude that addition of a carboxylic acid such as UDA induces the release $OlNH_2$ from the Cu NC surface and suppresses the interaction of MeOH with this surface.

To evaluate in more detail the relation between UDA addition and $OlNH_2$ release, we titrated a purified dispersion of as-synthesized, $OlNH_2$-capped Cu NCs with UDA. As shown in Figure 4.4, we started in this case with Cu NCs having a bound $OlNH_2$ surface concentration σ_{OlNH_2} of 2.3 nm^{-2}, and

added up to 3 equiv of UDA, relative to the initial $OlNH_2$ concentration. It can be seen from Figure 4.4 that in the initial stages of the titration, UDA exchanges almost quantitatively for $OlNH_2$. Further increasing the amount of UDA in the dispersion leads to a progressive enrichment of the ligand shell in bound UDA, yet adding 1 equiv of UDA does not suffice to remove all $OlNH_2$. Nevertheless, it can be seen from Figure 4.4 that the increase of bound UDA in the ligand shell resembles reasonably well the loss of bound $OlNH_2$ across the entire titration curve.

4.3.4 Model 1, One-by-one Ligand Exchange

4.3.4.1 Description of the Thermodynamic Equilibrium

A first model to describe the effect of UDA addition on the bound $OlNH_2$ involves a one-to-one exchange in which bound $OlNH_2$ is substituted for bound UDA:

$$(\mathrm{Cu})[\mathrm{OlNH_2}] + \mathrm{UDA} \rightleftharpoons (\mathrm{Cu})[\mathrm{UDA}] + \mathrm{OlNH_2} \tag{4.1}$$

Using subscripts b and f to indicate bound and free ligands and denoting both ligands by L and M, respectively, this equilibrium can be written more compactly as:

$$\mathrm{L}_b + \mathrm{M}_f \rightleftharpoons \mathrm{M}_b + \mathrm{L}_f \tag{4.2}$$

Table 4.2: Mass balance for the exchange between bound L and bound M as described by Eq 4.2, assuming an initial concentration of bound L and free M.

Extent of Reaction	$[\mathrm{L}_b]$	$[\mathrm{L}_f]$	$[\mathrm{M}_b]$	$[\mathrm{M}_f]$
0	$[\mathrm{L}_0]$	0	0	$[\mathrm{M}_0]$
α	$-\alpha$	α	α	$-\alpha$
Concentration	$[\mathrm{L}_0]-\alpha$	α	α	$[\mathrm{M}_0]-\alpha$

Assuming ideal dilute solutions and Langmuir adsorption, we take molar concentrations as the activity of the free ligands and fractional surface occupations as the activity of bound ligands. Since we have equal numbers of bound species at both sides of Eq 4.2, the ratio of the fractional surface occupation will be identical to the ratio of the overall concentration of the respective bound ligands in the sample. Accordingly, we can write the equilibrium equation as:

$$\frac{[\mathrm{M}_b][\mathrm{L}_f]}{[\mathrm{L}_b][\mathrm{M}_f]} = K \tag{4.3}$$

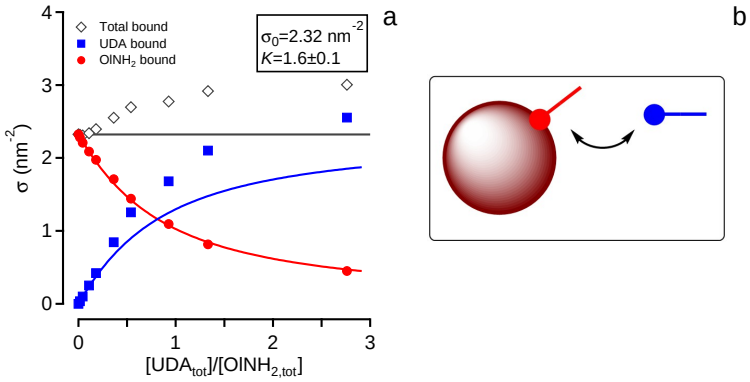

Figure 4.5: (a) Representation of (markers) the experimental titration of $\mathrm{OlNH_2}$-capped Cu nanocrystals with UDA and (full lines) a simulation of the $\mathrm{OlNH_2}$/UDA titration according to the one-by-one exchange model. The annotation provides the initial surface concentration σ_0 of bound $\mathrm{OlNH_2}$ and the equilbrium constant K as determined from a best fit of the surface concentration of bound $\mathrm{OlNH_2}$ to Eq 4.4. (b) Graphical representation of the one-by-one exchange model.

Finally, assuming initial conditions for the different species and the corresponding mass balance as indicated in Table 4.2, this equation can be written in terms of the extent of the reaction α as:

$$K = \frac{\alpha^2}{([\mathrm{L}_0] - \alpha)([\mathrm{M}_0] - \alpha)} \tag{4.4}$$

By solving Eq 4.4 for α and using the mass balance, the concentrations $[\mathrm{L}_b]$ and $[\mathrm{M}_b]$ of bound ligands can be obtained as a function of the total concentration of M in the dispersion.

By identifying $[\mathrm{L}_0]$ with the initial concentration of bound $\mathrm{OlNH_2}$ and $[\mathrm{M}_0]$ with the total concentration of UDA added, we used this model to simulate the concentration of bound $\mathrm{OlNH_2}$ and bound UDA throughout the titration of a dispersion of $\mathrm{OlNH_2}$-capped Cu nanocrystals by UDA additions. The result is represented in Figure 4.5. Here, we converted concentrations into surface concentrations and we used an equilibrium constant K as obtained from fitting the evolution of the bound $\mathrm{OlNH_2}$ concentration to Eq 4.4. Using the mass balance (see Table 4.2), the concentration of bound UDA can be calculated at each states of the titration from the bound $\mathrm{OlNH_2}$ concentration. As can be seen, this yields a good description of the release of UDA in the initial stages of the titration. However, the approach underestimate the amount of bound UDA with increasing additions of UDA to the

dispersion. This is intrinsic to Eq 4.1, which describes an exchange process where the total concentration of bound ligands remains constant. For the experimental titration, this is not the case.

4.3.4.2 The Ligand Shell Composition at Low UDA Concentrations

Although the one-to-one exchange model failed to describe the experimental data at higher UDA concentration, it does account for the quantitative exchange between bound $OlNH_2$ and added UDA at low UDA concentrations. To show that this initial behavior is an intrinsic property of the one-to-one exchange model, we analyzed the solutions to Eq 4.4 in the limit $[M_0] \to 0$. In this case, also the extent of the reaction α will go the zero, such that we can expand α as a Taylor series in $[M_0]$ without constant term:

$$\alpha = \alpha_1[M_0] + \frac{\alpha_2}{2}[M_0]^2 \tag{4.5}$$

Entering this expansion in Eq 4.4 and keeping only terms that contribute up to second order in $[M_0]$, we obtain:

$$\frac{\alpha_1^2[M_0]^2}{([L_0] - \alpha_1[M_0])((1-\alpha_1)[M_0] - \frac{\alpha_2}{2}[M_0]^2)} = K \tag{4.6}$$

In Eq 4.6, the numerator of the reaction quotient scales with $[M_0]^2$. To obtain a non-zero, finite equilibrium constant, the denominator in the reaction quotient must scale with $[M_0]^2$ as well. Hence, we have:

$$\alpha_1 = 1 \tag{4.7}$$

Since for small UDA concentrations, the linear term in Eq 4.5 will dominate, the extent of the reaction becomes based on Eq 4.7:

$$\alpha = [M_0] \tag{4.8}$$

Using the mass balance (Table 4.2), we thus obtain:

$$[M_b] = [M_0] \tag{4.9}$$

$$[L_b] = [L_0] - [M_0] \tag{4.10}$$

In agreement with the isotherms shown in Figure 4.5, we thus find that at low concentration of UDA, the one-by-one exchange model predicts a quantitative exchange between bound $OlNH_2$ and free UDA.

4.3.5 Model 2, Competition for Homogeneous Binding Sites

4.3.5.1 Description of the Thermodynamic Equilibrium

The increase in ligand coverage throughout the UDA titration suggests that the Cu nanocrystals offer binding sites for UDA that were initially not occupied by $OlNH_2$. Since UDA can quantitatively displace $OlNH_2$, one could assume that $OlNH_2$ can also bind to these initially empty surface sites. Taking this perspective, the variation of the ligand shell composition during a UDA titration can be described by a set of two coupled adsorption equilibria, a first describing $OlNH_2$ binding and a second describing UDA binding, that involve a single type of surface site. Hence our description of this model as a competition for homogeneous binding sites.

$$\mathrm{UDA} + (\mathrm{Cu})[\circ] \rightleftharpoons (\mathrm{Cu})[\mathrm{UDA}] \tag{4.11}$$

$$\mathrm{OlNH_2} + (\mathrm{Cu})[\circ] \rightleftharpoons (\mathrm{Cu})[\mathrm{OlNH_2}] \tag{4.12}$$

Writing again the two ligands as L and M and indicating free surface sites as S, the competition for homogeneous binding sites can be expressed by the following set of reaction equations:

$$\mathrm{L}_f + \mathrm{S} \rightleftharpoons \mathrm{L}_b \tag{4.13}$$

$$\mathrm{M}_f + \mathrm{S} \rightleftharpoons \mathrm{M}_b \tag{4.14}$$

Referring to the coupled mass balance outlined in Table 4.3, these equilib-

Table 4.3: Mass balance in the case of competition between homogeneous binding sites as expressed by Eqs 4.13 and 4.14. The extent of these respective reactions have been written as α and β, respectively.

Extent of Reaction	$[\mathrm{L}_b]$	$[\mathrm{L}_f]$	$[\mathrm{M}_b]$	$[\mathrm{M}_f]$	$[\mathrm{S}]$
0	0	$[\mathrm{L}_0]$	0	$[\mathrm{M}_0]$	$[\mathrm{S}_0]$
α	α	$-\alpha$	0	0	$-\alpha$
β	0	0	β	$-\beta$	$-\beta$
Concentration	α	$[\mathrm{L}_0]-\alpha$	β	$[\mathrm{M}_0]-\beta$	$[\mathrm{S}]-\alpha-\beta$

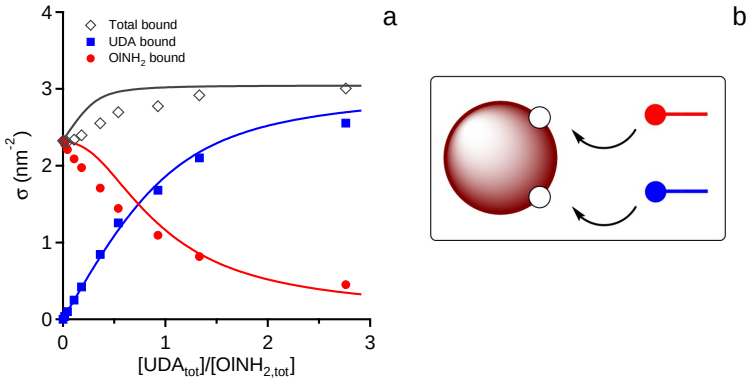

Figure 4.6: (a) Representation of (markers) the experimental titration of $OlNH_2$-capped Cu nanocrystals with UDA and (full lines) a simulation of the $OlNH_2$/UDA titration assuming competition for homogeneous surface sites. Here, the parameters were set so as the fit the surface concentration of bound UDA. (b) Graphical representation of the homogeneous exchange model.

rium reactions yield a set of 2 coupled equilibrium equations:

$$K_L = \frac{\alpha}{([\mathrm{L}_0] - \alpha)([\mathrm{S}_0] - \alpha - \beta)} \tag{4.15}$$

$$K_M = \frac{\beta}{([\mathrm{M}_0] - \beta)([\mathrm{S}_0] - \alpha - \beta)} \tag{4.16}$$

This set of equations can be numerically solved for α and β, which yields in combination with the mass balance the variation of $[\mathrm{L}_b]$ and $[\mathrm{M}_b]$ as a function of $[\mathrm{M}_0]$.

Figure 4.6 represents the evolution of the surface concentration of bound $OlNH_2$ and bound UDA as a function of the amount of UDA added to a dispersion of $OlNH_2$ stabilized Cu nanocrystals. Here, K_L was determined from Eq 4.15 using the initial concentration of bound and free $OlNH_2$ in the absence of any additional UDA – so taking α as the intial bound $OlNH_2$ concentration and β as 0 – while we used the limiting concentration of bound UDA to estimate $[\mathrm{S}_0]$. Next, we adjusted K_M such that the binding of UDA as a function of the total UDA concentration agrees with the experimental data. As can be seen in Figure 4.6, this approach can account for the eventual increase in ligand surface concentration, yet it fails at describing the initial quantitative displacement of bound $OlNH_2$ by UDA.

4.3.5.2 The Ligand Shell Composition at Low UDA Concentrations

To understand better the evolution of the ligand shell composition at low UDA concentrations with the competition for homogeneous binding sites model, we again looked at the equilibrium equations 4.15 and 4.16 in the limit $[M_0] \to 0$. Also in this case, this analysis starts from an expansion of the extent of both reactions as a function of $[M_0]$:

$$\alpha = \alpha_0 + \alpha_1[M_0] + \frac{\alpha_2}{2}[M_0]^2 \tag{4.17}$$

$$\beta = \beta_1[M_0] + \frac{\beta_2}{2}[M_0]^2 \tag{4.18}$$

Here, we took L for $OlNH_2$ and M for UDA and took into account that reaction 4.13 is shifted towards bound $OlNH_2$ prior to UDA addition (so $\alpha_0 \neq 0$) whereas reaction 4.14 cannot proceed in the absence of UDA (so $\beta_0 = 0$).
Using the above expansions, and keeping only terms that will contribute up to second order in $[M_0]$, Eq 4.16 can be rewritten as:

$$K_M = \frac{\beta_1[M_0]}{(1-\beta_1)[M_0]([S_0] - \alpha_0 - \alpha_1[M_0] - \beta_1[M_0])} \tag{4.19}$$

Looking at the term that is zero order in $[M_0]$, Eq 4.19 yields β_1 as:

$$\beta_1 = \frac{K_M([S_0] - \alpha_0)}{1 + K_M([S_0] - \alpha_0)} \tag{4.20}$$

In the same way, Eq 4.15 can expressed using the expansion of α and β as:

$$K_L = \frac{\alpha_0 + \alpha_1[M_0]}{([L_0] - \alpha_0 - \alpha_1[M_0])([S_0] - \alpha_0 - \alpha_1[M_0] - \beta_1[M_0])} \tag{4.21}$$

Here, we have retained all the terms in the reaction quotient that will contribute up to first order in $[M_0]$. Since α_0 must take the value that solves Eq 4.15 in the absence of any M, Eq 4.21 can be rewritten as:

$$K_L = K_L \frac{1 + \frac{\alpha_1[M_0]}{\alpha_0}}{\left(1 - \frac{\alpha 1[M_0]}{[L_0]-\alpha_0}\right)\left(1 - \frac{\alpha_1[M_0]}{[S_0]-\alpha_0} - \frac{\beta_1[M_0]}{[S_0]-\alpha_0}\right)} \tag{4.22}$$

Since the right hand side of Eq 4.22 must be constant, the contribution first order in $[M_0]$ must vanish. This condition enables us to express α_1 as a function of β_1:

$$\alpha_1 = -\frac{\beta_1}{1 + \frac{[S_0]-\alpha_0}{\alpha_0} + \frac{[S_0]-\alpha_0}{[L_0]-\alpha_0}} \tag{4.23}$$

According to Eq 4.23, $|\alpha_1|$ will always be smaller than $|\beta_1|$, which implies that more UDA will bind than $OlNH_2$ will release upon increasing the concentration of UDA. Moreover, we typically start from dispersions where most of the $OlNH_2$ is bound, *i.e.*, $[L_0] \approx \alpha_0$. Accordingly, the denominator at the right hand side of Eq 4.23 will be signficantly larger than 1, which implies that $|\alpha_1| \ll |\beta_1|$. This is indeed what we see in the simulations represented in Figure 4.6, where the initially added UDA binds without inducing any significant release of the originally bound $OlNH_2$. This behavior at low UDA concentration is not in agreement with the experimental observation, which suggests that a model implementing a competition for homogeneous binding sites does not accurately describe the exchange of $OlNH_2$ for UDA at the surface of Cu nanocrystals.

4.3.6 Model 3, Heterogeneous Binding Sites

4.3.6.1 Description of the Thermodynamic Equilibrium

The exchange models developed in section 4.3.4 and 4.3.5 both lead to a partial description of the actual $OlNH_2$/UDA titration. Whereas the one-by-one ligand exchange does account for the initial quantitative exchange between bound $OlNH_2$ and added UDA, it fails to describe the increase in overall ligand surface concentration when more UDA is added. The model based on competition for homogeneous binding sites, on the other hand, does allow for an increase of the ligand surface concentration, yet it fails to describe the initial release of bound $OlNH_2$ upon addition of UDA. Both aspects can be, however, comprehensively described under the assumption that the additional binding sites can bind UDA, yet have no affinity for binding $OlNH_2$.

Table 4.4: Mass balance in the case of competetion between homogeneous binding sites as expressed by Eqs 4.13 and 4.14. The extent of these respective reactions have been written as α and β, respectively.

Extent of Reaction	$[L_b]$	$[L_f]$	$[M_b]$	$[M_b^\star]$	$[M_f]$	$[S^\star]$
0	$[L_0]$	0	0	0	$[M_0]$	$[S_0^\star]$
α	$-\alpha$	α	α	0	$-\alpha$	0
β	0	0	0	β	$-\beta$	$-\beta$
Concentration	$[L_0]-\alpha$	α	α	β	$[M_0]-\alpha-\beta$	$[S_0^\star]-\beta$

$$\mathrm{UDA} + (\mathrm{Cu})[\mathrm{OlNH_2}] \rightleftharpoons (\mathrm{Cu})[\mathrm{UDA}] + \mathrm{OlNH_2} \tag{4.24}$$

$$\mathrm{UDA} + (\mathrm{Cu})[\circ] \rightleftharpoons (\mathrm{Cu})[\mathrm{UDA}] \tag{4.25}$$

Sticking to the L and M notation, this model can be again expressed by a set of two chemical equilibrium reactions:

$$\mathrm{M}_f + \mathrm{L}_b \rightleftharpoons \mathrm{M}_b + \mathrm{L}_f \tag{4.26}$$

$$\mathrm{M}_f + \mathrm{S}^\star \rightleftharpoons \mathrm{M}_b^\star \tag{4.27}$$

Here, the superscript $\star$ denotes the additional binding sites that show affinity for M but not for L.
The equilibrium expressed by Eqs 4.26 and 4.27 can once more be translated into a set of two coupled equilibrium equations. Using the coupled mass balance (see Table 4.4), these read:

$$K_1 = \frac{\alpha^2}{([\mathrm{L}_0] - \alpha)([\mathrm{M}_0] - \alpha - \beta)} \tag{4.28}$$

$$K_2 = \frac{\beta}{([\mathrm{S}_0^\star] - \beta)([\mathrm{M}_0] - \alpha - \beta)} \tag{4.29}$$

Taking into account that the surface coverage only increases from $2.3\,\mathrm{nm}^2$ to $3.0\,\mathrm{nm}^2$ upon addition of UDA and that the initial stage of the titration is well described using the one-by-one exchange model, we will look at Eqs 4.28 and 4.29 under the condition $\beta \ll \alpha$. Under these conditions, the equilbrium equations become:

$$K_1 = \frac{\alpha^2}{([\mathrm{L}_0] - \alpha)([\mathrm{M}_0] - \alpha)} \tag{4.30}$$

$$K_2 = \frac{\beta}{([\mathrm{S}_0^\star] - \beta)([\mathrm{M}_0] - \alpha)} \tag{4.31}$$

Note that in this case, $[\mathrm{L}_b]$ is decoupled from the binding of UDA to the additional sites $\mathrm{S}^\star$. Moreover, as Eq 4.30 is identical to Eq 4.4, $[\mathrm{L}_b]$ will follow the same evolution with increasing UDA concentration as in the one-by-one exchange model.

Figure 4.7 shows the result of a simulation of the experimental titration to this heterogeneous binding site exchange model. Here, we determined K_1 from a best fit of the bound $\mathrm{OlNH_2}$ concentration to Eq 4.30, using the UDA concentration as the independent variable and taking $[\mathrm{L}_0]$ is the initial bound $\mathrm{OlNH_2}$ concentration. Next, K_2 was determined from a best

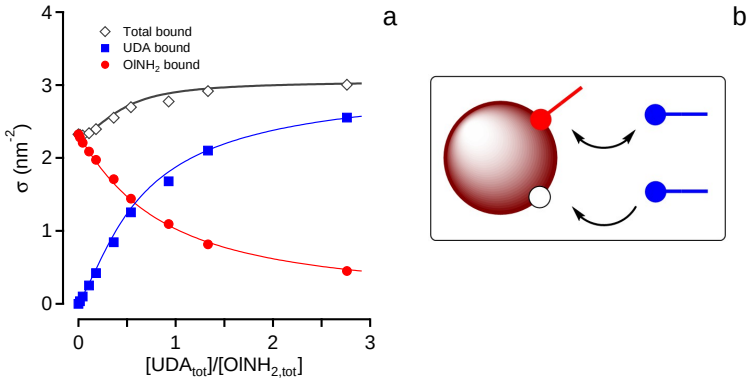

Figure 4.7: (a) Representation of (markers) the experimental titration of $OlNH_2$-capped Cu nanocrystals with UDA and (full lines) a simulation of the $OlNH_2$/UDA titration according to the model assuming additional sites that exclusively bind UDA. Here, K_1 was chosen so as the fit the surface concentration of bound $OlNH_2$ and the other parameters, notably K_2 and $[S_0^\star]$ were fitted to the experimental variation of the bound UDA concentration. (b) Graphical representation of the heterogeneous exchange model.

fit of the excess of bound UDA, *i.e.*, β or the part of bound UDA that did not replace bound $OlNH_2$, to Eq 4.29. Here, we used the concentration of free UDA, *i.e.*, $[M_0] - \alpha - \beta$ as the independent variable, and took $[S_0^\star]$ is a second fitting parameter. The different fitting parameters thus obtained have been listed in Table 4.5.

Table 4.5: Best fit values for the parameters K_1, K_2 and $[S_0^\star]$ as obtained from fitting the experimental bound $OlNH_2$ and bound UDA concentration during a UDA titration using the heterogeneous binding site model. $[S_0^\star]$ has been expressed as a surface concentration $\sigma_{S_0^\star}$.

Parameter	K_1	K_2	$\sigma_{S_0^\star}$ (nm^{-2})
Best fit	1.6 ± 0.1	$(4 \pm 1)\ 10^5$	0.75

4.3.6.2 The Ligand Shell Composition at Low UDA Concentrations

We formulated the condition $\beta \ll \alpha$ based on the observation that the number of additional binding sites is considerably smaller than the number of sites binding $OlNH_2$. This, however, does not warrant that the same condition applies at low UDA concentration. To verify this, we return to the original set of equilibrium equations (Eqs 4.28 and 4.29) and solve them again in the limit $[M_0] \to 0$ by introducing series expansions for α and β:

$$\alpha = \alpha_1[M_0] + \frac{\alpha_2}{2}[M_0]^2 \tag{4.32}$$

$$\beta = \beta_1[M_0] + \frac{\beta_2}{2}[M_0]^2 \tag{4.33}$$

Entering these expressions in Eqs 4.28 and 4.29 and keeping terms that contribute up to second order in $[M_0]$, we obtain:

$$K_1 = \frac{\alpha_1^2[M_0]^2}{([L_0] - \alpha_1[M_0])\left((1 - \alpha_1 - \beta_1)[M_0] - \frac{\alpha_2+\beta_2}{2}[M_0]^2\right)} \tag{4.34}$$

$$K_2 = \frac{\beta_1[M_0] + \frac{1}{2}\beta_2[M_0]^2}{([L_0] - \alpha_1[M_0])\left((1 - \alpha_1 - \beta_1)[M_0] - \frac{\alpha_2+\beta_2}{2}[M_0]^2\right)} \tag{4.35}$$

To avoid the reaction quotient in Eq 4.34 from diverging or reaching 0 in the limit $[M_0] \to 0$, we have:

$$\alpha_1 + \beta_1 = 1 \tag{4.36}$$

Combining this relation with the same requirement that the reaction quotient in Eq 4.35 yields a finite, non-zero number, we have:

$$\beta_1 = 0 \tag{4.37}$$

Hence, we find that in the limit $[M_0] \to 0$, α will scale proportional to $[M_0]$, whereas β will scale with $[M_0]^2$. Hence, the condition $\beta \ll \alpha$ will always apply in the limit $[M_0] \to 0$. This means that one-by-one exchange as expressed by Eq 4.26 will always describe the first stages of the heterogeneous model developed in this section; a point in agreement with the experimental $OlNH_2$/UDA titration.

We thus conclude that the addition of a carboxylic acid such as UDA to $OlNH_2$-capped Cu NCs has two effects; as described by the equilibrium reactions 4.24 and 4.25, UDA both exchanges with bound $OlNH_2$ and binds to empty sites at the Cu NC surface. From the equilibrium constants obtained

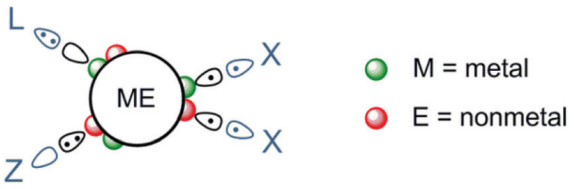

Figure 4.8: Schematic representation of the covalent bond classification. X-type ligands are one-electron donors, L-type ligand are Lewis bases and Z-type ligands are Lewis acids. Reprinted from reference [11]

from a best fit of this so-called heterogeneous binding site model to the experimental titration curves, we estimate that the free energy change of the UDA/OlNH$_2$ exchange is a mere $-1.1\,\mathrm{kJ}\cdot\mathrm{mol}^{-1}$, whereas the free energy of UDA adsorption amounts to $\sim -30\,\mathrm{kJ}\cdot\mathrm{mol}^{-1}$. This was estimated Note that the increased coverage of binding sites after UDA addition may also account for the observation that UDA addition suppresses the interaction between MeOH and the Cu NC surface.

4.3.7 Binding motif of UDA ligands

Understanding the ligand-surface interaction remains a key question for metal NC research. [12] In the case of semiconductor and metal oxide NCs, significant progress resulted from the introduction of the covalent bond classification to describe ligand binding motifs. [11;13] Here, ligands are classified as L, X or Z depending on the number of electrons the equivalent neutral compound contributes to the ligand-NC bond as shown in Figure 4.8. In this respect, L-type and Z-type ligands are Lewis bases and Lewis acids, that contribute 2 electrons or take two electrons to form the ligand-NC bond, respectively. X-type ligands, on the other hand, are radicals that form a two-electron bond with a NC by bringing in one electron and taking one electron from a NC surface atoms. In practice, this makes X-type ligands often appear as cations or anions, such as aliphatic carboxylates, phosphonates or thiolates.

Since the entire NC-ligand object must be charge neutral in apolar dispersions, [14;15] the negative charge acquired by the X-type ligands is compensated by an excess of metal cations in the case of NCs of binary compounds such as CdSe, PbS or InP. [16–18] A different behavior was reported for metal oxide NCs such as HfO_2. Here, it was found that the binding of a carboxylate was accompanied by the adsorption of a proton at the NC surface,

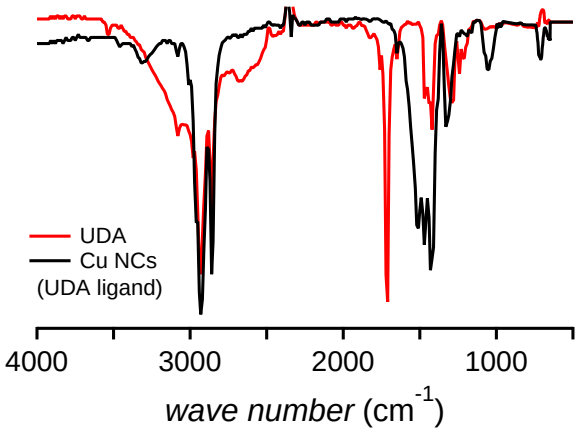

Figure 4.9: Solution FTIR spectra of UDA (red) and Cu NCs after addition of UDA (black).

forming a neutral pair of X-type ligands.[19] In a rare study on binding of secondary phosphine oxide X-type ligands ($R_1R_1PO^\bullet$) to gold NCs on the other hand, it was demonstrated that charge neutrality was ensured by the formation of Au^{1+} surface atoms.[20]

A key difference between the binding of a pair of X-type ligands and a single X-type ligand is the exchange behavior with respect to an L-type ligand such as an alkylamine. The need to preserve charge neutrality prevents such a direct exchange in the case that single X-type ligands are bound to metal-rich binary compounds or, for one thing, partially oxidized pure compounds. As a result, exposure of CdSe or PbS to alkylamines leads to the displacement of entire metal carboxylate moieties.[21] A pair of X-type ligands, on the other hand, can associate to form a neutral moiety that can be exchanged for or displaced by a neutral L-type ligand.[4] Keeping that finding in mind, we investigated the binding of UDA to Cu NCs in more detail.

Figure 4.9 represents the IR spectrum of UDA and of a dispersion of Cu NCs passivated with UDA. As expected, the UDA reference spectrum shows the characteristic signatures of the carboxyl group, including the C=O stretch vibration at 1720 cm^{-1}, the in-plane C-O-H bend vibration at 1420 cm^{-1}, and the C-O stretch vibration at 1300 cm^{-1}. In addition, a broad feature ranging from 3500 to 2500 cm^{-1} can be seen, which can be assigned to the O-H stretch vibration. In the case of the Cu NC dispersion, however, the C=O stretch vibration and the broad feature assigned to the O-H

stretch vibration are notably absent. In addition, new features appear at around 1500 cm^{-1} that are often assigned to both asymmetric and symmetric stretching of a metal-bound carboxylate. Given the requirement that the exchange reaction 4.1 be charge neutral in apolar media, we thus conclude that UDA dissociates upon binding to Cu NCs in a carboxylate and a proton, not unlike the binding motif carboxylic acids feature upon interaction with metal oxide NCs.

4.4 Surface chemistry model

Figure 4.10 summarizes the conclusions of the above sections in a surface chemistry model of Cu NCs. As synthesized Cu NCs have a capping consisting of tightly bound $OlNH_2$ that interacts as an L-type ligand with acidic surface sites, which we interpret as surface-bound Cu^{1+}. This result is not unlikely, Cu is a known oxygen scavenger and little presence of O_2 in solvents or environment can result in slight superficial oxidation. While alkylamines are weak, dynamic ligands for binary compounds such as CdSe and PbS,[3] octadecyalamine and oleylamine were shown to bind tightly to Cu^{1+} compounds such as $CuInS_2$.[22] As outlined in Figure 4.4, exposure of $OlNH_2$-capped Cu NCs to UDA results in the replacement of $OlNH_2$ by dissociated UDA at these copper oxide surface sites. This outcome agrees with previous studies on ligand binding to Cu_2O, where it was shown that the interaction of oleic acid with Cu_2O leads to the formation of strongly bound oleate.[23] Finally, the surface chemistry model represented in Figure 4.10 also includes the addition of UDA to unoccupied copper oxide sites, a process that accounts for the observed increase in ligand surface concentration upon UDA exposure. This latter point suggests that, in line with recent studies on CdSe NCs,[24–26] Cu NCs offer a heterogeneous set of binding sites, where some have little affinity for $OlNH_2$ while still binding UDA. This miscellaneous surface composition is allegedly causing the polydispersity of the NCs size distribution that provides a set of facets where organic ligands can bind with different affinities.[27]

As most metals are prone to oxidation, controlling the concentration of oxides at the surface of a metal NCs such as Cu is difficult. In a recent study, for example, Cure *et al.* reported that even if alkylamines can strongly suppress the full oxidation of copper NC, initial surface oxidation occurs rapidly.[28] The finding that the surface chemistry of Cu NCs depends on the presence of surface oxides therefore implies that the surface concentration of ligands and the occurrence or not of ligand exchange reactions can strongly depend on synthesis and processing conditions. This conclusion highlights

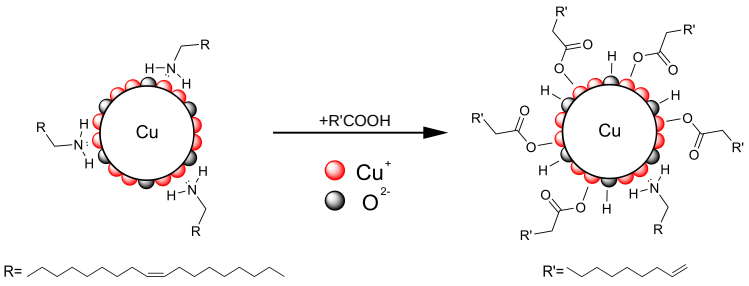

Figure 4.10: Surface chemistry model of the Cu NCs before and after addition of a carboxylic acid. The binding of the carboxylate to the metal is indicative and not meant to represent a specific binding mode.

the case for in-depth surface chemistry studies, where surface termination by ligands is studied as a function of the composition of the NC surface as exemplified by recent work on silver NCs.[29]

4.5 Conclusion

We have presented a comprehensive study of the surface of Cu NCs. We demonstrated that the initially bound $OlNH_2$ can be replaced by a carboxylic acid through mass-action. Based on the thermodynamic description of the amine/carboxylic acid titration curves, we argue that carboxylic acids directly replace $OlNH_2$ and bind to additional surface sites that show little affinity for $OlNH_2$. We proved that carboxylic acids dissociate upon binding on such surfaces, forming an X_2 binding motif. Since such a binding motif requires an amphoteric surface that offers acidic and basic binding sites, we argue that ligand binding to Cu nanocrystals is determined by the presence of surface oxides, rather than by the properties of the pristine metal surface.

References

[1] Alexander Kamyshny and Shlomo Magdassi. *Conductive Nanomaterials for Printed Electronics.* Small, 10(17):3515–3535, 2014.

[2] Ashley M. Smith, Kathryn A. Johnston, Scott E. Crawford, Lauren E. Marbella, and Jill E. Millstone. *Ligand Density Quantification on Colloidal Inorganic Nanoparticles.* Analyst, 142(1):11–29, 2017.

[3] Zeger Hens and Jose C. Martins. *A Solution NMR Toolbox for Characterizing the Surface Chemistry of Colloidal Nanocrystals.* Chem. Mater., 25(8):1211–1221, 2013.

[4] Jonathan De Roo, Yolanda Justo, Katrien De Keukeleere, Freya Van den Broeck, Jose C. Martins, Isabel Van Driessche, and Zeger Hens. *Carboxylic-Acid-Passivated Metal Oxide Nanocrystals: Ligand Exchange Characteristics of a New Binding Motif.* Ang. Chem. Int. Ed., 54(22):6488–6491, 2015.

[5] Xiao Sun, Ya-Wen Zhang, Rui Si, and Chun-Hua Yan. *Metal (Mn, Co, and Cu) Oxide Nanocrystals from Simple Formate Precursors.* Small, 1(11):1081–1086, 2005.

[6] Manjeet Singh, I. Sinha, M. Premkumar, A.K. Singh, and R.K. Mandal. *Structural and Surface Plasmon Behavior of Cu Nanoparticles Using Different Stabilizers.* Colloids Surfaces A Physicochem. Eng. Asp., 359(1-3):88–94, 2010.

[7] Petri Kanninen, Christoffer Johans, Juha Merta, and Kyösti Kontturi. *Influence of Ligand Structure on the Stability and Oxidation of Copper Nanoparticles.* J. Colloid Interf. Sci., 318(1):88–95, 2008.

[8] Arnaud Glaria, Jérémy Cure, Kilian Piettre, Yannick Coppel, Cédric-Olivier Turrin, Bruno Chaudret, and Pierre Fau. *Deciphering Ligands' Interaction with Cu and Cu2O Nanocrystal Surfaces by NMR Solution Tools.* Chemistry, 21(3):1169–78, 2015.

[9] Spartak S. Khutsishvili, Tamara I. Vakul'Skaya, Nadezhda P. Kuznetsova, Tamara G. Ermakova, Alexandr S. Pozdnyakov, and Galina F. Prozorova. *Formation of Stable Paramagnetic Nanocomposites Containing Zero-Valence Silver and Copper in a Polymeric Matrix.* J. Phys. Chem. C, 118(33):19338–19344, 2014.

[10] Lauren E. Marbella and Jill E. Millstone. *NMR techniques for noble metal nanoparticles.* Chem. Mater., 27(8):2721–2739, 2015.

[11] J. De Roo, K. De Keukeleere, Z. Hens, and I. Van Driessche. *From Ligands to Binding Motifs and Beyond; the Enhanced Versatility of Nanocrystal Surfaces.* Dalt. Trans., 45(34):13277–13283, 2016.

[12] Rongchao Jin, Chenjie Zeng, Meng Zhou, and Yuxiang Chen. *Atomically Precise Colloidal Metal Nanoclusters and Nanoparticles: Fundamentals and Opportunities.* Chem. Rev., 116(18):10346–10413, 2016.

[13] Jonathan Owen. *The Coordination Chemistry of Nanocrystal Surfaces.* Science, 347(6222):615–616, 2015.

[14] M Shim and P Guyot-Sionnest. *Permanent Dipole Moment and Charges in Colloidal Semiconductor Quantum Dots.* J. Chem. Phys., 111(15):6955–6964, 1999.

[15] Marco Cirillo, Filip Strubbe, Kristiaan Neyts, and Zeger Hens. *Thermal Charging of Colloidal Quantum Dots in Apolar Solvents: A Current Transient Analysis.* ACS Nano, 5(2):1345–1352, 2011.

[16] Oleksandr Voznyy. *Mobile surface traps in CdSe nanocrystals with carboxylic acid ligands.* J. Phys. Chem. C, 115(32):15927–15932, 2011.

[17] Arnaud Cros-Gagneux, Fabien Delpech, Celine Nayral, Alfonso Cornejo, Yannick Coppel, and Bruno Chaudret. *Surface Chemistry of InP Quantum Dots: A Comprehensive Study.* J. Am. Chem. Soc., 132(51):18147–18157, 2010.

[18] Iwan Moreels, Yolanda Justo, Bram De Geyter, Katrien Haustraete, José C Martins, and Zeger Hens. *Size-Tunable, Bright, and Stable PbS Quantum Dots: A Surface Chemistry Study.* ACS Nano, 5(3):2004–2012, 2011.

[19] Jonathan De Roo, Freya Van Den Broeck, Katrien De Keukeleere, José C. Martins, Isabel Van Driessche, and Zeger Hens. *Unravelling the Surface Chemistry of Metal Oxide Nanocrystals, the Role of Acids and Bases.* J. Am. Chem. Soc., 136(27):9650–9657, 2014.

[20] Israel Cano, Miguel A. Huertos, Andrew M. Chapman, Gerd Buntkowsky, Torsten Gutmann, Pedro B. Groszewicz, and Piet W. N. M. van Leeuwen. *Air-Stable Gold Nanoparticles Ligated by Secondary Phosphine Oxides as Catalyst for the Chemoselective Hydrogenation of Substituted Aldehydes: a Remarkable Ligand Effect.* J. Am. Chem. Soc., 137(24):7718–7727, 2015.

[21] Nicholas C. Anderson, Mark P. Hendricks, Joshua J. Choi, and Jonathan S. Owen. *Ligand Exchange and the Stoichiometry of Metal Chalcogenide Nanocrystals: Spectroscopic Observation of Facile Metal-Carboxylate Displacement and Binding.* J. Am. Chem. Soc., 135(49):18536–18548, 2013.

[22] Ruben Dierick, Freya Van den Broeck, Kim De Nolf, Qiang Zhao, Andre Vantomme, Jose C. Martins, and Zeger Hens. *Surface Chemistry of $CuInS_2$ Colloidal Nanocrystals, Tight Binding of L-Type Ligands.* Chem. Mater., 26(20):5950–5957, 2014.

[23] Douglas R. Kauffman, Paul R. Ohodnicki, Brian W. Kail, and Christopher Matranga. *Selective Electrocatalytic Activity of Ligand Stabilized Copper Oxide Nanoparticles.* J. Phys. Chem. Lett., 2(16):2038–2043, 2011.

[24] Kenneth O. Aruda, Victor A. Amin, Christopher M. Thompson, Bryan Lau, Alexander B. Nepomnyashchii, and Emily A. Weiss. *Description of the Adsorption and Exciton Delocalizing Properties of p-Substituted Thiophenols on CdSe Quantum Dots.* Langmuir, 32(14):3354–3364, 2016.

[25] Emile Drijvers, Jonathan De Roo, Jose C. Martins, Ivan Infante, and Zeger Hens. *Ligand Displacement Exposes Binding Site Heterogeneity on CdSe Nanocrystal Surfaces.* Chem. Mater., 30(3):1178–1186, 2018.

[26] Mersedeh Saniepay, Chenjia Mi, Zhihui Liu, E. Paige Abel, and Remi Beaulac. *Insights into the Structural Complexity of Colloidal CdSe Nanocrystal Surfaces: Correlating the Efficiency of Nonradiative Excited-State Processes to Specific Defects.* J. Am. Chem. Soc., 140(5):1725–1736, 2018.

[27] Aaron Puzder, Andrew J. Williamson, Natalia Zaitseva, Giulia Galli, Liberate Manna, and A. Paul Alivisatos. *The Effect of Organic Ligand Binding on the Growth of CdSe Nanoparticles Probed by Ab Initio Calculations.* Nano Lett., 4(12):2361–2365, 2004.

[28] Jérémy Cure, Arnaud Glaria, Vincent Collière, Pier-Francesco Fazzini, Adnen Mlayah, Bruno Chaudret, and Pierre Fau. *Remarkable Decrease in the Oxidation Rate of Cu Nanocrystals Controlled by Alkylamine Ligands.* J. Phys. Chem. C, 121(ii):acs.jpcc.6b12877, 2017.

[29] Kathryn A. Johnston, Ashley M. Smith, Lauren E. Marbella, and Jill E. Millstone. *Impact of As-Synthesized Ligands and Low-Oxygen Con-*

ditions on Silver Nanoparticle Surface Functionalization. Langmuir, 32(16):3820–3826, 2016.

5

Sintering of Copper Nanocrystals: From Particles to Conductive Films[1]

We analyze the sintering of Cu nanocrystals as a function of two different nanocrystal properties. In the first part we study the transformation into films of 4 nm particles capped with carboxylic acid ligands upon thermal sintering in different gases. We analyze the grain size and reduction temperature of the resulting layer depending on the capping ligand. In the second part we evaluate the transformation of a range of particle sizes and the effect that the sintering temperature has on the conductivity of the final patterns.

5.1 Introduction

In chapter 4, we demonstrated that oleylamine ($OlNH_2$) caps the surface of as-synthesized Cu NCs, which facilitates the formation of stable disper-

[1] *Adapted from:* **Arnau Oliva Puigdomènech**, Jonathan De Roo, Jakob Kuhs, Christophe Detavernier, Jose C. Martins, Zeger Hens. *Ligand Binding to Copper Nanocrystals: Amines and Carboxylic Acids and the Role of Surface Oxides.* Chemistry of Materials, 31 (6), 2058–2067, **2019**.

sions in apolar solvents. We proved by means of NMR spectroscopy that $OlNH_2$ can be replaced by a carboxylic acid, undecenoic acid (UDA), by mass-action. Such exchange reactions are most useful since they enable us to modify the chemical properties of Cu NCs by changing the surface termination. In view of applications in printed electronics, ligand exchange could be used for example to make the NCs compatible with more polar solvents. In addition, we showed in chapter 3 that metallic Cu NCs of different sizes can be obtained through simple changes to the reaction chemistry.

In this chapter, we aim at understanding the relation between NCs properties such as particle size and surface chemistry and the conversion of Cu NCs into conductive layers by thermal annealing. First, we introduce 2-[2-(2-methoxyethoxy)ethoxy]acetic acid (MEEAA) as a ligand that can stabilize Cu NCs in polar media. We then study the relation between the oxidation rate of 4 nm Cu NCs and the surface termination. While different ligands have little impact on the oxidation rate, we find that oxidized Cu NCs can be reduced to metallic Cu by thermal sintering in inert atmosphere. Subsequently, we evaluate the influence of different carboxylic acid ligands on the reduction temperature and on the grain size of the sintered films. Finally, we investigate the relation between the NC size and the transformation behavior during thermal annealing. We find that larger particles are passivated by an initial oxide layer that protects the core from further oxidation, remaining mainly metallic. However, this surface oxide layer is only reduced at higher temperature than small copper oxide NCs. On the other hand, after annealing, films with larger Cu NCs attain a higher conductivity. Such observations highlight the trade-offs involved when changing the Cu NC size, where an improved conductivity is only attained at the expense of a higher conversion temperature.

5.2 Experimental Section

Chemicals. In this work, the following chemicals were used: copper(II) formate tetrahydrate (Alfa Aesar, 98%), oleylamine (Acros Tech, 80-90%), n-dodecane (Merck Millipore, $\leq$99%), acetonitrile (VWR, $\leq$99.5%), n-hexane (VWR, 98%), methanol (VWR, $\leq$99.8%), undecenoic acid (Sigma-Aldrich, 98%), 2-[2-(2-methoxyethoxy)ethoxy]acetic acid (Sigma-Aldrich, technical grade), oleic acid (Sigma-Aldrich, technical grade), deuterated methanol (Sigma-Aldrich, $\leq$99.8%).

NMR analysis. Samples for NMR analysis were prepared by drying the purified reaction product under a nitrogen flow and redispersing the result-

ing powder in toluene-d_8. To prevent oxidation, all purification and sample preparation was performed under an inert atmosphere in a nitrogen-filled glovebox and the samples were loaded in air-tight screw-capped NMR tubes. NMR spectra were recorded either on a Bruker Avance III Ascend Spectrometer operating at a ^{1}H frequency of 500.13 MHz and equipped with a BBI-Z probe or on a Bruker Avance II Spectrometer operating at a ^{1}H frequency of 500.13 MHz and equipped with a TXI-Z probe. The sample temperature was set at 298.15 K. Quantitative ^{1}H spectra were recorded with 20 s delay between scans to ensure full relaxation of all NMR signals and concentrations were determined using the Digital ERETIC method. Diffusion-Ordered Spectroscopy (DOSY) experiments were performed using a double stimulated echo sequence for convection compensation and with monopolar gradient pulses. The diffusion decay was recorded in 64 steps of squared gradient strength from 95% to 2% of the probe's maximum value. The gradient pulse duration and diffusion delay were optimized so as to guarantee at least a 10-fold attenuation of the signal throughout the gradient strength scan.

Ligand Exchange to UDA or OA. In an oxygen-free environment, excess carboxylic acid (5-fold to $OlNH_2$) was added to a dispersion of $OlNH_2$ capped Cu NCs in hexane. After keeping the dispersion at room temperature for 30 minutes, the Cu NCs were precipitated by addition of acetonitrile and methanol as non-solvents and the thus obtained Cu NC powder was redispersed in hexane. This process was repeated a second time, followed by multiple purification cycles.

Ligand Exchange to MEEAA. In an oxygen-free environment, an hexane solution of $OlNH_2$ capped Cu NCs was dried under N_2 flow. After, 2-[2-(2-methoxyethoxy)ethoxy]acetic acid (MEEAA) and methanol were added and the solution was left under stirring until the NCs were fully dispersed in the methanol solution. The resulting solution of MEEAA capped NCs was washed of excess MEEAA and released $OlNH_2$ using a combination of methanol, isopropanol and hexane where the first and second act as solvents and the last as non-solvent.

***In-situ* XRD.** *In-situ* X-ray diffraction (XRD) was used to monitor the sintering of the Cu nanocrystals as a function of temperature. While linearly increasing the temperature of the sample in a controlled ambient, XRD patterns were obtained using a Bruker D8 Discover equipped with a Cu Kα x-ray source and a linear detector. The series of diffractograms were plotted as a function of temperature and diffraction angle using a color-scale map

for the recorded intensities, where red represents a higher intensity. Cu_2O to Cu transition temperature has been determined at the maximum derivative of the integrated intensity of the Cu plane (111) at 43.3°.

***In-situ* Resistance** *In-situ* resistance measurements were performed in a sealed chamber equipped with a 4-point probe and a heating plate. The chamber was flushed and the temperature of the sample increased regularly under a constant flow of N_2. I-V was continuously recorded to fit resistance which was normalized a posteriori by an *ex-situ* 4-point probe.

5.3 Principles of Sintering

Sintering is a processing technique in which metal or ceramic powders are compacted without melting by applying thermal energy. The driving force of this process is the reduction of the total interfacial energy of the system, a phenomenon achieved by coarsening - reducing the solid/solid interfacial area - and densification - reducing the solid/gas interfacial area - (see Figure 5.1).[1;2] The sintering of nanocrystals has unique characteristics that differ from micron-sized powders, such as lower sintering temperature and more pronounced grain growth.[3;4] Moreover, in the nanoscale, the grain growth is usually intertwined with the densification of the coating, resulting in the loss of the singular NC properties. This phenomenon is usually considered a drawback in light of catalysis applications when individual nanoscale effects needs to be preserved,[5] yet proves beneficial for conductive applications when the goal is to obtain a continuous, dense metallic coating where electrons can travel without much resistance.[6]

The presence of an oxide shell plays an important role on the sintering of metals. Whilst some oxide-coated metals such Al, Mg or In will not even undergo densification when sintered at temperatures close to their melting point,[7] a Cu_2O oxide shell increments the necessary energy to sinter the particles and results in the formation of weaker junctions.[8] However, a report from Ramakrishnan *et al*[9] claims that an oxide layer promotes the formation of a more dense layer in micron-scale particles. In this report, it is argued that the reduction of the oxide shell exposes a highly reactive metallic surface which increase the speed of surface migration. Nevertheless, sintering of micron-scale Cu particles under a N_2 atmosphere require temperatures close to 800°C to fully reduce the cuprite shell.[7–9]

The effect of an oxide shell becomes more relevant when sintering nano copper due to the densification occurring at much lower temperatures (150-400°C). This enhanced reactivity may be related to the higher curvature of

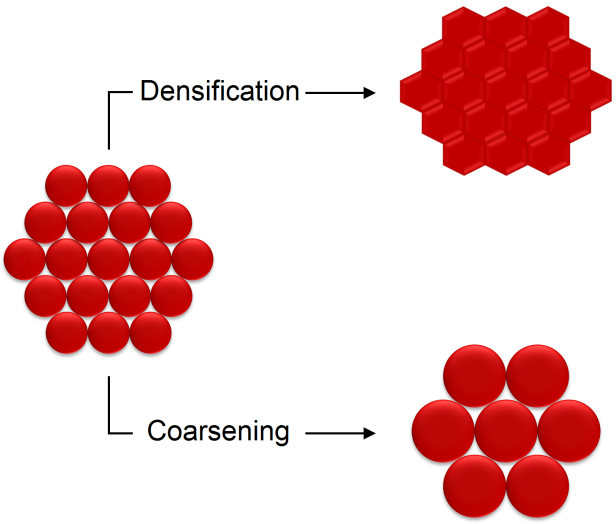

Figure 5.1: Graphical representation of an arrangement of particles undergoing densification and coarsening, the two basic phenomena that lead to sintering.

the NCs, which exposes a large extent of reactive surface defects.[4] Champion *et al*[10] studied the sintering under hydrogen gas of 35 nm copper nanocrystals with a 3 nm oxide shell and concluded that the sintering of the particles starts right after the oxide shell has been reduced, in other words, the presence of oxide controls the densification of the layers. Hence, controlling the reduction of the oxide shell becomes primordial in order to obtain sintered, conductive films. In this chapter, we evaluate the effect of both ligands and particle size on the reduction temperature and we establish a benchmark for the optimal thermal sintering conditions depending on such particle properties.[11]

5.4 Transfer of Cu Nanocrystals to Polar Solvents by Ligand Exchange

Recently, 2-[2-(2-methoxyethoxy)ethoxy]acetic acid (MEEAA) was put forward as a versatile ligand that enables dispersions of semiconductor and

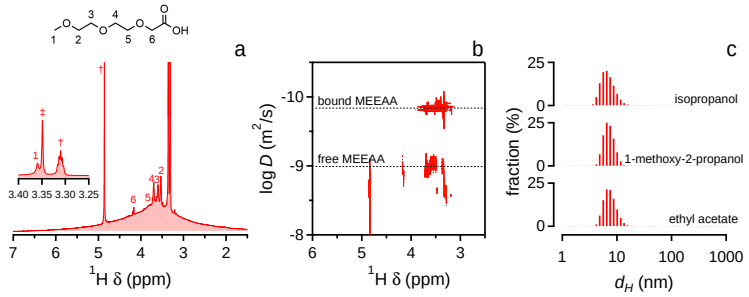

Figure 5.2: (a) 1D ^{1}H NMR of Cu NCs after ligand exchange to MEEAA and dispersed in methanol-d_4. (b) DOSY spectra of the same Cu NCs dispersion. (c) Hydrodynamic diameter distribution by Dynamic light scattering (DLS) of Cu NCs capped with MEEAA in different solvents. Labeled resonances are identified as (1-6) MEEAA resonances, (‡) methanol and (†) residual methanol-d_4.

metal oxide NCs to be stabilized in a variety of solvents, ranging from toluene to water.[12] The replacement of the original $OlNH_2$ ligands by UDA as demonstrated in the previous chapter suggests that MEEAA could be an equally versatile ligand for Cu NCs. As outlined in the Experimental Section, we found that a solution of MEEAA in methanol indeed disperses a dry powder of $OlNH_2$-capped Cu NCs; a dispersion that can be purified using hexane as the non-solvent and methanol or isopropanol as the solvent.

Figure 5.2a-b represents the ^{1}H 1D and DOSY spectrum of a dispersion of Cu NCs in methanol-d_4 prepared as outlined above. It can be readily seen that no resonances of the originally present $OlNH_2$ remain in the 1D ^{1}H NMR spectrum. Instead, a broad signal ranging from 6 to 1.5 ppm is obtained, together with a few superimposed narrow resonances. The latter could be assigned either to MEEAA, methanol or residual methanol-d_4 (see Appendix A.2.1). According to DOSY, the narrow resonances have a diffusion coefficient $D = 805 \pm 18\,\mu m^2/s$, which agrees with the diffusion coefficient of MEEAA in methanol. The broad background resonance, on the other hand, features a markedly smaller diffusion coefficient of $139 \pm 1 \mu m^2/s$, a number corresponding to a hydrodynamic diameter of 5.76 ± 0.01 nm in methanol. Since this figure agrees with the expected for MEEAA-capped Cu NCs, we assign the broad resonance to tightly bound MEEAA. Note that similarly as seen in chapter 4, the resonance is significantly broader than the reported resonances of MEEAA bound to HfO_2 or CdSe NCs.[12]

To highlight the versatility of MEEAA as a ligand to stabilize Cu NCs in

polar solvents, we assessed the particle distribution of nanocolloids made by dispersing MEEAA-capped Cu NCs in ethyl acetate, isopropanol and 1-methoxy-2-propanol using dynamic light scattering (DLS). Figure 5.2c represents the particle size distributions as recorded on dispersions of the same batch of Cu NCs in each of these solvents. A monomodal size distribution is obtained in each case, that systematically attains a maximum at around 7 nm. As this solvodynamic diameter agrees with the value determined using DOSY for MEEAA-capped Cu NCs dispersed in methanol, we conclude that in each of these solvents, a MEEAA capping results in stable dispersions of individual Cu NCs. In this respect, it is worth mentioning that MEEAA has a boiling point of a mere 140°C, as compared to the 360°C of $OlNH_2$. This suggests that upon annealing films of MEEAA stabilized Cu NCs, dense Cu films without organic impurities could be obtained at a relatively low temperature.

5.5 Sintering and Surface Termination

5.5.1 Ligand-Dependent Oxidation of Cu Nanocrystals

We investigated the impact of the different surface ligands introduced in the previous and current chapter on the oxidation of 4 nm Cu NCs studied here. To assess the oxidation rate, unoxidized Cu NCs capped with different ligands were exposed to ambient conditions, after which we regularly recorded the absorbance spectrum of the dispersion. As shown in Figure 5.3a, permanent air exposure induces a rapid redshift of the surface plasmon, a shift we already assigned to Cu oxidation in Figure 4.1c of chapter 4. Similarly, as depicted in Figure 5.3b, the SPR peak area starts decreasing approximately 1 minute after air exposure, indicating a reduction in the size of the metallic Cu core. Probably, this delayed drop of the SPR area results from a trade-off between an increase in the local field – which enhances the absorption coefficient – and a reduction of the Cu volume. Indeed, the initial growth of a Cu_2O shell with a dielectric constant higher than the solvent, n-hexane, (9 and 2.0 respectively) will reduce dielectric screening and thus promote an increase of the SPR area. This effect may compensate for the decrease of the metal Cu core volume during the first instances of the oxidation upon air exposure.[13–15]

Interestingly, oxidation is somewhat slower with Cu NCs capped with carboxylic acids than with oleylamine, yet the difference is small. Possibly, this difference in oxidation rate reflects the higher ligand surface concentration of carboxylic acids, which may render the Cu surface less accessible

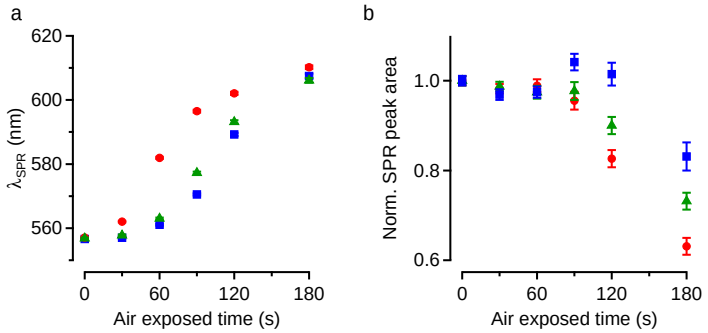

Figure 5.3: (a) Peak wavelength and (b) peak area of the surface plasmon resonance after starting the permanent exposure of a dispersion of Cu NCs to air. The different data sets pertain to Cu NCs capped by (red circles) $OlNH_2$, (blue squares) UDA, and (green triangles) oleic acid.

to oxygen. Even so, the rapid shift of the surface plasmon in both cases indicates that neither an $OlNH_2$ nor a carboxylate ligand shell effectively protects 4 nm Cu NCs from oxidation in the long term, in line with current literature.[21]

5.5.2 Sintering of Cu Nanocrystals capped with different ligands

To address the relation between surface ligands and sintering behavior, we cast different dispersions of 4 nm Cu NCs on glass substrates and monitored the x-ray diffraction pattern of the films thus formed during sintering under inert or reductive atmospheres. Figure 5.4a depicts the evolution of the crystallographic phases of the film sintered under ambient atmosphere. At temperatures lower than 280°C, a single broad signal at 36.4°attributed to the (111) planes of Cu_2O is present in the plot. Hence, in line with the results shown in Figure 5.3, we find that air exposure of the dropcast films lead to the oxidation of the initial Cu NCs to Cu_2O. After reaching 280°C the peak at 36.4°gives way to several signals at 35.6°, 38.8°and 48.8°, characteristic of CuO, indicating further oxidation of the particles.

Figure 5.4b represents the outcome of an annealing experiment on UDA-capped Cu NCs sintered under N_2. At temperatures below 200°, the diffractogram is once more dominated by a diffraction peak centered at 36.4°characteristic of the (111) planes of Cu_2O. In the temperature range between 200 and 300°C, the diffraction signatures of Cu_2O disappear and two new

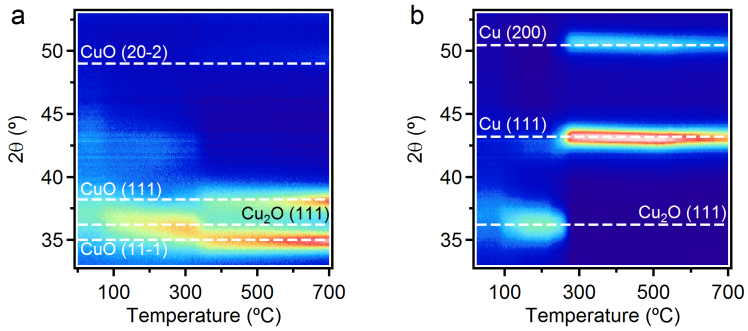

Figure 5.4: Contour plots of x-ray diffractograms of films of dropcast, UDA-capped Cu NCs recorded *in-situ* during annealing under ambient (a) and N_2 (b). Equivalent plots of $OlNH_2$, oleic acid (OA) and MEEAA-capped Cu NCs are available in the appendix section A.2.3.

diffraction peaks appear at around 43.3˚and 50.4˚, which correspond to the (111) and (200) planes of Cu. Hence, mild thermal sintering suffices to reduce 4 nm Cu_2O NCs and form metallic Cu. This conclusion points to the benefit of utilizing nanocrystals instead of bulk-like material, which cannot be reduced unless a reducing gas is introduced at high temperatures (see appendix A.2.4). Just recently, a study from Dai *et al.*[16] illustrated the same phenomena. In their work, $OlNH_2$-capped Cu NCs with an oxide shell were reduced upon sintering under N_2 without aid of any external reducing agent. According to their report, the driving force for the reduction of the Cu_2O shell was the H_2 released from $OlNH_2$ decomposition catalyzed by the Cu surface. The reducing effect of carboxylic acids on Cu_2O surfaces was also already observed in the literature albeit in that case they were added in the ink formulation or vaporized during sintering.[17;18] We also point this reduction to the thermodynamics of the equilibrium between of Cu_2O/Cu at lower concentrations of O_2. An Ellingham Diagram of this equilibrium is shown in the appendix demonstrating the impact of oxygen concentration on the thermodynamics of the process.A.2.2 In practice, we observed the same reduction phenomena both in amine and carboxylic acid capped Cu NCs (see appendix A.2.3) and the results are summarized in figure 5.5, where we compare the reduction temperature and the grain size for different ligands.

Comparing sintering of Cu NCs with three different carboxylic acid ligands under N_2, we find that more volatile ligands give rise to somewhat lower transition temperatures, from ∼280˚C in the case of oleic acid (OA) to

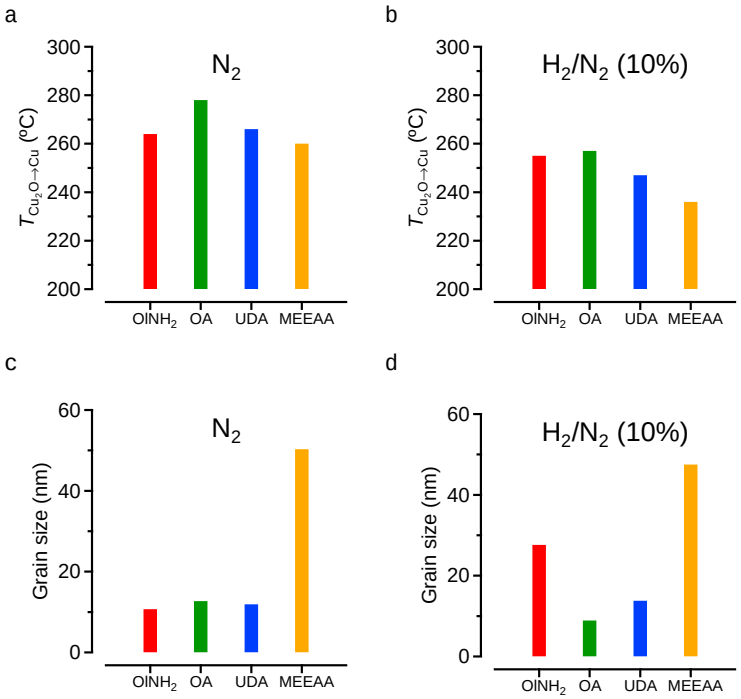

Figure 5.5: (a-b) Transition temperature characterizing the reduction of Cu_2O NCs to Cu, depending on the ligand and the annealing atmosphere. (c-d) Grain size of the crystallites as obtained from the diffractogram recorded at 300°C, depending on the ligand and annealing atmosphere. Each bar represents a different ligand: (red) $OlNH_2$, (green) oleic acid, (blue) UDA and (orange) MEEAA.

∼260°C in the case of MEEAA (see Figure 5.5a). The same trend appears during sintering in a reducing $N_2 : H_2$ environment, where MEEAA-capped Cu_2O NCs reduce to form Cu at a transition temperature of only ∼240°C (see Figure 5.5b). Comparing $OlNH_2$ with its equivalent carboxylic acid, OA, we can observe that the transition temperature is somewhat reduced for the amine under N_2 (∼262°C). We attribute this difference to the Cu surfaces catalyzing the decomposition of $OlNH_2$ and generating reducing gas H_2 (see equation 5.1).[16] This is confirmed by sintering already under H_2 flow, where NCs capped by either oleyl ligands exhibit a similar transition temperature of around ∼255°C.

$$OlNH_2 \rightarrow H_2 \uparrow + OlNH_2 \text{fragments} \tag{5.1}$$

While the difference in sintering temperature upon changing ligands is modest, sintering leads to considerably larger crystallites in the case of MEEAA ligands. This finding can be signficant. Films with smaller grains typically have a lower conductivity since grain boundaries enhance the scattering of electrons, a process that reduces the conductivity.[19] Analysing, for example, the various diffractograms recorded at 300°C by means of the Debye–Scherrer equation, we estimate that sintering OA or UDA capped Cu_2O NCs under a reductive atmosphere results in a grain size of ∼9 and ∼14 nm, respectively. In the case of MEEAA-capped NCs, on the other hand, we obtain a grain size close to 50 nm. Possibly, this difference is related to MEEAA being the only assessed ligand with a boiling point lower than the transition temperature. This implies that sintering occurs in a layer from which most of the organic fraction has evaporated; an aspect that seems to facilitate the formation of larger crystallites.

When comparing $OlNH_2$ to OA we do not observe representative differences in the grain size when sintered under N_2 atmosphere. Differently, presence of H_2 in the mixture resulted in larger grains of the sintered $OlNH_2$-capped NCs (∼26nm). We argue that since the decomposition of $OlNH_2$ is already triggered between 150°C and 290°C,[16] H_2 can access and reduce the Cu_2O shell at lower temperatures than in the long carboxylic acid cases, facilitating in that manner the formation of connections between particles.[8;10] Note that the crystallite size of the films has been estimated by the Debye–Scherrer method, which does not account for strain-induced broadening. We tried performing a Williamson-Hall analysis to account for the internal stress; however, since only two Cu signals are visible in the 33°-53°region the plot could not be reliably fitted.[20]

5.6 Sintering and Cu Nanocrystal Size

To analyze the effect of the particle size on the sintering temperature and conductivity of the films, we deposited 3 different size ranges of Cu NCs and monitored the x-ray diffractogram during a thermal treatment under a controlled atmosphere. The left column in Figure 5.6 represents TEM images of washed solutions of Cu NCs. By modifying the molar ratio $OlNH_2/Cu(HCO_2)_2$, different sizes of Cu NCs have been obtained: (a) 112.8 ± 65.4 nm, (b) 30.3 ± 13.9 nm and (c) 14.8 ± 1.9 nm. As exemplified in chapter 3 figure 3.5, the reduction of the equivalence of $OlNH_2$ in the reaction mixture leads to larger and more polydisperse particle size distributions. At the right of each TEM image, the evolution of the crystallographic phases upon thermal annealing under N_2 or N_2:H_2 (10%) is shown.

Differently from the previous section, unsintered films present mainly crystallographic planes of metallic Cu as visible by the signals at ∼43.3°(111) and ∼50.4°(200). This is confirmed by observing the XRD spectra in an extended 2θ range (see appendix A.2.5). That is, even if the NCs are synthesized and processed in contact with oxygen, it appears that an initial oxide shell passivates the NC surface and stalls further oxidation. An estimation from high-resolution TEM images establishes a 1.5-2 nm oxide shell thickness two weeks after synthesis and air exposure of the metallic particles (see appendix A.2.6); agreeing with a recent study on the oxidation rate of Cu NCs capped by alkylamines.[21]

By subjecting the films to a constant increase of temperature, we observe two phenomena: a shift of the diffraction peaks to smaller diffraction angles and the disappearance of the Cu_2O peak at ∼36.4°(111). The shift of the peaks results from the thermal expansion of the crystal lattices of the film.[22] The difference between the thermal expansion coefficient of copper and silicon also caused the films to peel off after sintering.[23;24] In Figure 5.6, we can also perceive a relation between the temperature at which the oxide shell is reduced and the particle size. At a constant heating rate of 10°C/min, the temperature range where the reduction occurs is proportional to the size of the particles. This is visible in the *in-situ* XRD plots. In the case of annealing in a N_2 atmosphere, for example, 113 nm Cu NCs are reduced between 300-380°C and 15 nm between 260-290°C. Differently from figure 5.4, where 4 nm NCs rapidly reduced at a specific temperature; larger and more polydisperse particle distributions are reduced through a prolonged temperature range.

In a second set of experiments, we tracked the resistance of the Cu NC films during sintering. In figure 5.7, we present the evolution of the resistivity of the films (in red) in combination with the intensity of the diffraction peak attributed to the (111) plane of Cu_2O as extracted from figure 5.6 (in blue). In general, both curves behave similarly. At low temperatures a more or less constant value indicates that neither the composition nor the resistivity of the films show a significant change with temperature. At higher temperatures, the amount of oxide exhibits a sudden drop, and so does the resistivity. Considering the low temperature resistivity first (figure 5.7c), it can be seen that the smallest NCs yield the most resistive films. Probably, this reflects the combined effect of more grain boundaries, a larger fraction of copper oxide and higher concentration of organic ligands; three characteristics that reduce the conductivity of a layer. Interestingly, films made of the larger NCs are somewhat conductive even before sintering. At 125 $\mu\Omega \cdot$ cm for the 113 nm and 175 $\mu\Omega \cdot$ cm for the 30 nm Cu NCs, such

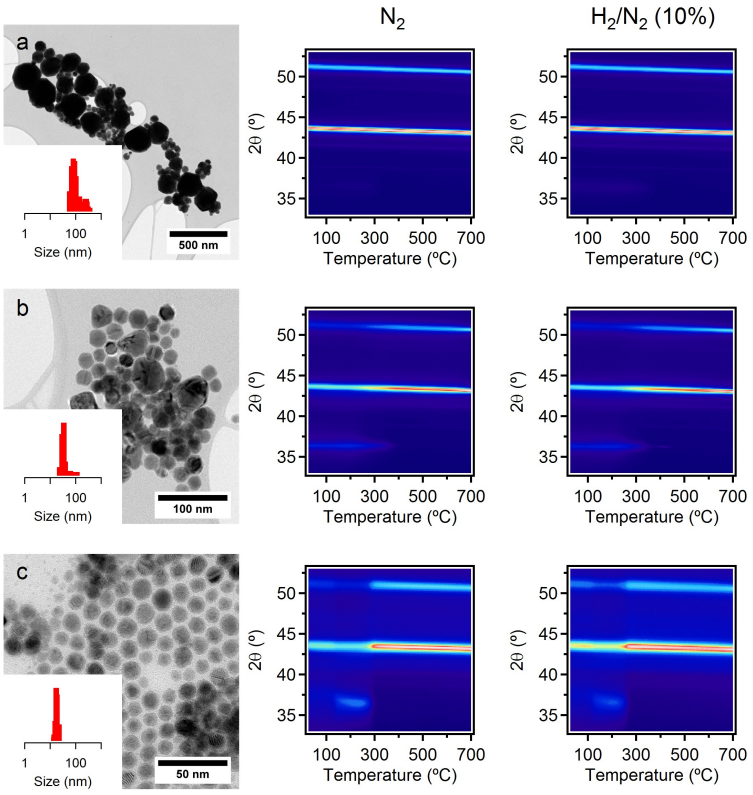

Figure 5.6: Low-resolution, brightfield TEM images of Cu NCs synthesized in an open atmosphere according to the protocols described in chapter 3: 0.4M $Cu(HCO_2)_2$ and (a) 0.4M: 113 nm, (b) 0.8M: 30 nm, (c) 1.2M: 15 nm $OlNH_2$. Contour plots of x-ray diffractograms of films of dropcast, $OlNH_2$-capped Cu NCs recorded *in-situ* during annealing under N_2 or N_2 : H_2 at a constant heating rate of 10°C/min. Average particle diameter was determined by sizing of 200 different particles

films may be promising for cut-rate, lower performance applications that use temperature-sensitive substrates such as PET or paper.

Upon increasing temperature, both the oxide content and the resistivity exhibit a sudden drop in a temperature range that depends on the size of the NCs comprising the film. Interestingly, however, both changes do not occur at exactly the same temperature. A closer look shows that the disappearance of the oxide phase precedes the drop in resistivity of the film. This result suggests that pure metallic Cu NCs are formed before

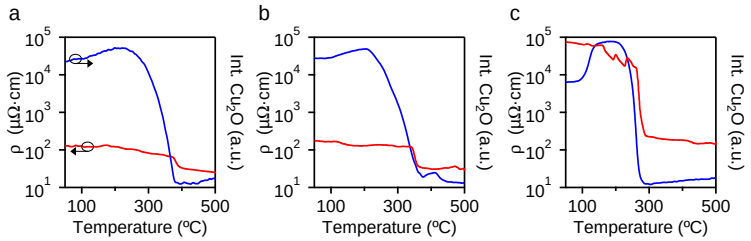

Figure 5.7: Resistivity (red) and integrated intensity of the peak attributed to the diffraction plane (111) of Cu_2O (blue) of films undergoing thermal treatment in N_2. The coatings were performed with a drawdown bar with theoretical wet film of 6 μm. The solutions contained toluene and a specific range of Cu NCs: 113 nm (a), 30 nm (b) and 15 nm (c). Heating rate was kept at 10°C/min, equal as in figure 5.6. Thickness and *ex-situ* resistance was measured before and after sintering to calculate the residual resistivity of each film and correct the increase due to temperature effects during thermal treatment.

densification. This is a key factor that can promote the formation of Cu films with bulk-like conductivities. Indeed, if sintering and reduction would occur simultaneously, the oxide could diffuse into a dense layer, and hampering electronic conduction by impurity scattering. This argument is supported by a prior work from Champion *et al.*, where a dilatometric analysis detected that shrinkage of a layer of Cu/Cu_2O nanocrystals only occurs at the end of the cuprite reduction.[10]

The absolute resistivity achieved by the 30 nm and 113 nm films after sintering to 500°C was 31 and 25 $\mu\Omega \cdot$ cm respectively, values in line with similar studies in literature.[25;26] Despite an abrupt reduction in resistivity at lower temperature, the layer consisting of 15 nm NCs achieved only 142 $\mu\Omega \cdot$ cm, a value comparable to the unsintered films of the larger NCs. Probably, this difference reflects the larger fraction of organic ligands in the dispersions of smaller NCs, which hinders a clean densification of the layers. Alternatively, an ink comprising both 115 nm and 15 nm NCs could benefit of the advantages of both sizes, where smaller particles are reduced first and act as a bonding material to connect the larger and more conductive ones.[27]

Although the reduction temperatures observed in the films suggests a clear limitation to only temperature resistant substrates, alternative sintering methods could open a window to the application of Cu NCs in low-cost plastics. Here, tape lamination followed by a flash lamp procedure, could

facilitate curing of a continuous copper film on temperature sensitive substrates.[28] Other strategies to enable the production of conductive films at low temperature involve a post-treatment with a densification promoter such as poly(diallyldimethylammonium chloride)[29] or the formation of the metastable compound CuH after treatment with hypophosphorus acid.[30]

Besides sintering, the final properties of the film depend on parameters such as solvent of choice, additives, printing method, etc., which are not optimized for this study.[31] In fact, the work presented in this chapter focused on the relation between particle properties (size and ligand coverage) and transformation properties – temperature range and eventual conductivity. A further optimization of more practical parameters involved in ink formulation is discussed in chapter 6.

5.7 Conclusion

We analyzed the effect that ligands have on the oxidation and reduction of the NCs and studied the sintering behavior of the Cu NCs. We demonstrated that a dispersion in polar solvents could be obtained by exchanging the ligand to a MEEAA, a volatile carboxylic acid. We showed that even if slightly stalled, carboxylic acids are not able to prevent oxidation of the NCs after air exposure. Nonetheless, we proved that oxidation can be reversed by thermal annealing in a N_2 atmosphere and we studied how the capping ligand and particle size affect the reduction temperature. In the case of 4 nm Cu NCs, MEEAA-capped particles presented the lowest reduction temperature amongst the studied ligands and an enhanced 50 nm grain size, featuring its case as a promising ligand for Cu NCs in conductive ink formulations. Using $OlNH_2$-capped NCs, we showed a clear relation between particle size and Cu_2O-Cu transition temperature. Films consisting of larger particles ($\geq$113 nm) presented improved conductivity both before and after thermal sintering despite requiring a higher temperature to achieve copper oxide reduction. Overall, these conclusions highlights the relevance of the capping ligand and particle size in the pursuit of conductive films and pinpoints the relevant particle parameters to formulate and print a conductive ink.

References

[1] F. Thümmler and W. Thomma. *The Sintering Process.* Met. Mater. Metall. Rev., 12(115), 1967.

[2] Suk-Joong L. Kang. *Sintering Processes.* In Sintering, pages 3–8. Elsevier, 2005.

[3] Conyers Herring. *Effect of Change of Scale on Sintering Phenomena.* J. Appl. Phys., 301(21):4–7, 1950.

[4] O Dominguez, Y Champion, and J Bigot. *Liquidlike Sintering Behavior of Nanometric Fe and Cu Powders: Experimental Approach.* Metall. Mater. Trans. A Phys. Metall. Mater. Sci., 29(12):2941–2949, 1998.

[5] Jonathan De Roo, Isabel Van Driessche, José C. Martins, and Zeger Hens. *Colloidal metal oxide nanocrystal catalysis by sustained chemically driven ligand displacement.* Nat. Mater., 15(5):517–521, 2016.

[6] Z. Z. Fang and H. Wang. *Sintering of ultrafine and nanosized particles.* Woodhead Publishing Limited, 2010.

[7] Z A Munir. *Surface Oxides and Sintering of Metals.* Powder Metall., 24(4):177–180, 1981.

[8] P. J. Heath and P. E. Evans. *Sintering, fracture and oxide films.* J. Mater. Sci., 9(12):1955–1960, 1974.

[9] P. Ramakrishnan and G. S. Tendolkar. *Influence of Thin Oxide Films On the Mechanical Properties of Sintered Metal-Powder Compacts.* Powder Metall., 7(13):34–49, 1964.

[10] Yannick Champion, Frédéric Bernard, Nadine Guigue-Millot, and Pascal Perriat. *Sintering of copper nanopowders under hydrogen: an in situ X-ray diffraction analysis.* Mater. Sci. Eng. A, 360(1-2):258–263, 2003.

[11] Krishna Balantrapu, Meaghan McMurran, and Dan V. Goia. *Inkjet printable silver dispersions: Effect of bimodal particle-size distribution on film formation and electrical conductivity.* J. Mater. Res., 25(5):821–827, 2010.

[12] Jonathan De Roo, Nuri Yazdani, Emile Drijvers, Alessandro Lauria, Jorick Maes, Jonathan S. Owen, Isabel Van Driessche, Markus Niederberger, Vanessa Wood, Jose C. Martins, Ivan Infante, and Zeger Hens. *Probing Solvent-Ligand Interactions in Colloidal Nanocrystals by the NMR Line Broadening.* Chem. Mater., 30(15):5485–5492, 2018.

[13] Frederick I Mopsik. *Dielectric constant of n-hexane as a function of temperature, pressure, and density.* J. Res. Natl. Bur. Stand. Sect. A Phys. Chem., 71A(4):287, 1967.

[14] Arnaud Glaria, Jérémy Cure, Kilian Piettre, Yannick Coppel, Cédric-Olivier Turrin, Bruno Chaudret, and Pierre Fau. *Deciphering Ligands' Interaction with Cu and Cu2O Nanocrystal Surfaces by NMR Solution Tools.* Chemistry (Easton)., 21(3):1169–1178, 2015.

[15] Kennethh R. Lawless. *The oxidation of metals.* Reports Prog. Phys., 231(37):231–316, 1974.

[16] Xiaofeng Dai, Wen Xu, Teng Zhang, and Tao Wang. *Self-Reducible Cu Nanoparticles for Conductive Inks.* Ind. Eng. Chem. Res., 57(7):2508–2516, 2018.

[17] Anna Pajor-Świerzy, Yousef Farraj, Alexander Kamyshny, and Shlomo Magdassi. *Effect of carboxylic acids on conductivity of metallic films formed by inks based on copper@silver core-shell particles.* Colloids Surfaces A Physicochem. Eng. Asp., 522:320–327, 2017.

[18] Kyoohee Woo, Youngwoo Kim, Byungyoon Lee, Jonghee Kim, and Jooho Moon. *Effect of carboxylic acid on sintering of inkjet-printed copper nanoparticulate films.* ACS Appl. Mater. Interfaces, 3(7):2377–2382, 2011.

[19] S. M. Rossnagel and T. S. Kuan. *Alteration of Cu conductivity in the size effect regime.* J. Vac. Sci. Technol. B Microelectron. Nanom. Struct., 22(1):240, 2004.

[20] A. Khorsand Zak, W. H. Abd. Majid, M. E. Abrishami, and Ramin Yousefi. *X-ray analysis of ZnO nanoparticles by Williamson-Hall and size-strain plot methods.* Solid State Sci., 13(1):251–256, 2011.

[21] Jérémy Cure, Arnaud Glaria, Vincent Collière, Pier-Francesco Fazzini, Adnen Mlayah, Bruno Chaudret, and Pierre Fau. *Remarkable Decrease in the Oxidation Rate of Cu Nanocrystals Controlled by Alkylamine Ligands.* J. Phys. Chem. C, 121(9):5253–5260, 2017.

[22] Masahisa Wada and Ritsuko Hori. *X-Ray Diffraction Study of the Thermal Expansion Behaviorof Cellulose Triacetate I.* J. Polym. Sci. Part B Polym. Phys., 47:517–523, 2009.

[23] F.C. Nix and D. MacNair. *The Thermal Expansion of Pure Metals: Copper, Gold, Aluminum, Nickel, and Iron.* Phys. Rev., 60:597–605, 1941.

[24] P. Becker, P. Scyfried, and H. Siegert. *The lattice parameter of highly pure silicon single crystals.* Zeitschrift für Phys. B Condens. Matter, 48(1):17–21, 1982.

[25] Wan-Ho Chung, Hyun-Jun Hwang, and Hak-Sung Kim. *Flash light sintered copper precursor/nanoparticle pattern with high electrical conductivity and low porosity for printed electronics.* Thin Solid Films, 580:61–70, 2015.

[26] Juha Niittynen, Robert Abbel, Matti Mäntysalo, Jolke Perelaer, Ulrich S. Schubert, and Donald Lupo. *Alternative sintering methods compared to conventional thermal sintering for inkjet printed silver nanoparticle ink.* Thin Solid Films, 556:452–459, 2014.

[27] Yusuke Yasuda, Toshiaki Morita, and Yoshio Kobayashi. *EP 2 587 899 A1*, 2013.

[28] James P Novak, Valerie Ginsberg, and Related U S Application Data. *US 2014/0314966 A1*, 2014.

[29] Shlomo Magdassi and Alexander Kamyshny. *US 2012 / 0168684 A1*, 2012.

[30] Michael Grouchko. *WO2018025271A1*, 2017.

[31] Adrian Rose. *Considerations in Formulation and Manufacturing of Thick Film Inks.* Electrocompon. Sci. Technol., 9(1):43–49, 1981.

6

Formulation of a Copper-Nanocrystal-based Conductive Ink

Using a design of experiments, we develop a nano copper conductive ink. This ink is based on Cu nanocrystals made using a high solid-loading synthesis that yields unoxidized Cu NCs at a 50 g scale. We create a definitive screening design and evaluate the effect of processing conditions and additives on ink properties such as adhesion and conductivity to formulate a nano copper screen printing ink. Conductive RFID antennas are printed with this ink, demonstrating its value for applications in printed electronics.

6.1 Introduction

Until now, we presented a holistic characterization of the Cu NCs. We studied from a synthesis perspective how parameters such heating rate, precursor or ligand concentration affect the crystallographic state or size of the particles; we analyzed the surface ligands and the effect they have in the chemical

properties of the NCs and finally we studied how the NCs transform into metallic and dense films depending on the previously tuned particle properties. To capitalize on a conductive ink other study elements such as ink formulation or printing method are equally important to evaluate. [1;2]

In this chapter, we introduce an adaptation of the synthesis method. By increasing the precursor concentration, we produce up to ∼6 grams of unoxidized Cu NCs in a 100 mL reaction volume. We use the produced conductive material to optimize an ink formulation using Design of Experiments (DOE) as a method of study. We use a definitive screening design to optimize quantitatively the ink additives in terms of resistance and adhesion. By this means we obtain a conductive pattern with a resistivity of 2.57 $\mu\Omega \cdot$cm, a value corresponding to 66% of Cu bulk conductivity. We increase further the volume of the reaction to 1 L, producing 60 g of slightly oxidized Cu NCs in a sole synthesis. We adapt the formulation for screen printing by adding a thixotropic agent. We print RFID antennas on both PET and glass.

6.2 Experimental section

Chemicals. In this work, the following chemicals were used: copper(II) formate tetrahydrate (Alfa Aesar, 98%), oleylamine (Acros Tech, 80-90%), n-dodecane (Merck Millipore, ≤99%), 4-hydroxy-4-methyl-2-pentanone, referred as diacetone alcohol (Merck Millipore, 99%), Disperbyk-180 (Byk), Byk-333 (Byk), Polyvest HT (Evonik), Tixogel-MP (Byk).

Design of experiments. A Definitive Screening Design (DSD) experiment was set around five factors (k = 5), sintering temperature (χ^1), particle size (χ^2), disperbyk-180 (χ^3), polyvest-HT (χ^4), byk-333 (χ^5). The factor levels (minimum, center, maximum) were chosen according to previous data in chapter 5 (χ^1, χ^2) and according to recommended levels in the technical data sheets (χ^3, χ^4, χ^5). By including a qualitative factor (χ^2), an expanded design comprised of 18 experiments (instead of 13) was chosen to identify the factors causing a significant nonlinear effect. Two main responses are examined: adhesion (Y_1) and log(resistivity) (Y_2).

Ink preparation. To prepare 1 g of ink, we first prepared the vehicle by mixing the solvent, 4-hydroxy-4-methyl-2-pentanone (diacetone alcohol), with the additives according to the table 6.2. The volume of added diacetone alcohol varied up to reach a 0.5 g total weight of the vehicle. Then, 0.5 g Cu NCs were added to the solution thus obtaining an ink consisting of 50% solid

loading. The solution was stirred and sonicated for 1 h to ensure maximum dispersion of the NCs.

Responses characterization. Adhesion was determined by a tape-test standard method ASTM D3359, 2010. In this test method, an X-cut is made through the film to the substrate, then pressure-sensitive tape is applied over the cut and removed; adhesion is assessed qualitatively on the 0 to 5 scale.[3] Thickness was determined by scratching a sample and measuring the step height between sample and coating with a Taylor-Hobson Talystep mechanical profilometer. The square resistance was measured using a custom-build 4-point probe with equal spacing between probes. In a 4-point probe set-up, a current is passed through the outer probes and it induces a voltage in the inner voltage probes. The measured voltage is independent of the resistance of the probe tips and determines the resistance of the film by Ohm's law. The absolute resistivity of the layers was calculated by multiplying the square resistance by the thickness and the correction factor.[4]

6.3 Design of Experiments

Formulating an ink is an optimization task in which multiple factors, such as the solvent, the additives, and the printing method play a role. Moreover, the modification of a single parameter is a time-consuming effort that does not even guarantee that an optimal result is achieved because of possible interdependencies of the different factors. A common approach for formulators to analyze and optimize inks is the use of design of experiments (DOE).[5] Designing an ink formulation experiment by DOE allows researchers to investigate interactions among variables in a limited amount of runs. The data obtained is fitted to a mathematical model that relates the factors with the results and predicts responses for any combination of factors. In that manner, the optimal experimental conditions can be outlined without any prior knowledge of the outcome of the programmed experiments.

To estimate the relations between the factors, a regression analysis is typically usually to describe the data. Mainly, an empirical model is fitted to the data in a polynomial linear regression equation. For example, a first-order model consisting of two variables x, a response y, regression coefficients parameters β and error ϵ is expressed by the following relation:[6]

$$y = \beta_0 + \beta_1 x_1 + \beta_2 x_2 + \epsilon \tag{6.1}$$

Clearly, such a model puts forward x_1 and x_2 as independent factors and can only accounts for the main effects of these factors. Non-linear effects such interactions between factors and quadratic relations between the outcome and a factor can be included in more involved relations such as:

$$y = \beta_0 + \beta_1 x_1 + \beta_2 x_2 + \beta_{12} x_1 x_2 + \beta_{11} x_1^2 + \beta_{22} x_2^2 + \epsilon \tag{6.2}$$

To study all the factors and their interactions, a full factorial design is needed to describe the system. However, most experiments involve more than two factors in the design. In a full factorial design all main effects and interactions are studied, and the number of runs increase exponentially with the number of factors. For example, a two-level experiment with 5 factors consists in 32 runs where only 5 degrees of freedom account for the main effects and 17 for 3-factor interactions or more, which are usually negligible according to the sparcity-of-effects principle. Two-level experiments are perilous because a linear effect of the factors is assumed. If three levels are considered then the number of runs increases to 243, which results in a workload overkill. [6]

The amount of runs required to obtain information on the main effects and low-level interactions can be reduced by using fractional factorial designs. Fractional factorial designs are typically used in screening experiments - where many factors are studied with the objective of identifying those that have an effect. However, as the number of runs decreases, some effects cannot be distinguished from each other (i.e. interactions are confounded). An important property of fractional factorial designs is their resolution, defined as the ability to separate main effects and interactions from one another or, in other words, to avoid confounding. Then, the most common designs can be classified according to the resolution as:

1. Resolution III: Main effects are not confounded with any other main effect, but may be confounded with two-factor interactions. Example: A one-half fraction design of a two-level, 3 factors, experiment: 2^{3-1}
2. Resolution IV: Main effects are not confounded with any other main effect nor two-factor interactions. Two-factor interactions may be confounded with other two-factor interactions. Example: 2^{4-1}
3. Resolution V: Main effects are not confounded with any other main effect nor two- or three-factor interactions. Three-factor interactions may be confounded with other two-factor interactions. Example: 2^{5-1}

Once the main factors contributing to a response are screened and narrowed down, response surface methods are usually used to optimize those factors

to obtain an ideal response. A typical design used by formulators to optimize an ink formulation is a mixture experiment. Mixture designs are a special class of response surface experiment in which the factors are composed of several ingredients of a product wherein the measured response is assumed to depend only on relative proportions of the factors.[7] However, classic mixture experiments can only account for ingredients contributing to the mixture properties. To include process variables such as temperature, we need to create an experiment where the mixture design is included at each location generated by the process variables. Mixture–process variable experiments are frequent in the pharmaceutical industry, yet these types of experimental designs become considerably large as the number of mixture components and process variables increase.[8]

Recently, a new three-level design for screening in the presence of second-order effects was introduced by Jones and Nachtsheim.[9;10] This method, dubbed Definitive Screening Design (DSD), allows assessment of the curvature in the factor–response relationship and is able to estimate the model coefficients of the main effects, two-factor interactions and quadratic effects with only twice as many runs as there are factors plus one.[11] A DSD experiment structure is shown in table 6.1.

The proposed design has several advantages compared to full or fractional factorial designs:[9]

1. Only 2k+1 runs are required, with a minimum of 13 runs.
2. Main effects are independent of two-factor interactions.
3. Two-factor interactions are not completely confounded with other two-factor interactions though might be correlated.
4. Quadratic effects are estimable.
5. Quadratic effects are orthogonal to main effects and not completely confounded though might be correlated.
6. For six factors or more, quadratic models involving three or fewer factors are estimable.

In summary, a DSD permits, in a low number of runs, the unambiguous identification of active main effects, quadratic effects and two-way interactions with a moderate level of sparsity. This represents an advantage in respect to resolution III, where main effects can be confounded with two-factor interactions as well as resolution IV, where two-factor interactions can be confounded with other two-factor interactions. Moreover, the explicit use

Table 6.1: General structure of a definitive screening design with k factors and 2k+1 runs.[9]

Foldover pair	Run (i)	Factor levels				
		$x_{i,1}$	$x_{i,2}$	$x_{i,3}$	$\cdots$	$x_{i,k}$
1	1	0	$\pm$	$\pm$	$\cdots$	$\pm$
	2	0	$\mp$	$\mp$	$\cdots$	$\mp$
2	3	$\pm$	0	$\pm$	$\cdots$	$\pm$
	4	$\mp$	0	$\mp$	$\cdots$	$\mp$
3	5	$\pm$	$\pm$	0	$\cdots$	$\pm$
	6	$\mp$	$\mp$	0	$\cdots$	$\mp$
$\vdots$	$\vdots$	$\vdots$	$\vdots$	$\vdots$	$\vdots$	$\vdots$
k	2k-1	$\pm$	$\pm$	$\pm$	$\cdots$	0
	2k	$\mp$	$\mp$	$\mp$	$\cdots$	0
Centerpoint	2k+1	0	0	0	$\cdots$	0

of three levels throughout the experiment results in unique identification of curvature effects unlike resolution III, IV or V even with added center runs. For all that, DSD situates itself in the middle ground between fractional factorial designs, which lead to ambiguous effects, and full-factorial or response surface designs, which require a large number of runs.[12]

6.4 Synthesis of Cu nanocrystals for ink formulation

A high-concentration synthesis was develop to produce pristine conductive material to test ink formulation. In a 250 mL flask, a 1 M solution of $Cu(HCO_2)_2$ was formed by dissolving the precursor in a 100 mL solution of dodecane and $OlNH_2$ while vigorously stirring at 50°C. Then, the mixture was heated up to 140°C and soaked at the same temperature for 10 minutes, cooled down and washed multiple times using a toluene and ethanol as solvent and non-solvent respectively. Particle size was tuned by modifying the equivalence of $OlNH_2$ with respect to $Cu(HCO_2)_2$. A 1 equivalent synthesis

resulted in a polydisperse set of Cu NCs (a phenomenon already discussed in chapter 3) with an average diameter of 117.3 ± 62.4 nm as visible in Figure 6.1a. A 2 equivalent synthesis resulted in an ensemble of Cu NCs with an average diameter of of 21.3 ± 10.9 nm diameter (see Figure 6.1b). Most importantly, the XRD diffractograms only presented peaks of the metallic phase of Cu, indicating that such reactions conditions lead to unoxidized particles. The washed powders were dried and weighted, yielding 6.26 g for the ∼120 nm and 5.64 g for the ∼20 nm, equivalent to 98.5% and 88.8% respectively of the expected Cu weight.

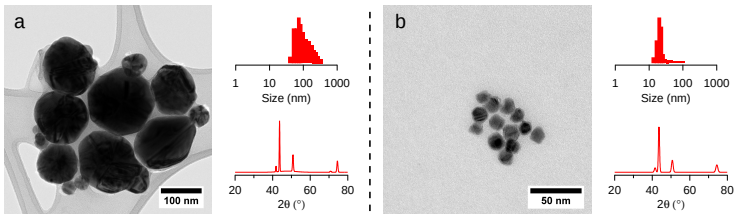

Figure 6.1: Low resolution, brightfield TEM images of Cu NCs synthesized at 1M $Cu(HCO_2)_2$ concentration and different $OlNH_2$ concentrations: (a) 1M $OlNH_2$ or (b) 2M $OlNH_2$. Average particle diameter was determined by sizing of 200 different particles. The XRD patterns under each histogram show the presence of only metallic Cu phases. The small peaks left to each signal are artifacts caused by the Cu filament.

6.5 Definitive screening design for ink formulation

In the thesis introduction we described the components that compose a conductive ink. Until now, we studied the properties of the filler, Cu NCs, and how to produce and modify to our liking this essential part of the ink. Even if the Cu NCs are the main responsible for the properties of the films, a careful choice of solvent and additives is vital to ensure the proper application of the ink to the substrate.[13] Thus, we searched for a method to study how the concentration of each additive and the processing conditions affect the conductivity and adhesion of the films. Design of experiments (DOE), and more precisely, a definitive screening design (DSD), is the tool that allowed us to study such in a minimal time.

Here, we set a DSD experiment with 5 factors: sintering temperature (χ^1),

particle size (χ^2), dispersing agent: disperbyk-180 (χ^3), binder: polyvest-HT (χ^4) and wetting agent: byk-333 (χ^5). Other relevant factors such as solvent (diacetone alcohol), solid loading (50%), application method (k-bar) and sintering time (1h) were kept constant throughout the experiments. Then, 2 responses were evaluated: adhesion (Y_1) and resistivity (Y_2). Even if the main goal of a conductive ink is to achieve minimal resistivity, proper adhesion is crucial to ensure integration and long-term performance of the coatings.[14] Adhesion is defined as the interatomic and intermolecular interaction at the interface of two surfaces.[15]It depends on several factors such as surface chemistry, physics, rheology... and identifying the mechanisms that explain the adhesion is an intricate task out of the scope of this thesis. Even so, the evaluation of adhesion can be straightforward. Following the standard test method ASTM D3359 (see experimental section), adhesion is quantified from 0 to 5 by assessing the adhered surface on the tape after scratching and placing/removing the tape on the film.[3]

We monitored the absolute resistivity of the films by independently analyzing its two components: thickness and resistance. We formulated the inks with a theoretical constant solid loading which should result in a constant dry film thickness. However, due to the variable concentration of dispersing agent and possible experimental inconsistency we determined the thickness in an empirical manner. Thickness was determined by finely scratching the film until the substrate was visible and measuring the height step difference with a mechanical profilometer. Resistance was measured with a 4-point probe to neglect the inherent resistance of the tips as described in the experimental section.[4]

DSD is a three-levels design, therefore -1,0 and 1 factor levels had to be determined. These factor levels should be as broad as possible, yet at the same time, they need to ensure that all responses are still measurable. For instance, in the case of large Cu NCs, the $OlNH_2$ capping may not suffice to keep the particles from agglomerating and precipitating, limiting the achievable solid loading. Hence, a minimal amount of added dispersant is imperative to ensure that the NCs are incorporated into the dispersion and effectively deposited. Based on the transformation temperatures of super-10 nm NCs upon sintering under N_2 (see chapter 5), a minimum temperature of 300°C(-1,χ^1) and maximum of 500°C(1,χ^1) were selected. For the particle size, only two levels were selected corresponding to the NCs synthesized at high concentrations (Figure 6.1), corresponding to ∼120nm (L1 χ^2) and ∼20 nm (L2 χ^2). This implies, that the factor had to be considered qualitative since a 0 level was not used, causing the experiment to include extra runs to compensate for the increment of confounding generated by a qualitative

Table 6.2: Definitive screening design of 5 factors: Sintering temperature, χ^1, average diameter of the Cu NCs, χ^2, disperbyk-180, χ^3, polyvest HT, χ^4 and byk-333, χ^5. 2 responses are measured in the definitive screening design: adhesion (Y_1) and log(resistivity) (Y_2).

Run	χ^1 °C	χ^2 nm	χ^3 %	χ^4 %	χ^5 %	Y_1 a.u.	Y_2 $\log(\mu\Omega \cdot \mathrm{cm})$
1	400	20	4	4	0.3	4.5	1.181
2	400	120	1	0	0	1	1.101
3	500	120	2.5	4	0.3	2	1.383
4	300	20	2.5	0	0	4.5	2.419
5	500	20	1	2	0.3	0	1.415
6	300	120	4	2	0	5	2.068
7	500	20	1	0	0.15	1	1.733
8	300	120	4	4	0.15	5	2.217
9	500	20	4	0	0	3.5	1.360
10	300	120	1	4	0.3	5	1.698
11	500	120	1	4	0	3.5	1.602
12	300	20	4	0	0.3	2.5	1.652
13	500	120	4	0	0.3	0.5	0.411
14	300	20	1	4	0	5	2.108
15	500	20	4	4	0	4	2.304
16	300	120	1	0	0.3	0	0.651
17	400	120	2.5	2	0.15	4.5	1.280
18	400	20	2.5	2	0.15	1.5	1.317

factor.[16]

The levels of the additive factors were selected according to the recommended values from the technical data sheets and preliminary tests. In that way, the levels of the dispersing agent, Disperbyk-180 were situated at 1% (-1,χ^3) and 4% (1,χ^3); for the binder, Polyvest HT, the levels were 0% (-1,χ^4) and 4% (1,χ^4); and for the wetting agent, Byk-333 the chosen levels were 0% (-1,χ^5) and 0.3% (1,χ^5). The experiment was designed by JMP® software as if six continuous factors and one categorical were to be studied and subsequently dropping two of the continuous factors as suggested by the inventors.[16;17] The different runs of the experiment and their responses are listed in table 6.2. Note that the logarithm of the response resistiv-

ity (Y_2) is used instead of the real value. We did this adjustment because we observed that the residuals of the resistivity tended to higher values as the nominal value of the response increased. By fitting the model to the logarithm we confirmed that the goodness of the fit greatly improved. A comparison of both models and residuals is included in the appendix A.3.1 showing a simplified relationship with the predictor variable and simpler model in the case of the logarithmic response.

The adhesion of the film to the substrate varied strongly throughout the experiments: whilst some films had absolutely no adhesion, 0, others showed perfect adherence after sintering, 5. In terms of resistivity, the absolute values ranged between 262.7 and 2.56 $\mu\Omega\cdot$cm. This latter value represented a remarkable improvement as compared to the results of chapter 5, where 25 $\mu\Omega\cdot$cm was the lowest resistivity obtained. Furthermore, 2.56 $\mu\Omega\cdot$cm is equivalent to 66% of the bulk conductivity of Cu, a promising result at par with the finest state-of-the-art Cu NCs-based conductive films. [18;19]. The coefficients of the significant factors for each response are listed in Table 6.3. The model of choice was selected based on the Akaike information criterion, where the preferred model is chosen based on a trade-off between the goodness of the fit and the number of independently adjusted parameters within the model. [20–22]

The model equations for each response are expressed according to the coefficient parameters listed in table 6.3:

$$\begin{aligned} Y_1 =& 2.944 - 0.893(\frac{\chi^1 - 400}{100}) + 0.679(\frac{\chi^3 - 2.5}{1.5}) + \\ &+ 1.143(\frac{\chi^4 - 2}{2}) - 0.857(\frac{\chi^5 - 0.15}{0.15}) \end{aligned} \tag{6.3}$$

$$\begin{aligned} Y_2(120\text{nm}) =& 1.335 - 0.213(\frac{\chi^1 - 400}{100}) + \\ &+ 0.486(\frac{\chi^4 - 2}{2}) - 0.299(\frac{\chi^5 - 0.15}{0.15}) \end{aligned} \tag{6.4}$$

$$\begin{aligned} Y_2(20\text{nm}) =& 1.713 - 0.213(\frac{\chi^1 - 400}{100}) + \\ &+ 0.020(\frac{\chi^4 - 2}{2}) - 0.299(\frac{\chi^5 - 0.15}{0.15}) \end{aligned} \tag{6.5}$$

Equation 6.3 shows that adhesion is largely effected by the % of Polyvest HT present in the formulation (χ^4), proving that the binder of choice fulfills its

Table 6.3: Model coefficients of the significant factors for each of the measured responses with their respective p-values. A p-value $\leq$0.05 is an indicator that the measured factor has a significant effect on the response. p-values were computed by the software. 120 nm NCs are considered for the coefficients related to χ^2; 20 nm NCs coefficients are of the opposite sign.

Significant factors	Y_1 Adhesion	Y_2 $\log(\rho)$
R^2	0.77	0.80
Constant	2.944	1.524
p	<0.0001	<0.0001
χ^1 Sintering T	-0.893	-0.213
p	0.0064	0.0186
χ^2 Size NCs		-0.189
p		0.0193
χ^3 Disperbyk-180	0.679	
p	0.0283	
χ^4 Polyvest HT	1.143	0.253
p	0.0011	0.0072
χ^5 Byk-333	-0.857	-0.299
p	0.0082	0.0240
$\chi^2 \cdot \chi^4$		0.233
p		0.0116

purpose. Temperature (χ^1) has an unfavorable effect probably due to organics molecules that benefit adhesion volatilizing at higher temperatures. The other two additives have an opposite effect. Byk-333 (χ^5), a silicone-based surfactant, hampers the adhesion of the films whilst disperbyk-180 (χ^3), an alkylol ammonium salt of a copolymer, favors an improved adhesion. These last effects highlight the potential of a DOE, where effects from unexplored factors can be predicted and modeled without premises or expected outcomes. It is worth noting that particle diameter has no significant effect on the adhesion, illustrating that such ink property is determined by processing and a minor, but important, fraction of the formulation components.

Equations 6.4 and 6.5 present the effect of the significant factors on the resistivity. Two separated equations are taken for each level of the qualitative factor, particle size χ^2, thus simplifying the expression. The difference in

the constant factor indicates that larger NCs have in general terms a lower resistivity, in line with the observed trend of figure 5.7 of chapter 5. Also, the effect of sintering temperature was anticipated from the data of the previous chapter, where higher sintering temperature promoted oxide shell reduction and sintering of the NCs, hence obtaining less resistive films. Byk-333 (χ^5) has a startling favorable effect in the resistivity of the films. This additive is a polydimethylsiloxane-based surfactant added at most in a 0.3% of the total formulation weight. Its limited presence proves to be clearly beneficial to the formation of the films whilst not hindering the conductivity whatsoever. The effect of the last factor, Polyvest HT (χ^4), is interacting with the effect of particle size (χ^2). This interaction results in two completely different effects depending on the particle diameter. Films consisting of 120 nm NCs become largely more resistive as the % of the binder increases: $\beta(\chi^4)$=0.486. This is not an unexpected result since Polyvest HT structure entity is a hydroxyl-terminated unsaturated polymer with electrical insulating properties. However, in equation 6.5 the coefficient for χ^4 is only 0.020, meaning that the resistivity films deposited from the 20 nm NCs is barely affected by the amount of binder in the formulation.

Given the above, films obtained with 120 nm NCs can attain lower resistivity, however, the presence of the binder limits greatly this potential minimal resistivity. In contrast, 20 nm-based coatings, despite being generally less conductive, are hardly insulated by the binder meaning that a trade-off between low resistivity and proper adhesion can be achieved with such smaller Cu NCs.

6.6 Upscaled synthesis for screen-printing ink formulation

A large-scale reaction was carried out to test the industrialization potential of the synthesis method and formulate an ink for screen printing applications. In an open 3 L flask, a 1 M solution of $Cu(HCO_2)_2$ was formed by dissolving the precursor in a 1 L solution of dodecane and 1 M $OlNH_2$ while vigorously stirring with a mechanical stirrer at 50°C (see Figure 6.2a). Then, the mixture was heated up to 140°C and soaked at the same temperature for 10 minutes, cooled down and washed multiple times in toluene, decanting after centrifugation.

The washed powder was characterized via TEM and XRD as shown in Figure 6.2b. The particles presented an average diameter of 240 ± 39 nm, a larger and narrower particle size distribution than the analogous synthe-

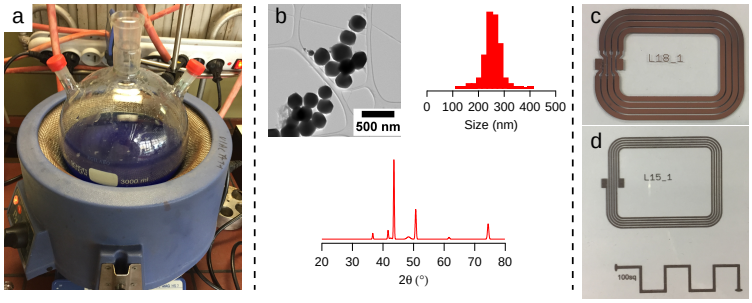

Figure 6.2: (a) Initial solution mixture prior to large-scale synthesis. An open 3 L round-bottom flask was used as vessel and a corresponding heating mantle was used as heating method. (b) Low resolution, brightfield TEM image of Cu NCs synthesized at 1M $Cu(HCO_2)_2$ concentration and 1M $OlNH_2$ in a 1 L volume. Average particle diameter was determined by sizing of 100 different particles. The XRD diffractogram shows mainly presence of crystalline Cu and minor presence of Cu_2O. RFID antennas screen-printed by Quad Industries in (c) glass and (d) PET.

sis in 100 mL, where precursor concentration and precursor-$OlNH_2$ ratio were identical. We attribute this difference to the larger reaction volume, which caused a decrease in the heating rate of the solution to approximately 3°C/min. A slower heating rate induced a slower reaction. In slow reactions less nucleation events occur, hence promoting the formation of larger particles.[23] This also implied that the synthesis could not evolve rapidly enough to prevent oxygen intake during nucleation and growth, a phenomenon discussed in chapter 3 (figure 3.4), thus resulting in slightly oxidized Cu NCs as visible in the XRD pattern with the peaks at 37.0, 42.6 and 62.4° attributed to Cu_2O.

To formulate an ink for screen printing, we followed the optimal conditions for resistivity according to the DSD experiment. Then, 50 g of Cu NCs were incorporated to a constantly stirring vehicle containing diacetone alcohol (45.7%), byk-333 (0.3%) and disperbyk-180 (4%) and sonicated for an hour to ensure full dispersion. Screen printing of the ink was performed by an external partner, Quad Industries, a company specialized in screen-printing techniques for PE. Unfortunately, rheological properties were not studied and the delivered ink viscosity was too low for screen printing, which resulted in ink dripping and sagging. To adapt our ink formulation for screen printing, a rheological additive that increased the viscosity and provided a thixotropic behavior was required to be incorporated to the formulation.

Thixotropy is a shear thinning property which implies a time-dependent decrease of the viscosity induced by flow - a property common in everyday products like yogurts.[24] Thixotropic inks can be pushed through the screen (under pressure of the squeegee) while dripping of the ink is avoided when there is no squeegee pressure. This thixotropic behavior also ensures there is no flow of the ink after it has been printed reducing the smearing effect. Therefore, to the previous ink formulation we added 2% of Tixogel-MP, a thixotropic agent based on silicate platelets with a hydrophobic coating which drastically improved the printability.

Well-defined RFID antennas were printed both in glass (figure 6.2c) and PET (figure 6.2d). The PET-printed antenna showed that the formulated ink was printable onto a plastic substrate. However, no characterization was performed since no adequate sintering method for temperature sensitive substrates was available at the time of the experiments. Further work should involve the study of alternative sintering methods such as IR or laser curing to determine if the developed ink is compatible with plastic substrates. The glass-printed antenna was sintered in a nitrogen-filled oven at 400°C for 1 hour and the resistance measured in the edges of the squared tracks as the one shown in the bottom of figure 6.2d. The resulting thickness-independent resistance of the tracks was 0.52 $\Omega/\square$, a sufficiently low value to power a chip and generate an inductive response to the interrogator.

6.7 Conclusions

We introduced a high-concentration adaptation of the synthesis method, producing ∼6 g per 100 ml of unoxidized Cu NCs. The produced Cu NCs enabled the optimization of an ink formulation using a definitive screening design (DSD). We determined the significant factors that impact on the resistivity and adhesion of the ink. Optimal processing conditions yielded to highly conductive films, attaining a resistivity of 2.57 $\mu\Omega \cdot$ cm, a value corresponding to 66% of Cu bulk conductivity. We then increased further the volume of the reaction to 1 L, producing slightly oxidized ∼60 g of Cu NCs in a sole synthesis. We enabled screen printing and production of conductive RFID antennas by adapting the optimal formulation adding a thixotropic agent.

References

[1] Rita Faddoul, Nadège Reverdy-bruas, and Anne Blayo. *Formulation and screen printing of water based conductive flake silver pastes.pdf.* Mater. Sci. Eng. B Solid-State Mater. Adv. Technol., 177:1053–1066, 2012.

[2] Aurore Denneulin, Julien Bras, Fiona Carcone, Charles Neuman, and Anne Blayo. *Impact of ink formulation on carbon nanotube network organization within inkjet printed conductive films.* Carbon N. Y., 49(8):2603–2614, 2011.

[3] ASTM. International. *Standard Test Methods for Measuring Adhesion by Tape Test. D3359 – 09.* Astm, pages 1–7, 2010.

[4] F M Smits. *Measurement of Sheet Resistivities with the Four-Point Probe.* Bell Syst. Tech. J., 37(3):711–718, 1958.

[5] Jose Maria Lopez Pedrosa and Mark Bradley. *A high-throughput and design of experiment mediated optimization of pigment-based ink formulations.* Pigment Resin Technol., 37(3):131–139, may 2008.

[6] Douglas C Montgomery. *Design and Analysis of Experiments - Eighth Edition.* John Wiley & Sons, 9th edition, 2013.

[7] J. M. Gozálvez and J. C. García-Díaz. *Mixture Design Experiments Applied to the Formulation of Colorant Solutions.* J. Chem. Educ., 83(4):647, 2009.

[8] Christine M. Anderson-Cook, Heidi B. Goldfarb, Connie M. Borror, Douglas C. Montgomery, Kelly G. Canter, and John N. Twist. *Mixture and mixture-process variable experiments for pharmaceutical applications.* Pharm. Stat., 3(4):247–260, 2004.

[9] Bradley Jones and Christopher J. Nachtsheim. *A class of three-level designs for definitive screening in the presence of second-order effects.* J. Qual. Technol., 43(1):1–15, 2011.

[10] Bradley Jones and Christopher J. Nachtsheim. *Efficient designs with minimal aliasing.* Technometrics, 53(1):62–71, 2011.

[11] Jonas Billet, Wouter Dujardin, Katrien De Keukeleere, Klaartje De Buysser, Jonathan De Roo, and Isabel Van Driessche. *Size Tunable Synthesis and Surface Chemistry of Metastable TiO2- Bronze Nanocrystals.* Chem. Mater., 30(13):4298–4306, 2018.

[12] Catarina P. Santos, Tiago J. Rato, and Marco S. Reis. *Design of Experiments: A comparison study from the non-expert user's perspective.* J. Chemom., 33(1):1–18, 2019.

[13] Adrian Rose. *Considerations in Formulation and Manufacturing of Thick Film Inks.* Electrocompon. Sci. Technol., 9(1):43–49, 1981.

[14] K.L. Mittal. *Adhesion measurement of films and coatings.* VSP, 1995.

[15] Firas Awaja, Michael Gilbert, Georgina Kelly, Bronwyn Fox, and Paul J. Pigram. *Adhesion of polymers.* Prog. Polym. Sci., 34(9):948–968, sep 2009.

[16] Bradley Jones and Christopher J. Nachtsheim. *Definitive screening designs with added two-level categorical factors.* J. Qual. Technol., 45(2):121–129, 2013.

[17] Bradley Jones. *Proper and improper use of Definitive Screening Designs (DSDs)*, 2016.

[18] Wanli Li, Lingying Li, Yue Gao, Dawei Hu, Cai Fu Li, Hao Zhang, Jinting Jiu, Shijo Nagao, and Katsuaki Suganuma. *Highly conductive copper films based on submicron copper particles/copper complex inks for printed electronics: Microstructure, resistivity, oxidation resistance, and long-term stability.* J. Alloys Compd., 732:240–247, 2018.

[19] Youngil Lee, Jun Rak Choi, Kwi Jong Lee, Nathan E. Stott, and Donghoon Kim. *Large-scale synthesis of copper nanoparticles by chemically controlled reduction for applications of inkjet-printed electronics.* Nanotechnology, 19(41), 2008.

[20] Hirotugu Akaike. *A New Look at the Statistical Model Identification.* IEEE Trans. Automat. Contr., 19:716–723, 1974.

[21] Kiyoshi Yamaoka, Terumichi Nakagawa, and Toyozo Uno. *Application of Akaike ' s Information Criterion (AIC) in the Evaluation of Linear Pharmacokinetic Equations.* J. Pharmacokinet. Biopharm., 6(2):165–175, 1978.

[22] Wei Pan. *Akaike's Informat ion Criterion in Generalized Estimating Equations.* Biometrics, 57:120–125, 2001.

[23] Z. Hens. *Economical routes to colloidal nanocrystals.* Science (80-.)., 348(6240):1211–1212, 2015.

[24] Jan Mewis and Norman J. Wagner. *Thixotropy.* Adv. Colloid Interface Sci., 147-148:214–227, aug 2009.

7

Summary and perspectives

7.1 Summary

Copper nanoparticles (NPs) or nanocrystals (NCs) emerged as a cost-efficient alternative to silver in printed electronics applications. Cu features a bulk conductivity almost at the same level as silver while costing only 1% of Ag's price. In this thesis we first assessed the known synthesis methods for Cu NPs and the strategies to prevent oxidation. We then developed a synthesis method based on thermal decomposition to form size-tunable Cu NCs. We studied how different ligands interact with the surface of the Cu NCs. We learnt that both the capping ligand and particle size have an effect on the sintering of the particles into continuous films. We finally developed a formulation to print the Cu NCs and obtained conductive RFID antennas.

First, we realized an extensive investigation on the known methods to synthesize Cu NPs. We divided the methods in 3 categories, chemical, physical and biological. Chemical methods are the most common in the literature due to their accessibility and straight-forward adaptation of particle properties. The downside of the chemical methods is the frequent use of hazardous reducing agents and the amount of waste-product from the synthesis. Substitution of the reducing agent by ascorbic acid seems to be a promising ap-

proach to reduce the environmental impact of the synthesis and at the same time protect the Cu NPs from oxidation. Alternatively, shifting to methods based on thermal decomposition of copper precursors are promising since no extra reducing agent is required. Physical methods allow mass-production yet they usually require a more costly equipment. Their other issue is the lack of control on particle crucial properties such as size and colloidal stability. Biological synthesis of Cu NPs is based on the same mechanisms as the chemical methods but in a more environmentally-friendly perspective. Here, plant-extract based synthesis stand out from the rest as a green method to prepare well-defined Cu NPs. However, the low reaction times and yields of such synthesis causes that is still not a cost-effective manner to manufacture Cu NPs. In terms of oxidation prevention strategies, silica and carbon-based encapsulation proved to halt the oxidation process on Cu surfaces at the expense of a drastic conductivity decrease. Oppositely, Ag shelling through transmetallation on the surface of the NPs proved to preserve the conductive properties while protecting the Cu core from oxidation. A more economical approach is based on the adsorption of organic ligands and polymers on the surface of the NPs. Besides granting colloidal stability, their presence on the surface delayed the oxidation process sufficiently to eventually transform the Cu NPs into conductive films.

In chapter 3, we introduced our method to synthesize Cu NCs based on the thermal decomposition of copper formate in oleylamine. This method features an economical precursor and a one-pot, rapid synthesis to obtain Cu NCs. By saturating the initial solution with copper formate and implementing a specific temperature profile, we demonstrate a self-cleaning effect. Oxygen cannot access the nanocrystals during the reaction with non-oxidized nanocrystals as result. This is only possible if the reaction rate is high enough to ensure that oxygen has limited access during the formation of Cu^0 monomers. We demonstrated that size of the particles can be tuned from 4 to 200 nm by adjusting the initial concentration of precursor and the ratios precursor/oleylamine.

In chapter 4, we first presented a synthesis adaptation to form 4 nm Cu NCs, ideal for surface chemistry studies due to their high surface/volume ratio. We demonstrated that the initially bound $OlNH_2$ can be replaced by a carboxylic acid through mass-action. Based on the thermodynamic description of the amine/carboxylic acid titration curves, we argue that carboxylic acids directly replace $OlNH_2$ and bind to additional surface sites that show little affinity for $OlNH_2$. We proved that carboxylic acids dissociate upon binding on such surfaces, forming an X_2 binding motif. Since such a binding motif requires an amphoteric surface that offers acidic and basic binding sites, we

argue that ligand binding to Cu nanocrystals is determined by the presence of surface oxides, rather than by the properties of the pristine metal surface.

In chapter 5, we analyzed the effect that ligands have on the oxidation and reduction of the NCs and studied the sintering behavior of the Cu NCs. We demonstrated that a dispersion in polar solvents could be obtained by exchanging the initially bound $OlNH_2$ to a MEEAA, a volatile carboxylic acid. We showed that even if slightly stalled, carboxylic acids are not able to prevent oxidation of the NCs after air exposure. Nonetheless, we proved that oxidation can be reversed by sintering under N_2 and we studied how the capping ligand and particle size affect the reduction temperature. MEEAA-capped particles presented the lowest reduction temperature amongst the studied ligands and an enhanced 50 nm grain size, featuring its case as a promising ligand for Cu NCs in conductive ink formulations. We showed a clear relation between particle size and Cu_2O-Cu transition temperature. Films consisting in larger particles ($\geq$113 nm) presented improved conductivity both before and after thermal sintering despite requiring higher temperatures. Overall, these conclusions highlights the relevance of the capping ligand and particle size in the pursuit of conductive films and pinpoints the relevant particle parameters to formulate and print a conductive ink.

Finally, we introduced a high-concentration adaptation of the synthesis method, producing $\sim$6 g per 100 ml of unoxidized Cu NCs. The produced Cu NCs enabled the optimization of an ink formulation using a definitive screening design (DSD). We determined the significant factors that impact on the resistivity and adhesion of the ink. Optimal processing conditions yielded to highly conductive films, attaining a resistivity of 2.57 $\mu\Omega \cdot$ cm, a value corresponding to 66% of Cu bulk conductivity. We then increased further the volume of the reaction to 1 L, producing slightly oxidized $\sim$60 g of Cu NCs in a sole synthesis. We enabled screen printing and production of conductive RFID antennas by adapting the optimal formulation adding a thixotropic agent, obtaining a resistance of 0.52 $\Omega/\square$.

7.2 Perspectives

From my point of view there are 3 main elements that are needed to be taken into consideration in order to capitalize on Cu NCs-based inks for printed electronics: (i) a synthesis protocol to produce metallic Cu NCs, (ii) a method to prevent or stall oxidation while not hindering conductivity and (iii) a processing method to sinter the particles into conductive films. These elements are markedly connected with each other, for example, if oxidation is not avoided, harsher sintering conditions will be required to attain conductive patterns. Essentially, the crucial point in question is that the whole process must remain cost-effective at all stages; only in that manner will Cu replace Ag as the material of choice for conductive applications.

An extensive list of synthesis methods to produce Cu NCs is presented in chapter 2. Yet, there is no absolute answer for what is the best method, it depends on other factors such as equipment availability, post-processing or printing method. However, an essential factor that is barely treated in the scientific literature is the upscalability of the process which by no means is straightforward. Here, new challenges appear and a promising synthesis in a lab-scale can result in failure when performed in a larger scale. I could tell first hand these struggles when performing the developed synthesis in a 1 L scale. Our method features a low-cost precursor, rapid reaction times, high-solid loading and even the ability to be performed under oxygen presence. When we performed the synthesis in a 1 L scale we faced a dilemma, open-flask synthesis resulted in slightly oxidized particles due to the lower attainable heating rate and closed-flask synthesis was not feasible due the large amount of produced gases. This exemplifies that no synthesis is perfect, and that even if it improves known methods in some way, new problems can always appear when upscaling. Nevertheless, the known literature is thoroughly complete and I do not personally consider synthesis protocols to be the stalling element for the application of Cu-based conductive inks. For example if the goal is to produce large, irregular Cu NPs (>100 nm), ball-milling seems a cost-effective method of choice due to the large volume of material that can be produced. For ink-jet printing suitable NPs (<50 nm), chemical methods such chemical reduction and thermal decomposition still have the upper hand due to control of the size and morphology and rapid reaction times.

Oxidation is usually referred as the main contention point that stops Cu from becoming the preferred material for conductive applications. Two strategies can be follow to deal with the oxidation: prevention and reversion.

In the first, Ag-shelling has proven to greatly improve oxidation resistance while maintaining the electrical properties yet at expenses of a higher cost and processing time. A lower-cost remarkable strategy consisted of shelling the NCs with a copper formate layer. This layer prevented oxidation and decomposed into metallic Cu, H_2 and CO_2 upon sintering at 250°C under N_2 atmosphere. However, the objective of shelling the Cu NCs should be to avoid using high temperature sintering, which limits the range of substrates, or special atmospheres, that raises the cost of the process. A similar case occurred with our process, which focused on oxidation reversion. Even if we managed to synthesize pristine metallic Cu NCs and control the surface chemistry, highly conductive layers were only obtained after sintering at $\geq$300°C, which limited the substrates to glass and polyimide and increased the processing costs. To reduce this sintering temperature we introduced MEEAA, a promising low boiling point ligand, yet we did not success in formulating concentrated inks solely dispersed by MEEAA. Nevertheless, I honestly believe that our contributions to the fields of synthesis, surface chemistry and sintering of Cu NCs are significant and can be of considerable interest for future research. I would like to finish the perspectives by mentioning a promising alternative to obtain conductive films developed by Dr. Michael Grouchko. In his work he formulated Cu NCs with hypophosphorous acid (H_3PO_2), which react forming CuH, a metastable compound that decomposes into metallic Cu and H_2. The advantage of the method is that sintering can be performed with an office laminator in 1 minute, thus greatly reducing the processing expenses. I personally believe that research oriented towards the understanding and developing of this strategy are of great interest for future research in Cu-based conductive inks.

Finally, I would like to use this final section to express my personal view on science communication. During the last years I have heard so many times that a successful researcher should know how to "sell" his or her work in order to make it more appealing for the audience, creating a story by introducing a problem and developing how your data solves it. Although I agree that this helps in terms of structure and comprehension, and that is something I have been intending to improve upon as a scientist; one must be careful to not carry it too far. Even an ignorant like me realized that in some occasions authors tend to oversell their results to make their work more appealing. What the reader never knows is which unwanted results and data that weakens the story are discarded or ignored. Hence, valuable scientific contributions are probably foregone because "they did not fit into the story". The point I am trying to make is that we would all benefit if we would be critical with all obtained results rather than just the ones that fit our story. I do not pretend to give any kind of lesson with these

statements. This is just a reflection expressed as a reminder to myself and whoever wants to embrace it, just some values to always keep in mind. To summarize it, I would like to end this manuscript with this citation from Prof. Feynman autobiography:

"The first principle is that you must not fool yourself—and you are the easiest person to fool. So you have to be very careful about that. After you've not fooled yourself, it's easy not to fool other scientists. You just have to be honest in a conventional way after that."

— Richard P. Feynman, Surely You're Joking, Mr. Feynman!

A

Supporting Information

A.1 Supporting Information of Chapter 4

A.1.1 Oleylamine, ^{1}H NMR Resonance Assignment

Assignment of the different resonances in the 1D ^{1}H NMR spectrum of oleylamine ($OlNH_2$) was done through Homonuclear Correlation Spectroscopy (COSY). Whereas the 1D ^{1}H spectrum already indicated a distinct signal for the alkene resonance **4** and the bulk of the oleyl chain **2**, COSY provided a definitive assignment of all the resonances, where neighboring protons can be identified by cross peaks between the corresponding resonances. In the case of free $OlNH_2$, the resonances of the α-CH_2 protons **5** and the protons **3** next to the alkene group appear clearly resolved in the spectrum.

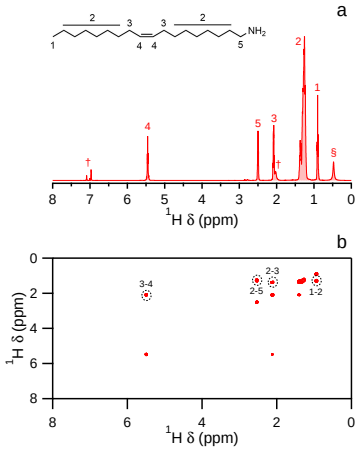

Figure A.1: (a) 1D ^{1}H NMR spectrum of a solution of 10 μl of $OlNH_2$ in toluene-d_8. (b) Correlation Spectroscopy (COSY) spectrum of the same solution.

A.1.2 A NMR Linewidth Benchmark, Oleate Bound to CdSe Nanocrystals

To benchmark the resonance linewidths measured for $OlNH_2$ bound to Cu nanocrystals before and after oxidation, we use the 1D ^{1}H NMR spectrum of oleate-capped CdSe NCs published by Fritzinger *et al.* (see Figure A.2).[1] From this spectrum, we obtain the full widths at half maximum as listed in Table 4.1 of the main manuscript. This numbers attest to the larger than usual line broadening for $OlNH_2$ bound to Cu nanocrystals; an excessive line broadening that disappears after oxidation of the Cu nanocrystals. This suggests that $OlNH_2$ bound to Cu nanocrystals experiences a different magnetic environment than $OlNH_2$ or oleate bound to a diamagnetic semiconductor nanocrystal such as Cu_2O or CdSe.

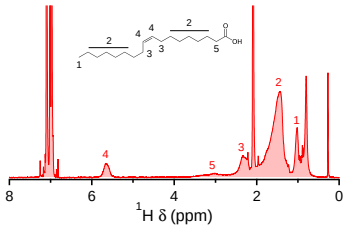

Figure A.2: 1D ^{1}H NMR spectra of a dispersion of 3.5 nm CdSe nanocrystals in toluene-d_8 as previously published by Fritzinger *et al.*. We obtained the full width at half maximum of the oleate resonance listed in Table 4.1 from this spectrum.

A.1.3 DOSY of Oxidized Cu Nanocrystals

We used diffusion ordered spectroscopy (DOSY) to verify the binding of $OlNH_2$ to oxidized Cu nanocrystals. Also here, the overview DOSY spectrum indicates that $OlNH_2$ has the small diffusion coefficient typical of a bound ligand. This is confirmed by analyzing the decay of the signal intensity as a function of the square of the field gradient strength, which yields a diffusion coefficient of $103\,\mu m^2/s$. This number is all but identical to that of $OlNH_2$ bound to pristine Cu nanocrystals, which indicates that $OlNH_2$ remains tightly bound ligand upon oxidation of the Cu to Cu_2O.

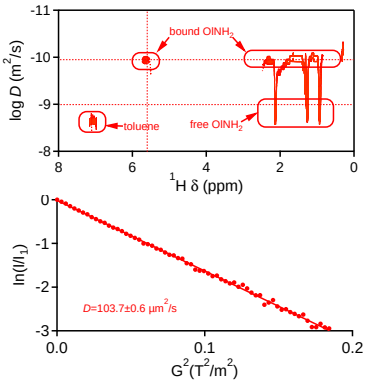

Figure A.3: (top) DOSY spectrum of a dispersion of Cu nanocrystals stabilized by $OlNH_2$ after 1 hour of air exposure. (bottom) Decay of the intensity of the alkene resonance at 5.5 ppm with increasing field gradient strength. Fitting the decay to a single exponential yields the diffusion coefficient as indicated.

A.1.4 Undecenoic Acid, ^{1}H NMR Resonance Assignment

To assign the different resonances of undecenoic acid (UDA), we used the same procedure as outlined in section A.1.1. Combining the 1D ^{1}H and the COSY spectra of UDA, all the UDA resonances can be unambiguously assigned to specific protons in UDA. The chemical shift of these different protons is different from what is measured for $OlNH_2$ protons, which makes that all the signals in an UDA-$OlNH_2$ mixture can be assigned. As compared to the pure compounds, resonances **g** and **f** of UDA and resonance **5** of $OlNH_2$ exhibit a downfield shift in the UDA-$OlNH_2$ mixture. This shift can be interpreted as caused by the formation of an UDA-$OlNH_2$ ion pair that provokes deshielding of the protons next to the interacting functional groups.[2] Most interestingly, the alkene resonances are well separated, which is useful to obtain separate concentrations for both species from the integrated signal intensity. This approach was used to monitor the concentration of bound and free ligands during a titration of an $OlNH_2$ capped Cu nanocrystal dispersion with UDA as shown in Figure 4.3c of the main text.

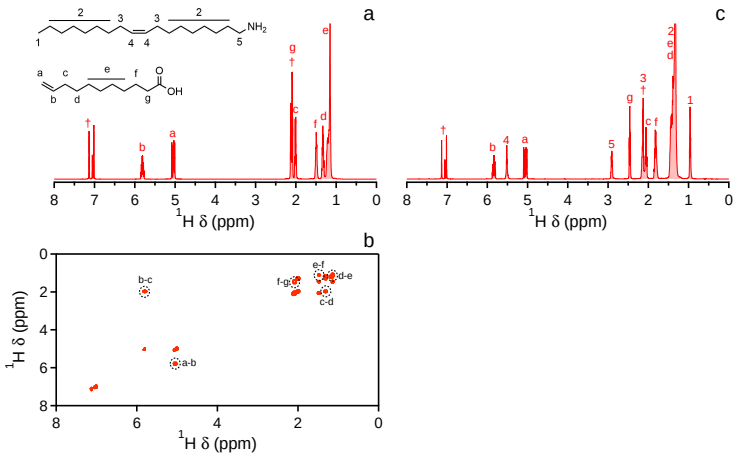

Figure A.4: (a) 1D ^{1}H NMR spectrum of UDA in toluene-d_8. (b) COSY spectrum of UDA in toluene-d_8, in which the different cross peaks have been assigned to couples of neighboring protons. (c) 1D ^{1}H NMR spectrum of $OlNH_2$ and UDA in toluene-d_8. Labeled resonances are identified as (1-5) $OlNH_2$ resonances, (a-g) UDA and (†) toluene-d_8.

A.2 Supporting Information of Chapter 5

A.2.1 2-[2-(2-Methoxyethoxy)ethoxy]acetic acid, ^{1}H NMR Resonance Assignment

We assigned the different proton resonances of 2-[2-(2-Methoxyethoxy)ethoxy]acetic acid (MEEAA) by 1D ^{1}H NMR. The position attributed was based on the assumption that protons closer to the terminal carboxylic acid present larger ^{1}H chemical shifts due to the deshielding effect from the carboxylic acid group. This assignment concurs with published work by De Roo *et al.*[3]. Due to its technical grade, signals at 4.18 and 4.27 are assumed to be minor impurities.

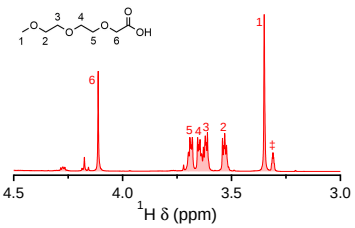

Figure A.5: 1D ^{1}H NMR spectrum of a solution of 10 μl of MEEAA in methanol-d_4. Labeled resonances are identified as MEEAA (1-6) and residual methanol (‡)

A.2.2 Ellingham diagram of the oxidation of Cu^0 to Cu_2O

We calculated the free energy of the reaction A.1 at O_2 concentration of 1ppm to simulate the conditions of the Cu NCs when sintered in a glovebox.

$$4Cu_{(s)} + O_{2(g)} \rightleftharpoons 2Cu_2O_{(s)} \tag{A.1}$$

Here, the gibbs free energy of the reaction is affected by both the partial pressure of the gases and the total pressure of the system:

$$\Delta G = \Delta G^{\circ} + RT\ln Q \tag{A.2}$$

where Q is:

$$Q = \frac{1}{P_{O_2}} \tag{A.3}$$

As seen in figure A.6, the reduction becomes thermodynamically favorable around ~420°C, indicating that the reduction observed upon sintering is greatly affected by the oxygen gas concentration during the process.

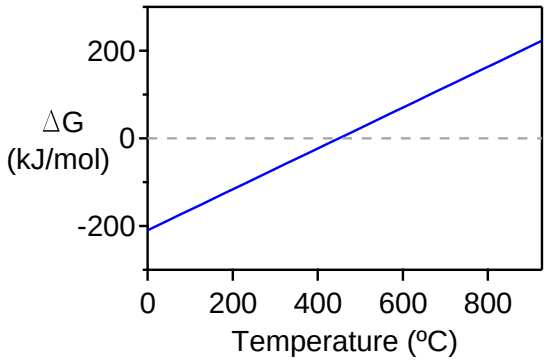

Figure A.6: Ellingham diagram of the reaction A.1 at a O_2 concentration of 1 ppm and a total pressure of 3 mbar.

A.2.3 Ligand effect on sintering of Cu NCs

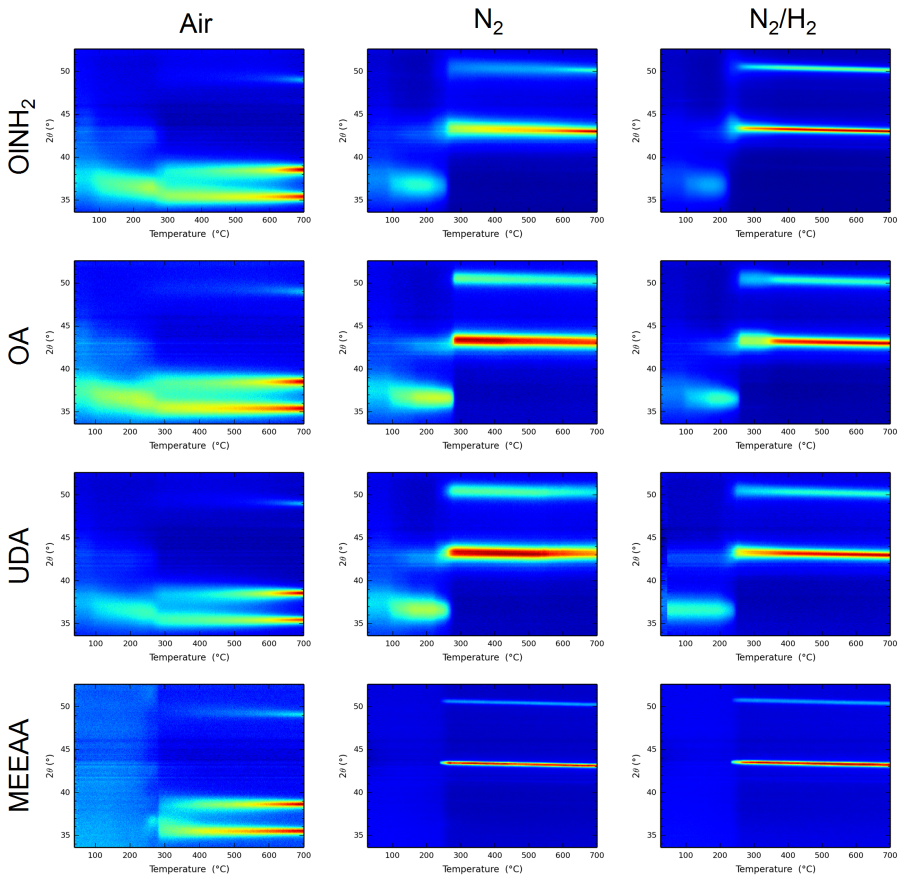

Figure A.7: *In-situ* XRD plots of Cu NCs capped either with $\mathrm{OlNH_2}$, OA, UDA and MEEAA sintered under different atmospheres (air, $\mathrm{N_2}$ and $\mathrm{N_2 : H_2}$.)

A.2.4 CuO XRD planes evolution upon heating

We deposited CuO powder on glass substrate and monitored the x-ray diffraction patterns of the films thus formed during sintering under inert or reductive atmospheres. Differently from Cu_2O NCs, thermal treatment in N_2 up to 700°C is not enough to reduce the material to Cu_2O or Cu^0. Presence of a reducing agent, H_2, suceeded in reducing the CuO powder first to Cu_2O and subsequently to Cu^0 yet at a high temperature >500°C.

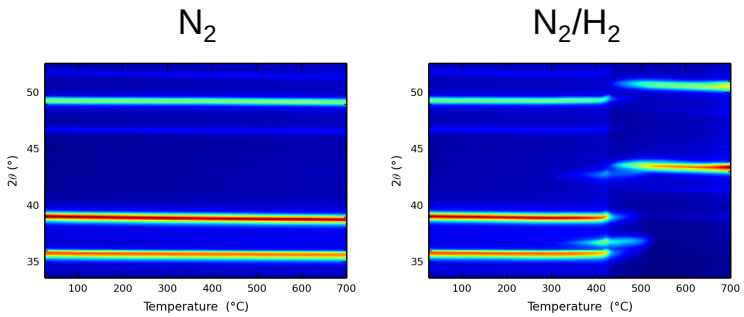

Figure A.8: *In-situ* XRD plot of comercial CuO heated up under different atmospheres (N_2 and $N_2 : H_2$.)

A.2.5 XRD spectra of the pristine Cu NCs synthesized under ambient conditions

As visible in figure A.9, sole presence of the metallic phase of Cu is proven by the peaks at 43.3˚and 50.5˚. No diffraction peak is visible at 37˚or 42.6˚, confirming the absence of Cu_2O. Signal at ∼41˚is a common satellite originated by the Cu coil. Large peaks at ∼62˚, ∼66˚and ∼69˚arise from the poorly chosen substrate for the measurements, Si.

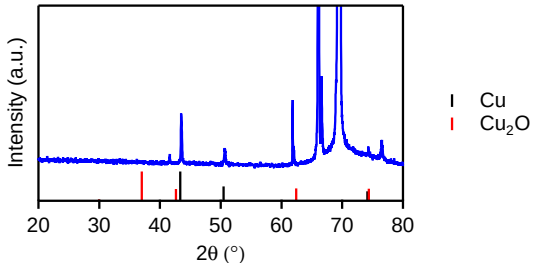

Figure A.9: XRD plot of as-synthesized Cu NCs described in Figure 5.6b.

A.2.6 High resolution TEM of Cu NCs 2 weeks after storage under ambient conditions

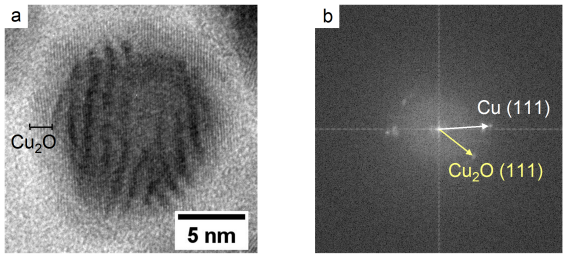

Figure A.10: (a) High-resolution, brightfield TEM image of Cu NCs synthesized in an open atmosphere 2 weeks before the imaging. The reagents concentrations were set at: 0.63M $Cu(HCO_2)_2$ and 1.26M $OlNH_2$. The synthesis proceeded with a heating rate of 10°C/min. until 140°C and then held at this temperature for 10 min. (b) Fast Fourier Transform of image (a), showing their indexed lattice planes.

A.3 Supporting Information of Chapter 6

A.3.1 Comparison of the linear regression models for the response resistivity

The coefficient of determination of the resistivity model is showing a low goodness of the fit (0.53). Also, the residuals distribution are showing a trend to higher absolute residuals as the value of the response increases suggesting that the response can be transformed to improve the fit. Transforming the response to the logarithm simplifies its relationship with the predictor variables and lead to a better description of the model. Right column of the figure plots the residuals after a transformation on the response variable to logarithm of the resistivity. Plotting the residuals versus the value of a fitted response produces a distribution of points with a more random scattering around 0 and model with a better fit to the experimental values (0.80).

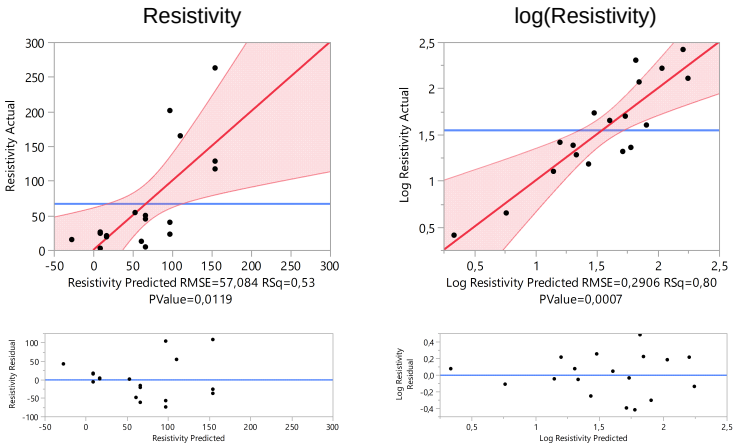

Figure A.11: Experimental data versus predicted in the model for both resistivity and log(resistivity), and residuals of the plots.

References

[1] B Fritzinger, R K Capek, K Lambert, J C Martins, and Z Hens. *Utilizing Self-Exchange To Address the Binding of Carboxylic Acid Ligands to CdSe Quantum Dots.* J. Am. Chem. Soc., 132(29):10195–10201, 2010.

[2] Jonathan De Roo, Maria Ibáñez, Pieter Geiregat, Georgian Nedelcu, Willem Walravens, Jorick Maes, Jose C. Martins, Isabel Van Driessche, Maksym V. Kovalenko, and Zeger Hens. *Highly Dynamic Ligand Binding and Light Absorption Coefficient of Cesium Lead Bromide Perovskite Nanocrystals.* ACS Nano, 10(2):2071–2081, 2016.

[3] Jonathan De Roo, Nuri Yazdani, Emile Drijvers, Alessandro Lauria, Jorick Maes, Jonathan S. Owen, Isabel Van Driessche, Markus Niederberger, Vanessa Wood, Jose C. Martins, Ivan Infante, and Zeger Hens. *Probing Solvent-Ligand Interactions in Colloidal Nanocrystals by the NMR Line Broadening.* Chem. Mater., 30(15):5485–5492, 2018.